University of Ghana http://ugspace.ug.edu.gh

THERMAL HYDRAULIC AND SAFETY ANALYSIS OF HEAT TRANSFER AND DISTRIBUTION IN THE GHANA RESEARCH REACTOR-1 (GHARR-1) CORE USING STAR-CCM+ CFD CODE

A thesis presented to the:

Department of **MEDICAL PHYSICS**
GRADUATE SCHOOL OF NUCLEAR AND ALLIED SCIENCES
UNIVERSITY OF GHANA

BY

SIMBARASHE MANGENA, 10542174
Bsc, Midlands State University, Zimbabwe, 2009

In partial fulfillment of the requirements of the award of

MASTER OF PHILOSOPHY

IN

NUCLEAR SCIENCE AND TECHNOLOGY PROGRAM

JULY, 2016

University of Ghana http://ugspace.ug.edu.gh

DECLARATION

This thesis is a result of research work undertaken by Simbarashe Mangena in the Department of Medical Physics, School of Nuclear and Allied Sciences (SNAS), University of Ghana, under the supervision of Professor G. Emi-Reynolds and Dr. V.Y. Agbodemegbe.

…… Date: …….

Simbarashe Mangena

(Student)

…… Date: ……

Prof. G. Emi Reynolds

(Principal Supervisor)

…… Date: ……..

Dr. V. Y. Agbodemegbe

(Co-supervisor)

University of Ghana http://ugspace.ug.edu.gh

ABSTRACT

Operational power of a nuclear reactor core is limited by thermal considerations. In principle, the allowable core power is restricted by the rate at which the heat can be transferred from the fuel to the coolant. Unlike in conventional combustion facilities where the heat is released in gas-flows, heat in the nuclear reactor core is mainly released in the structural material. If not properly removed the structural materials inevitably melt causing release of radioactive material.

STAR-CCM+ CFD code was used to perform thermal hydraulic analysis of the Miniature Neutron Source reactor also known as the Ghana Research Reactor-1 (GHARR-1). The reactor has a Highly Enriched Uranium (HEU) core consisting 344 fuel pins arranged in 10 multi-concentric circle layers at a pitch distance of 10.95 mm. The present study however considered only the first two concentric rings with varying power of 15 to 30kW. The choice of the first two concentric rings was informed by the results of the computation of local power peaking factors based on power densities. The result indicates that the maximum radial peaking factor of 2.02 occurred at the mid-plane of the core while the maximum axial peaking factor of 1.57 was at the region of the second ring. The extent of the domain considered in this work was also limited by the computational resources available.

Analysis of the temperature, pressure, mass flow rate and turbulent intensity in the first two concentric rings was performed to assess the steady state Thermal hydraulic behaviour of GHARR-1 core under natural convection cooling. Computational simulation was performed at 15 and 30 kW at a fixed mass flow rate of 0.11 kg/s. The mass flow rate was varied from 0.11 to 0.15 kg/s in steps of 0.02 kg/s at a fixed power of 30 KW.

University of Ghana http://ugspace.ug.edu.gh

Effective heat transfer and cooling of the reactor was achieved at the maximum coolant mass flow rate. Surface Average temperature increased along the flow channel from the inlet to the outlet in conformity with operating trends reported in the GHARR-1 Safety Analysis Report. The highest surface average temperature in the normal operating power range (15-30kW) was observed to be 296.21K at 30 kW and coolant mass flow rate of 0.11kg/s. The hottest channel is located between the inner and outer ring on the triangular pitch distance bounded by rods 4, 5 and 14.

The hottest segment has a temperature of 301.85K and is located at an axial distance of 0.2020cm. This is below the maximum cladding Temperature of 333.15K hence the reactor is operating safely. Computed Distribution of the mass flow rate generated in the domain varies proportionally with the assigned inlet mass flow rate for the normal operating powers (15-30kW) A turbulence surge at the inlet due to instantaneous injection of fluid coupled with a drop as a result of development of the flow was observed.

A general turbulence buildup was also observed as the flow develops and the fluid stabilises. Turbulent intensity was observed to peak at the upper part of the fuel rods consistent with the predictions of the GHARR-1 Safety Analysis Report. All computed accident situation temperatures were below the melting point of the U-Al alloy satisfying regulatory requirements for safe operations.

University of Ghana http://ugspace.ug.edu.gh

DEDICATION

This work is dedicated to my parents Mr and Mrs E.P Mangena, my sisters Grace Mangena-Chigeza and Tariro Mangena-Jemwa, my nieces Philipa Chigeza, Amara Jemwa and Tamara Jemwa, my nephews Flynn and Flloyd Chigeza. Last but not least my girlfriend Lorraine Rutendo Zhou for the time endured.

University of Ghana http://ugspace.ug.edu.gh

ACKNOWLEDGEMENTS

I would like to gratefully acknowledge the International Atomic Energy Agency (IAEA) and the Government of Zimbabwe for awarding me the opportunity to undertake studies in Ghana.

My profound gratitude to my supervisors Prof G. Emi- Reynolds and Dr V.Y Agbodemegbe whose guidance, conscientiousness and meticulous attention to detail was instrumental in the production of this thesis.

This acknowledgement would be incomplete without mention of Mr Edward Shitshi whose immense support was unquantifiable. Thank you "old man of SNAS" and may our dear Lord bless you abundantly. In the same vein, profound gratitude also goes to Prof Emeritus E.H.K Akaho, Prof C. Shandorf, Prof J.J Fletcher, Dr S.K Debrah, Dr Ampomah Amoako, Dr R.B. M Sogbadji, Dr Danso, Rev Dr A. Bamford, Dr H.C Odoi and Dr R. Abrefah for the priceless impartation of knowledge. Hats off to the Management of the Radiation Protection Authority of Zimbabwe for their confidence in me and awarding me this opportunity. Special mention to the Chief Executive officer Mr R.M Severa. May God bless and prosper you in all dimensions.

My Father, mentor and role model since childhood Mr E.P Mangena, an ocean of wisdom, knowledge and experience. I am proud of you Dad, I owe it all to you. Thank you for continuously refining and polishing me to be a man that people take pride in.

I would also like to record my heartfelt thanks to my family, friends, advocates, CD-ADAPCO and everyone who contributed in many different ways and provided continuous support in this effort.

University of Ghana http://ugspace.ug.edu.gh

TABLE OF CONTENTS

University of Ghana http://ugspace.ug.edu.gh

University of Ghana http://ugspace.ug.edu.gh

University of Ghana http://ugspace.ug.edu.gh

LIST OF TABLES

University of Ghana http://ugspace.ug.edu.gh

LIST OF FIGURES

University of Ghana http://ugspace.ug.edu.gh

University of Ghana http://ugspace.ug.edu.gh

NOMENCLATURE

Roman Letters

$\dot{Q}$	Heat generation rate
G	Energy produced per fission
N	Number of fissionable nuclei per unit volume
V_f	Volume of the fuel
$q^{"}$	Heat flux (heat transferred per unit area
K	Thermal conductivity of the fuel pellet
T	Temperature
R	Radius of the fuel pellet
h	Specific Enthalpy
h_c	Convective heat transfer Coefficient
h_g	Gap conductance
F	Buoyancy force per unit volume
g	Acceleration due to gravity
Gr	Grashof's number
L	Characteristic length of coolant channel
Ra	Rayleigh Number
Pr	Prandtl number
U, V *and* W	Momentum components in x, y and z directions
u, v *and* w	Velocity components in x, y and z directions
S	Source term

University of Ghana http://ugspace.ug.edu.gh

c	Specific heat capacity
P	Pressure
B	Constant
F_q	Power peaking factor
P_s	Power in each fuel rod segment
P_r	Operating power
A_s	Surface area
k	turbulent kinetic energy
Y+	Dimensionless variables with respect to the wall conditions

Greek Letters

σ_f	Microscopic fission cross section of the fuel
ϕ	Neutron flux
ρ	Material density
τ	Time
β	Volumetric thermal expansion coefficient
Δ	Change in a specific quantity
μ	Viscosity
v	Coolant velocity
ε	Turbulent dissipation
ω	Specific dissipation rate
α	Thermal diffusivity
τ	Viscous Stresses
δ	Boundary layer thickness

University of Ghana http://ugspace.ug.edu.gh

κ	Constant
Φ	Imposed Heat Flux
Σ	Summation

Subscripts

f	Fuel
c	Cladding
FS	Fuel pellet surface
Cl	Cladding inner radius
CS	Cladding outer radius
W	Bulk Coolant
AV	Average
Max	Maximum
x, y, and z	Direction components
i	internal energy
i, j and k	Direction Components in Cartesian tensor form
t	Turbulent
b	Buoyancy
w	Wall
ϕ	Scalar quantity
v	Volume
s	Surface

INTEGRI PROCEDAMUS

University of Ghana http://ugspace.ug.edu.gh

Abbreviations

GHARR-1	Ghana Research Reactor 1
MNSR	Miniature Neutron Source Reactor
HEU	Highly Enriched Uranium
STAR-CCM+	Simulation of Turbulent flow in Arbitrary Regions C++ Based
CFD	Computational Fluid Dynamics
U-Al	Uranium- Aluminium
Cd	Cadmium
CIAE	China Institute of Atomic Energy
SAR	Safety Analysis Report
SLOW-POKE	Safe Low Power Kritical Experimental
NAA	Neutron Activation Analysis
PARET	Program for the Analysis of Reactor Transients
MCNP	Monte- Carlo N-Particle
MATLAB	Matrix Laboratory
DNBR	Departure from Nucleate Boiling Ratio
MDNBR	Minimum Departure from Nucleate Boiling Ratio
COMSOL	Computer Solutions
3D-CAD	3-Dimensional Computer Aided Design
RELAP	Reactor Excursion and Leak Analysis Program
NIRR-1	Nigeria Research Reactor-1
PPFF	Power Peaking Factors
CHF	Critical Heat Flux

University of Ghana http://ugspace.ug.edu.gh

CHFR	Critical Heat Flux Ratio
SIMPLE	Semi Implicit Method for Pressure Linked Equations
NNRI	National Nuclear Research Institute
S/No	Specification Number
TLOFA	Total loss of flow accident
GAEC	Ghana Atomic Energy Commission
NIST	National Institute of Standards and Technology
Tke	Turbulent Kinetic Energy
Tdr	Turbulent Dissipation Rate
LEU	Low Enriched Uranium

University of Ghana http://ugspace.ug.edu.gh

CHAPTER 1

INTRODUCTION

This chapter outlines the phenomenon of heat transfer in the GHARR-1 and establishes the justification for the study in association with the problem statement. It also gives insight on the scope of the work as a regulatory requirement.

1.1. Background

Nuclear energy generation is strictly proportional to the generation of the neutron flux. Therefore depending on the size of the reactor core, there is a limit to the amount of fluid employed for the removal of thermal heat generated. Other parameters may affect the level of generated heat within the core, but it is limited by the ability of the fluid to cool the fuel pins. [1].

In this vein, adequate description of the process of transferring the fission heat released in materials due to nuclear reactions is both paramount and fundamental for the safe utilization of the thermal energy in the provision of useful heat. The study therefore seeks to provide knowledge of the heat generated in the core of the GHARR-1 in the first two concentric rings.

In the GHARR-1, U-Al alloy is used as the fuel meat and is in contact with the cladding, providing a small contact resistance. Due to the low power density the centre temperature of the meat is almost the same as cladding temperature when operating at the same reactor power. The temperature drop across the cladding is about $1^{o}C$. 344 fuel pins constitute the reactor core configuration at a nominal power 30 kW [2]. The configuration of fuel pins comprises arrangement in 10 multi-concentric circle layers at a pitch distance of 10.95 mm as shown in Figure 1.1

University of Ghana http://ugspace.ug.edu.gh

Figure 1.1: GHARR-1 Core showing the 10 concentric rings [2]

The work to be performed seeks to make use of features available in Computational Fluid Dynamics (CFD) models with the aim to analyse heat transfer and distribution in the GHARR-1 core. The present study will however consider the first two rings of the GHARR-1. STAR-CCM+ CFD code shall be employed for this application.

1.2 Overview of the GHARR-1

The GHARR-1 is a Miniature Neutron Source Reactor (MNSR) with a tank-in-pool design and a maximum power of 30kW similar to the Canadian SLOWPOKE (Safe Low Power Critical Experiment) reactor. It was designed, manufactured and constructed by China Institute of Atomic Energy (CIAE). The GHARR-1 is fueled by Highly Enriched Uranium (HEU) (90.2% enrichment) in aluminium alloy (UAl_4) fabricated into pins 4.3mm in diameter housed in a 0.6mm thick aluminium cladding. Each of the 344 fuel elements are concentrically arranged in 10 rings (figure 1.1) in the fuel assembly with a total length of 248mm and an active length of 230mm. The fuel assembly additionally contains 4 tie rods and 6 dummy pins mounted on a 50 mm thick bottom-Be reflector surrounded by a 100 mm thick annular-Be reflector in addition to a top-shim Be reflector

University of Ghana http://ugspace.ug.edu.gh

of variable thickness. A stainless steel cladded Cadmium (Cd) control rod is inserted and withdrawn through a central guide tube covering the active length of the core. The single control rod regulates the reactor power, compensates reactivity and shuts down the reactor during normal and abnormal operations [3]. Natural convection is employed for cooling the reactor which operates to a maximum thermal neutron flux of $1x10^{12}$ n/cm^{2}s. Figure 1.2 shows a schematic diagram of the MNSR. The reactor comprises 5 major components namely the reactor assembly, control console, auxiliary systems, irradiation system and the pool. It is designed for use in universities, hospitals and research institutes mainly for neutron activation analysis, production of short lived radioisotopes, education and manpower development.

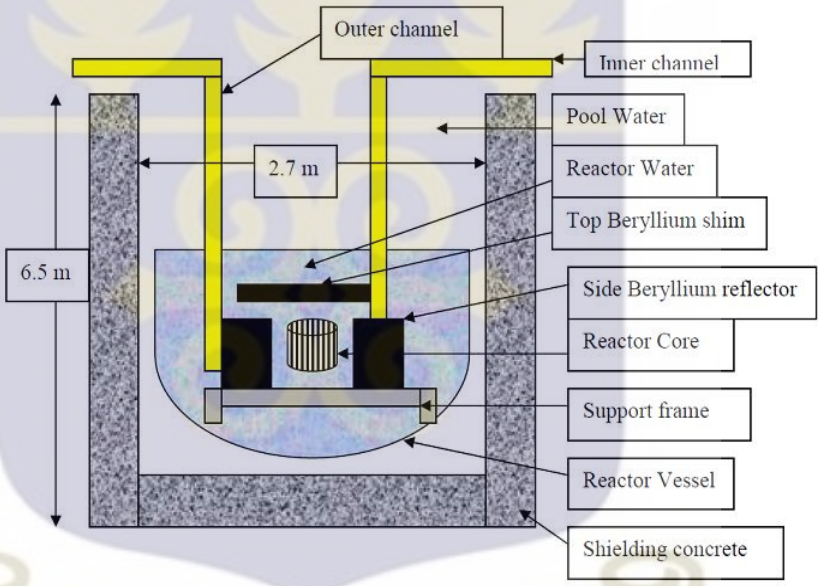

Figure 1.2: Schematic diagram of the MNSR (*side view*) [4]

Technical and thermal hydraulic specifications of the GHARR-1 are provided in tables 1.1 and 1.2 respectively.

University of Ghana http://ugspace.ug.edu.gh

Table 1.1: Technical Specifications for GHARR-1

Parameter	Description
Reactor Type	Tank in pool
Rated Thermal Power	30kW
Fuel	UAl_4
U-235 Enrichment	90.2%
Core shape	Cylinder
Core Diameter	23.1cm
Core Height	23.0 cm
Core loading	990.72 g
Number of fuel Elements	344
Number of dummy rods	6
No. of Irradiation Channels	10
Inner Channels	5
Flux in inner channel	$1x10^{12}$ n/cm^{2}s
Flux in outer channel	$5x10^{11}$ n/cm^{2}s
Reactor Cooling Mode	Natural Circulation
Height of inlet orifice	6mm
Height of Outlet orifice	7.5mm
Diameter of fuel meat	4.3mm
Diameter of fuel Element	5.5mm
Excess Reactivity	3.9mK

University of Ghana http://ugspace.ug.edu.gh

Table 1.2: Thermal Hydraulic Specifications for GHARR-1

Initial Condition	Magnitude
System Pressure	1bar
Reactor Water mass flow Rate	0.112 kg/s
Pool Water mass flow Rate	0.224-0.280kg/s
Inlet water temperature	303.15 K
Maximum cladding Temperature at 30kW	333.15 K
Coolant Density	1000kg/m^3

1.3 Heat Transfer in the GHARR-1 Core

The GHARR-1 core is located 4.7m under 1.5m^3 of water close to the bottom of a watertight reactor vessel. The water in the reactor relies upon natural convection and is the primary heat transfer medium which additionally serves the purpose of radiation shielding and moderation. A water-cooling coil located near the top of the vessel is also used for heat extraction. The water-filled reactor vessel is in turn immersed in a water-filled pool of 30m^3. Cold water is drawn through the inlet orifice by natural convection and flows through the hot fuel elements then exists the core through the outlet orifice. The heated water rises to mix with the large volume of water in the reactor vessel and to the cooling coil. Heat passes through the walls of the container and is dissipated in the pool water. The flow regime of the coolant in the core is at the transient phase from laminar flow to turbulent flow. The flow transition occurs when there is an increase in power as a result turbulence increases in the coolant towards the upper part of the fuel elements where the buoyancy force in natural circulation must overcome the friction [3]. A diagrammatic representation of heat removal under natural circulation is shown in Figure 1.3.

University of Ghana http://ugspace.ug.edu.gh

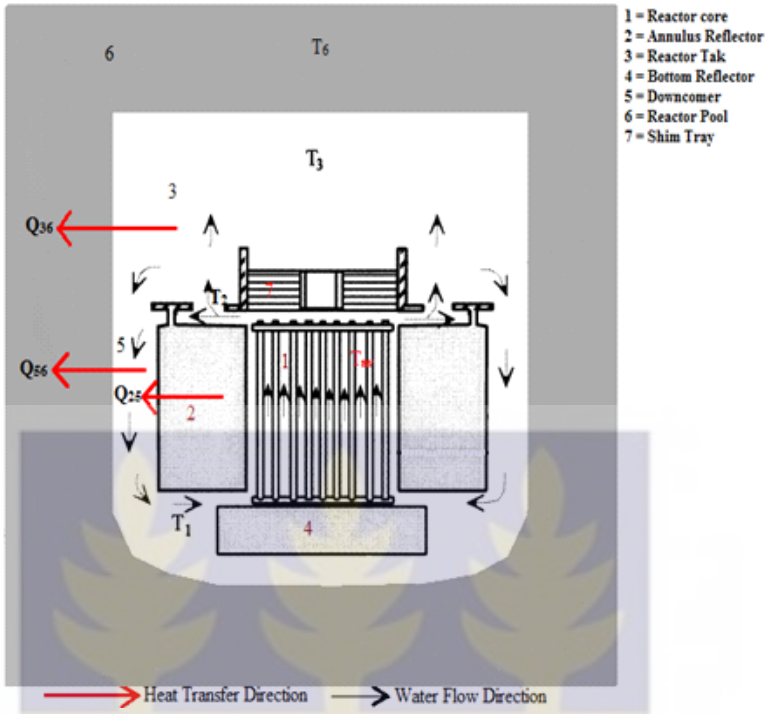

Figure 1.3: Heat transfer under natural circulation [5]

1.4 Statement of the Problem

There is no theoretical upper limit to the power production in a nuclear reactor as long as the heat released can be safely removed. From a safety analysis point of view, literature lacks comprehensive numerical data that can be used to predict heat transfer in the GHARR-1 core. Current knowledge [11, 19] is limited as a result of adaptations of the geometry consistent with the capabilities of analysis codes. Neutronics codes employed in previous studies were able to model the entire geometry of the GHARR-1 but they are limited to evaluation of Neutronics parameters. Studies performed by S. Mohammed et al., [19] modified the core and represented it as a single fuel pin. There is need for a more accurate representation of the core consistent with the available computational resources. The work seeks to accurately analyse heat transfer and distribution in the actual geometry of the GHARR-1 core focussing on the first two concentric rings. The study is expected to satisfy the regulatory requirement of ensuring safety of operation of the reactor at all times [6]

University of Ghana http://ugspace.ug.edu.gh

1.5 Objectives

To perform thermal hydraulic analysis of the heat generated in the GHARR-1 core paying particular attention to heat distribution from one ring to the other between the first two concentric rings.

- **Specific Objective**

1) To evaluate the steady state thermal hydraulic behaviour of GHARR-1 core under natural convection cooling by numerical simulation using STAR-CCM+ CFD code.
2) To perform fluid channel mapping and zoning of the GHARR-1 core in a bid to analyse heat transfer and distribution.
3) To provide adequate knowledge of the heat generated in the core of the GHARR-1 Miniature Neutron Source Reactor (MNSR)
4) To determine the extent to which failure of the heat transfer will compromise safe operation of the reactor based on limits approved by the Regulatory Authority.

1.6 Relevance & Justification

Nuclear thermal hydraulics is the science providing knowledge and mathematical tools for adequate description of the process of transferring the fission heat released in materials due to nuclear reactions into its environment. Properly arranged and controlled processes achieve this target. Improperly arranged processes or inappropriate controlled processes may lead to damages, resulting in partial or in some cases total loss of investment together with loss of life. Nuclear thermal hydraulics is thus a substantial part of reactor safety [7].

Accurate knowledge of the heat source is a prerequisite for analysis of the temperature field. It is on this basis that nuclear and physical properties of the fuel, coolant and structural material are defined. Both steady state and transient conditions of the reactor require the coupling of neutronic and thermal analysis. Thermal analysis is performed in order to predict the temperature field in the reactor core [8].

University of Ghana http://ugspace.ug.edu.gh

The use of computer based simulations helps to accurately analyse heat transfer in the GHARR-1 core in a bid to assess and enhance operational safety. In view of the above discourse, the study serves to provide analysis of heat transfer within the GHARR-1 core as a means of operational analysis for safety assessment during normal operation

1.7 Scope and Limitation

In a bid to optimize the available computational resources, the study will be limited to analysis of the first two concentric rings. Consistent with computations of local power peaking factors based on power densities as reported in the Safety Analysis Report, the maximum radial peaking factor of 2.02 occurred at the mid-plane of the core and the maximum axial peaking factor of 1.57 was at the region of the second ring with 6 fuel elements near the centre of the core as reported in the Safety Analysis Report. Analysis of heat transfer at these regions of maximum heat release will thus give an overall view of heat transfer in the core and hence the safety of the facility.

1.8 Thesis Structure

This thesis comprises five chapters. Chapter one provides an introduction and background to the study. It also emphasizes the importance of this work and its contribution to current knowledge on heat transfer and distribution in research reactors. Chapter two gives insight on the work performed in the study of heat transfer and distribution in MNSRs and highlights the knowledge gaps that need to be addressed by this research. A comprehensive discussion of the fundamentals of the STAR-CCM+ code and its relevant features utilized in the computational modelling and analysis of the GHARR-1 is also undertaken in this chapter. Chapter three vividly outlines the methodology employed for the analysis of heat transfer and distribution in the GHARR-1. It also discusses the geometry design, computational models used, boundary conditions and relevant parameters utilized in the research as well as explanations of the various processes undertaken by the code during computation. The results obtained from the study are clearly and logically presented in Chapter 4. Chapter five concludes the study and gives an overall summary of the research, recommendations, lessons learnt, overall contribution to current knowledge and possible recommendations for future studies.

University of Ghana http://ugspace.ug.edu.gh

CHAPTER TWO

LITERATURE REVIEW

Computational fluid dynamics codes provides a comprehensive understanding of heat transfer processes and fluid flow in complex geometries of nuclear reactors. In this work the application of CFD to undertake thermal-hydraulic analysis of the Miniature Neutron Source Reactor (MNSR) at the Ghana Atomic Energy Commission was carried out. This chapter presents a review of relevant literature on the work performed in the study of heat transfer on GHARR-1 as well as the approach adopted in the study of other Miniature Neutron Source Reactors (MNSRs) and the extent and limitations in these previous efforts directed at the study of MNSRs.

Commercial nuclear power reactors are designed to achieve optimum thermal hydraulic performance while maintaining sufficient safety margins. Research reactors, while not aiming at optimum thermal-hydraulic performance, are also required to permit sufficient safety margins between normal operations and hence ensure fuel and cladding integrity [9]. The work reported in this thesis serves to complement the previous work and provide a framework for operational safety analysis.

2.1 Previous Related Work on GHARR-1 and other MNSRs

Miniature Neutron Source Reactors (MNSRs) are Chinese versions of the Canadian Safe Low Power Kritical Experimental (SLOW-POKE) reactors. There are four operational MNSRs in China, while Ghana, Iran, Nigeria, Pakistan and Syria have one each [10]. The Ghana Research Reactor 1 (GHARR-1) was commissioned in March 1995 [11]. It has been used mainly as a teaching and training reactor, Neutron Activation Analysis (NAA) and small scale radioisotope production [4]. Studies on the GHARR-1 have been directed towards characterizing the core by computer simulation together with experimental work. These previous works provided information on, neutron fluxes, reactor parameters,

University of Ghana http://ugspace.ug.edu.gh

reactor transients, power peaking factors and burnup. However, simulation and experimental work with regards to coolant/moderator temperature distribution is limited.

Ampomah- Amoako et al., performed transient analysis of the GHARR-1 using PARET-thermal hydraulics code for the insertion of 2.1 mK, 4 mK and 6.71 mK reactivities. Program for the Analysis of Reactor Transients (PARET) code enables the reactor core to be represented by up to four regions with different power generation, coolant mass flow rate and hydraulic parameters. This setup mimics fuel pins and their associated coolant channels. Solution of the one-dimensional heat conduction equation enabled computation of heat transfer in each fuel element solution up to a maximum of 21 axial segments. The geometry of the present work was designed consistent to the maximum axial segments of the PARET code [12]. Power across the 21 axial sections was obtained from an MCNP neutronic computation [13, 14]. Power peaking factors were calculated from this work and used to compute heat fluxes that were used to study heat transfer in the present work.

Transient Temperature profiles within the fuel pin following a sudden loss of coolant accident were investigated by C.J Adjei et al., The transient conditions entailed the operation of the research reactor at maximum power (30 kW) in steady state and suddenly shutting down due to total loss of coolant without generation of subsequent internal heat together with decay heat from the fuel pins. Equations of transient temperature distribution were formulated mathematically and solved analytically using Bessel functions. The results obtained showed a high transient temperature distribution at the fuel element centreline, the least temperature was recorded at the fuel clad surface [15]. Although axial heat conduction was assumed to be negligible in their analysis, the present work provides detailed axial analysis of temperature, pressure mass flow rate and turbulent intensity in the core by through the use of STAR-CCM+ Computational Fluid Dynamics code. Furthermore, safety analysis of both normal operation and accident conditions will be performed.

N.A. Adoo et al., determined thermal hydraulic data for the GHARR-1 under reactivity insertion transients using the PARET/ANL code. The following parameters were analysed:

University of Ghana http://ugspace.ug.edu.gh

- peak clad and coolant temperatures
- temperature and void coefficients of reactivity
- power distribution and power peaking factors
- Heat flux at the hot spot.

Peak clad and coolant temperatures were observed to range from 59.18 ◦C to 112.36 ◦C and 42.95 ◦C to 79.42 ◦C respectively. Calculations of the Departure from Nucleate Boiling Ratio (DNBR) satisfied the design criteria for which no boiling occurs in the reactor core consistent with operational safety limits. The resultant thermal hydraulic data generated by the PARET code indicated that the high inherent safety feature of GHARR-1 limits power excursion and escalation of the cladding temperature as a result of the high negative reactivity feedback of the moderator. The advent of Computational analysis of the clad and coolant temperatures was a major development from the previous analytical transient temperature profile studies performed by Adjei et al [16]. The present work will employ injection of heat flux calculated from power peaking factors and analysis of the steady state thermal hydraulic behaviour of GHARR-1 under natural convection cooling.

Analysis of thermal hydraulic transients was performed by S.Yamoah et al., A mathematical model was used to simulate the effect of the pool upper section cooling coils on the thermal-hydraulic behaviour of the GHARR-1. The model was based on the lumped parameter description numerically solved by Matlab/Simulink. The cooling coil mechanism for heat removal in the core is based on circulating water from the coil in the reactor vessel to a refrigeration unit (chiller) which cools the water and returns it to the coil. The reactor vessel and core are cooled by the water as it circulates and heat is transferred by convection from the vessel wall to the reactor pool. The model incorporates fuel grids, cooling coils and radiant energy from the clad. An energy balance based on the average temperatures in these components was performed and partial differentials solved for the diffusion of heat through each fuel element in the core. Comparison of the predictions of model with experimental data showed good agreement of results [5]. The work performed augmented earlier thermal hydraulic studies which were conducted under reactivity insertion. In contrast to the lumped parameter model, the present work involves a finite volume discretization of the reactor core by application of

University of Ghana http://ugspace.ug.edu.gh

the STAR-CCM+ code and will focus on analysing heat transfer within the fuel rods and coolant circulating in the core.

Kyei A.Y. et al., modelled the velocity profile of the coolant flow in the GHARR-1 flow channel using a finite difference scheme by the Marker and Cell method. The model was based on mathematical formulation of the Navier-Stokes equations using a finite difference method for the coolant flow channel of the GHARR-1. The following assumptions were made;

- Coolant flow through the core was laminar.
- The fluid is incompressible with constant properties.
- The flow was between parallel plates.
- The geometry was considered as a plane

The fuel channels were discretized into nodal points in a bid to model the coolant flow Velocity at the nodal points was obtained from computations using the Navier-Stokes equations. The velocity distribution of the coolant flow at a nominal power of 30 kW was simulated by MATLAB. Results obtained from the simulation were validated by COMSOL Multiphysics code using the fluid dynamics module of the Navier- Stokes equation. Analysis of the results established a velocity distribution which ranged from 0.9 m/s to 1.9 m/s and consequently values for Reynolds Number which ranged from 460 to 970 consistent with the assumption of laminar flow [2]. The present work will employ a finite volume analysis of the actual flow regime of the GHARR-1 which transitions from laminar to turbulent on the upper part of the fuel elements. The k-ε turbulence model shall be used to capture the turbulent flux and its dissipation rate. The mean velocity of the coolant and its turbulent kinetic energy will be used to determine turbulent intensity at varying powers.

Control volume finite difference analysis of the transient temperature distribution and associated induced thermal stresses in the GHARR-1 reactor vessel due to coolant heating was performed by M Annor- Nyarko et al., The work sought to investigate the structural integrity of the vessel after 20 years of operation. Heat transfer in the GHARR-1 comprises temperature distributions within structural materials, thermal stress in solid components and the flow of reactor coolant. The heat produced by fission in the fuel

University of Ghana http://ugspace.ug.edu.gh

elements is transferred to the surface of the cladding by conduction and further transferred to the flowing coolant and out of the system through the reactor vessel by natural convection. Thus, heat removal is achieved by natural circulation and water recirculation. Thermal stresses induced by varied thermal gradients within the vessel wall along tangential, longitudinal and radial directions were calculated analytically using Bessel functions. MATLAB was used to generate data for analysis and simulations. Temperature and thermal stress distributions below the limits imposed by the vessel material composition (melting point of 933 K and allowable yield stress of 480 MPa) were obtained from the results. Therefore the structural integrity of the reactor vessel has been maintained to anticipate the incidence of crack propagation and other premature failure modes over the operational period [17]. The present work is limited to the core and will analyse temperature distribution in the fuel and coolant.

T. A. Annafi et al., performed a finite difference analysis of the transient temperature profile within a fuel element of the GHARR-1. A mathematical model of the transient heat distribution within the fuel element and related shutdown heat generation rates was developed [18]. The work utilized the transient temperature profile within the fuel pin of the GHARR-1 solved analytically using Bessel Functions by Adjei et al., [15] and shutdown heat generation rates (residual fission power and fission product decay power) after reactor shutdown due to a reactivity insertion accident estimated by Annafi et al. The residual fission power and fission product decay power was used as the heat source and the steady state temperature resembled the initial temperature before shutdown. A finite difference scheme for the discretization by implicit method was used for analysing the temperature variation and heat generation. MATLAB was utilized to determine the temperature distributions within the fuel element on the developed solution algorithms. A steady state temperature of approximately 341.3 K with a 2 % deviation from that reported in the GHARR-1 Safety Analysis report was obtained from the simulations. An approximate average temperature of 444 K lower than the melting point (913 K) the Aluminium cladding under transient conditions was obtained. The GHARR-1 fuel element was observed to be stable and thus there would be no release of radioactivity in the coolant during accident conditions [18]. CFD tools available in STARCCM+ will be

University of Ghana http://ugspace.ug.edu.gh

used for the analysis of the temperature profile, pressure, mass flow rate and turbulent intensity in 18 fuel pins under normal operation in this work.

S. Mohammed et al., investigated heat transfer and distribution in the GHARR-1 core using Star-CCM+ CFD code. A single fuel rod with 21 axial segments was modelled and hypothetically assumed to represent the core. The 3D-CAD parametric solid modeller embedded in the code was used to design the geometry which was then discretized by polyhedral, prism layer and surface remesher meshing models. Operating conditions of the GHARR-1set as the boundary conditions for the simulation. Heat flux for each axial segment was computed from power peaking factors obtained from Ampomah- Amoako et al [12] and surface area. The heat fluxes were applied at the wall of the flow channel. Mass flow and pressure were specified as the inlet and outlet boundary conditions respectively. The turbulent kinetic energy and dissipation rate were solved using a standard k-ε turbulent model. Experimental data from the GHARR-1 was used to validate the results of the simulation which were found to be fairly in agreement [19]. The geometry of the present work is designed to simulate heat transfer and distribution of 18 fuel pins in the first two concentric rings of the GHARR-1 core therefore a comprehensive and detailed analysis is postulated consistent with the available computational resources. Computations of hottest and average channels of the core were based on a single fuel pin in the previous work. The present work provides a more accurate representation of the hottest channel and envisages an in depth analysis of heat transfer and distribution due to the fact that all the fuel rods in the actual geometry are analysed. The present work will therefore provide sufficient knowledge to enable future analysis of heat transfer and distribution in all 344 pins of the reactor core.

H. Omar et al., performed thermal hydraulics analysis of the Syrian MNSR using Relap 5 Mode3.2/ code. The study entailed simulation of the complete MNSR system using a RELAP model. Periodic reactivity transients and reactivity insertion accidents were simulated under conditions of natural circulation. Core inlet and outlet temperature, flow velocity under nominal operation were calculated with measurements indicating the correct modelling of reactor core with its complicated geometry. The time development of the predicted reactor

University of Ghana http://ugspace.ug.edu.gh

Power, core inlet and outlet coolant temperature was observed to closely follow the measured data for the reactivity insertion. The maximum clad temperature was below the condition of onset of sub-cooled boiling due to the high negative reactivity feedback of moderator temperature under insertion of total available excess reactivity. The RELAP5 model for Syrian MNSR was therefore shown to be an appropriate model for the simulation. The predictions by the model were validated by comparison with experimental data and observed to correlate. Some adaptations were applied to achieve the best representation of MNSR components consistent with the features available in the one-dimensional RELAP5 code [20]. The present work will employ STARCCM+ 3-dimensional Computational Fluid Dynamics (CFD) code for the analysis of heat transfer and distribution in the core. Application of the code in geometry design is only limited by available computational resources. An 18 pin reactor core geometry will be used in this work. Characteristics of the thermal behaviour due to loss of flow will also be investigated by simulation at low coolant mass flow rate

An experimental testing of coolant flow rate and velocity in the core of Nigeria Research Reactor-1 was performed by S.A. Agbo et al., The study was aimed at safety assessment of reactor thermal hydraulic parameters in a bid to improve model predictions. Experiments to monitor core mass flow rate, coolant velocity, mass flux, density and Reynolds number at different power levels were conducted in a bid to cater for the absence of an installed device for measuring core mass flow rate in the NIRR-1. The heat balance utilized measurements of water inlet and outlet temperature to determine the mass flow rate through the core. The experiments confirmed the efficiency of natural circulation for heat removal in the reactor core [21]. The present work entails analysis of heat transfer and distribution at varying power and coolant mass flow rate using STARCCM+ CFD code.

University of Ghana http://ugspace.ug.edu.gh

2.2 Operational Limits and Conditions

2.2.1 Specifications for Fuel Parameters

(1) Enrichment 90.2 % U-235

(2) U-235 loading per pin 2.88 g

(3) Meat alloy UAl_4 in Al

(4) Clad alloy Type 303-1 Al alloy

(5) Dimension of pin 5.5 mm × 248 mm

(6) Clad thickness 0.6 mm

2.2.2 Reactor Core Specifications

(1) Maximum number of fuel elements is 344.

(2) Minimum number of dummy fuel elements is 6.

(3) Minimum number of fuel elements is 343.

(4) Maximum number of dummy fuel elements is 7.

(5) Core geometry is cylindrical and fixed.

(6) Reflectors are beryllium.

(7) Annulus reflector is 102 mm thick.

(8) Bottom reflector is 50 mm thick.

(9) Top reflector is initially water.

(10) Top Be reflector is 0 to 109.5 mm thick.

(11) Reactivity regulators up to 4, as required.

(12) Operating power level is 30 kW nominal [3]

University of Ghana http://ugspace.ug.edu.gh

2.3. Heat Removal and Transfer in MNSR

2.3.1 Heat Generation in the fuel meat

Thermal energy released in nuclear reactors is due to the fission process and at a much smaller degree to the non-fission neutron capture in the fuel, moderator, coolant and structural material. The smallest integral fuel bearing component of a nuclear reactor is the fuel element. Heat generated by fission consists almost entirely of fission fragments and beta particles and is deposited directly in the fuel material. This can be represented mathematically by the following equation:

$$\dot{Q} = GN\sigma_f \phi V_f \qquad (1.00)$$

Where

$\dot{Q}$ - Heat generation rate (W/sec)

G- Energy produced per fission (W/fission)

N- Number of fissionable nuclei per unit volume (atoms/cm^3)

σ_f - Microscopic fission cross section of the fuel (cm^2)

ϕ - Neutron flux (n/cm^{2}sec)

V_f - Volume of the fuel (cm^3) [22]

Heat transfer within the fuel pellet is described by the steady state Fourier equation. For 3-dimensional flow in the radial direction:

$$q'' = -k\frac{dT}{dr} = -k\nabla T \qquad (1.01)$$

Where;

q'' - Heat flux (heat transferred per unit area (w/m^2)

k- Thermal conductivity of the fuel pellet (w/m.K)

University of Ghana http://ugspace.ug.edu.gh

$\frac{dT}{dr}$-Temperature gradient (K/m)

The steady state heat balance can thus be written as:

$$\nabla^2 T + \frac{q'''}{k} = \rho C_P \frac{\partial T}{\partial t} \qquad (1.02)$$

Where:

T- Temperature (K)

q''' -energy generation per unit volume of the fuel material.

k- Thermal conductivity of the fuel pellet (w/m.K)

ρ- Material density

c_p -Heat capacity of the pellet

$\frac{dT}{dr}$- Temperature gradient (K/m) [8]

2.3.2 Heat Transfer to the Fuel Clad

The heat deposited in the fuel is transferred by conduction through the fuel across the boundary between the fuel and cladding and through the cladding to the cladding surface [22]. A schematic diagram of a fuel channel with a single rod is shown in fig 2.0 below.

University of Ghana http://ugspace.ug.edu.gh

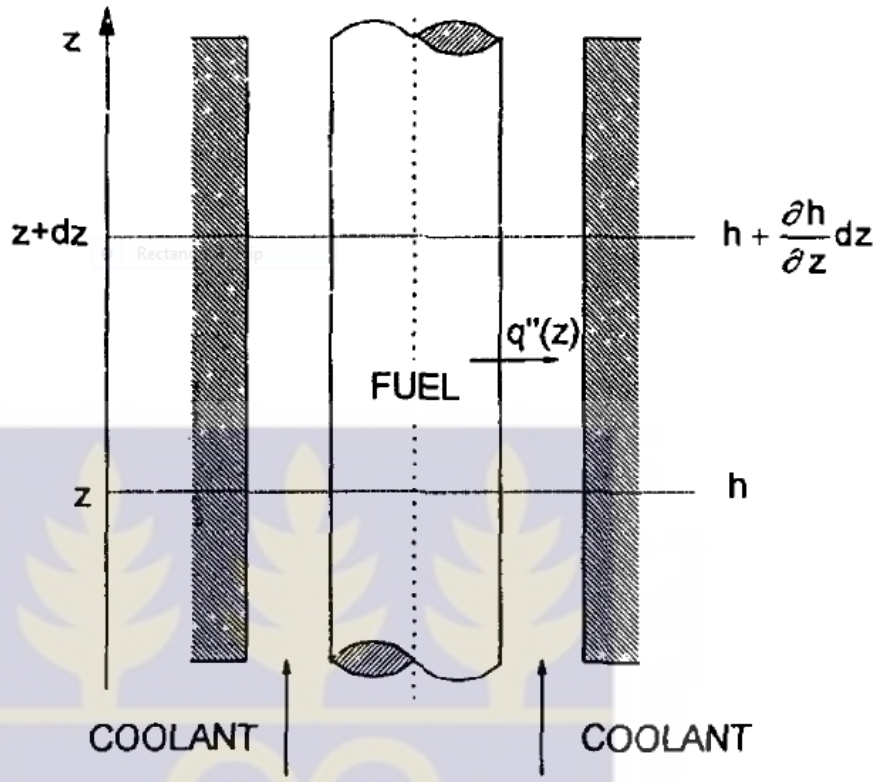

Figure 2.1: Fuel Channel with a Single Rod [23]

Heat conduction in the cladding is given by:

$$\frac{1}{r} k_c \frac{\partial}{\partial r}\left(r \frac{\partial t}{\partial r} \right) = \frac{\partial}{\partial \tau}(\rho_c c_c t) \qquad (1.03)$$

Where:

r- Radius of the fuel pellet

k_c - Conductivity of the cladding (w/m.K)

τ - Time (sec)

ρ_c -Specific mass of the cladding (kg/m^3)

c_c - Specific Heat (J/kg)

t- Temperature of the clad (K)

h- Specific Enthalpy (KJ/kg)

University of Ghana http://ugspace.ug.edu.gh

Heat convection at the cladding surface is given by:

$$-k_c\left(\frac{\partial t_c}{\partial r}\right)=h_c\left(t_c(r_c)-t\right) \quad (1.04)$$

Where:

h_c - Convective heat transfer Coefficient (W/m^2K)

$t_c(r_c)$ - Temperature of cladding outer surface (K)

t- Coolant Temperature (K)

r_c - Radius of the fuel element (m)

Heat Transfer at the fuel-cladding interface is given by:

$$q^{"}=h_g(t_f(r_c)-t_c(r_c) \quad (1.05)$$

Where:

h_g - Gap conductance (W/m^2K)

$t_f(r_c)$ - Temperature at the surface of the fuel (K)

$t_c(r_c)$ - Temperature at the inner surface of the cladding (K) [23]

2.3.3 Natural Convection

Natural convection occurs as a result of buoyancy forces within the fluid influencing the motion of the fluid [24]. Buoyancy occurs as a result of thermally induced density changes producing a fluid density gradient and a proportional body force [24, 25]. The fluid surrounding the heat source is heated and becomes less dense. The heated fluid rises to the surface and is replaced by the surrounding cooler fluid which in turn is heated repeating the same process. Consequently a convection current is formed as a result of this process [26]. Natural convection is responsible for drawing water through the inlet orifice in the GHARR-1. The water is drawn through the channels within the fuel elements and exits through the core outlet orifice [3].

Considering ρ_∞ as the density of the "undisturbed" cold fluid and ρ as the density of the warmer fluid, the buoyancy force per unit volume *F* of fluid is given by:

$$F=(\rho_\infty-\rho)g \quad (1.06)$$

University of Ghana http://ugspace.ug.edu.gh

Where:

g - Acceleration due to gravity

The density varies with temperature as expressed by the following relation:

$$\rho_{\infty} = \rho(1+\beta\Delta T)g \qquad (1.07)$$

Where:

β - Volumetric thermal expansion coefficient

ΔT - Temperature difference between the two fluid regions.

Substituting ρ_{∞} from equation into equation yields the buoyancy force per unit volume given as:

$$F = \rho g\beta\Delta T \qquad (1.08)$$

The ratio of buoyancy forces to the square of viscous forces in the fluid is described by Grashof's number.

$$Gr = \frac{\rho^2 g\beta\Delta TL^3}{\mu^2} \qquad (1.09)$$

Where:

L - Characteristic length of coolant channel

μ - Viscosity of the fluid

The buoyancy forces are large compared to the viscous forces at high Gr numbers thus the fluid particles are held together and therefore convection can occur.

The ratio of thermal energy liberated by buoyancy to the energy dissipated by heat conduction and viscous drag under natural convection can also be expressed by the Rayleigh Number.

$$Ra = Gr\,\mathrm{Pr} = \frac{g\beta\Delta TL^3}{\nu\alpha} \qquad (1.10)$$

Where:

Pr- Prandtl number

University of Ghana http://ugspace.ug.edu.gh

v - Coolant velocity

α - Thermal diffusivity [24]

2.3.4 Heat flux Profile

The heat flux is the heat transfer rate per unit surface area. While the heat flux can be referenced to any surface, in reactors the heat flux is most often referenced to the outer clad surface, i.e. the clad/coolant interface [27]. Figure 2.1 below shows the heat transfer geometry of a cylindrical fuel rod.

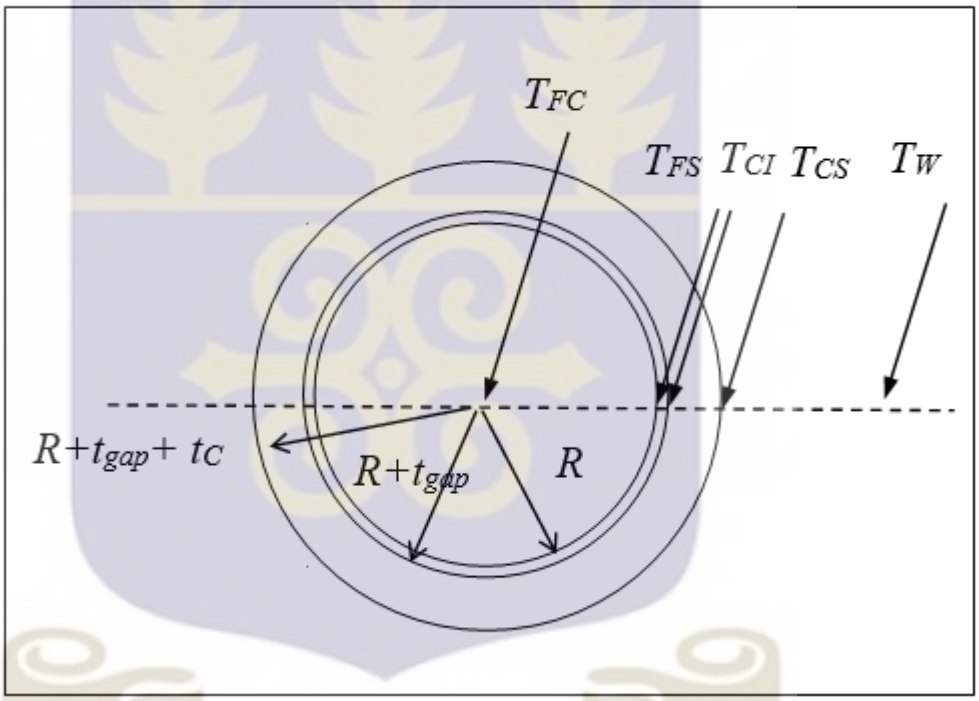

Figure 2.2: Fuel Rod Heat Transfer Geometry [28]

Radial heat flux distribution considers the heat flux from the center of the core out to the edges and axial heat flux distribution looks at flux from the bottom to the top of the core [29]. Heat is generated in the fuel pellet radius R and flows radially through the fuel, the pellet-cladding gap, and the cladding itself to reach the coolant. The axial temperature variation is relatively small and often neglected due to the small thermal gradient compared to the thermal gradient in the radial direction. This heat flux flows from the

University of Ghana http://ugspace.ug.edu.gh

fuel through the fuel-cladding gap then through the cladding and finally into the coolant. Heat transfer through the cladding occurs by conduction. Although heat transfer through the gap occurs through a gas, no flow or convective effects exist. As a result the process can be thought of as one of conduction with $\kappa_{gap} = h_{gap} t_{gap}$ where t_{gap} is the gap thickness and h_{gap} the convective heat transfer coefficient in the gap. The temperature drop through these two hollow cylinders is obtained by solving the heat transfer equations for the cladding which yield equations 1.11 and 1.12 respectively.

$$T_{FS} - T_{Cl} = q' \frac{\ln[(R + t_{gap}) / R]}{2\pi k_{gap}} \tag{1.11}$$

$$T_{Cl} - T_{CS} = q' \frac{\ln[(R + t_{gap} + t_C) / (R + t_{gap})]}{2\pi k_C} \tag{1.12}$$

Where:

T_{FS} - Fuel pellet surface Temperature (K)

T_{Cl} - Cladding inner radius Temperature (K)

T_{CS} - Cladding outer radius Temperature (K)

T_C - Cladding wall thickness Temperature (K)

T_W - Bulk Coolant Temperature (K) [29]

2.3.5 Power Peaking Factor (PPF)

The power peaking factor is defined as the highest local power density (LPD) divided by the average power density in the core [30]. Power peaking factors are established to account for power variations due to non-ideal geometries and/or uncertainties due to manufacturing tolerances and physical changes during operation [27]. The total power peaking factor is related to the non-homogenous spatial distribution of the heat flux over the core. This distribution determines that in certain spots of the core the local heat flux is

University of Ghana http://ugspace.ug.edu.gh

higher than the average value. For Thermalhydraulic calculations a cosine profile with a maximum power peaking factor value of 3 is conservatively adopted [31]. The GHARR-1 design criteria PPF<4 [3].

- The average heat flux $\left(q''_{Av}\right)$ is calculated as the power removed by the cooling system divided by the total heat transfer area.
- The maximum operational heat flux $\left(q''_{Max}\right)$ is obtained from the product of the average heat flux and the power peaking factor (PPF) [31].

2.4 Safety Considerations for Thermal Hydraulic Analysis of a Nuclear Reactor core:

2.4.1 Failure of Heat Removal and Consequences

S. Adu et al., investigated the core behaviour of the GHARR-1 MNSR during loss of flow with best estimate code RELAP 5/ MOD3.2. Partial and total blockage of the coolant to the reactor core transients was performed in a bid to study the behaviour of the reactor core. Boiling was observed to occur in the blocked channels leading to an increase in coolant and clad temperatures in the case of partial coolant blockage. However, the reactor gradually returned to a safe steady state due to unperturbed coolant flow in adjacent channels. Cladding and coolant temperatures were observed to be below the melting point of the structural material. In the case of total blockage the calculations indicated unsafe behaviour of the reactor. The study concluded that natural circulation is capable of cooling the reactor at 35% blockage without producing any significant threat to the fuel material integrity [32].

S. Adu et al., propound that due to the upward flow design of the GHARR-1 core configuration the probability of fuel swelling to block the flow channel is much higher than that of material falling into the pool to block the flow channel. Conversely, the latter can occur as a result of some object un-intentionally left in the flow channel during maintenance work. Nonetheless, since the reactor liquid flow is laminar and there are no external pumps, dragging material into the core is almost impossible [33].

University of Ghana http://ugspace.ug.edu.gh

2.4.2 Safety Design and Operational Limits to be observed

2.4.2.1 Closed tank-in-pool type design structure

This type of reactor design prevents anything from being dropped into the core. From a radiation protection perspective, the closed tank-in-pool reactor can prevent fission and activated gas from escaping into the reactor hall. The level of reactor water is the same as that of the pool water. The reactor water and pool water are separated from each other. Because of the geometrical arrangement, even if the pool water is lost, the reactor water and geometric arrangement still provide adequate shielding for the reactor hall against the radiation from the shutdown reactor [3].

2.4.2.2 Adaptation of natural circulation for cooling

The reactor operates by natural convection to remove heat from the core. Differences in fluid density and body force (gravity) force the hot fluid to move upwards and cooler fluid to move down in the large pool establishing a circulation pattern driven by buoyancy [34].

The water in the reactor is not pressurised and it relies upon natural convection. The problems of de-pressurisation or coolant flow pump failure are not posed. The reactor core is immersed in a large reactor vessel containing deionised water, which possesses a considerable heat capacity. Even under accident conditions, removal of heat is by natural circulation to this large heat sink [3].

2.4.2.3 Insufficient circulation

Due to the small size of the core, the distance from the inlet orifice to the outlet orifice is small. The water, after being heated in the core goes out through the upper part of the core. Part of the water does not get sufficiently cooled before it sinks down, resulting in part of outlet water being carried back into the core due to siphoning effect. This direct re-circulation of the part of hot water causes a rise of the inlet water temperature.

University of Ghana http://ugspace.ug.edu.gh

This phenomenon is referred to as insufficient circulation. It accelerates the rise in coolant temperature in the core and shortens the function time of the temperature effect. Therefore it is impossible to cause the inlet water temperature to rise in such a short time by heating the core only, but by the coupling action between the inlet and the outlet coolant. Consequently this offers some benefit to the reactor safety.

2.4.2.4 Use of U-Al alloy as the fuel meat

U-Al alloy possesses high thermal conductivity: The meat is in close contact to the cladding, providing a small contact resistance.

2.4.2.5 Low linear power density of fuel element of about 3.8 W/cm.

Due to the low power density the centre temperature of the meat is almost the same as cladding temperature when operating at the same reactor power. The temperature drop across the cladding is about $1^{o}C$ [35].

2.4.2.6 Negative feedback effect

This occurs when the temperature difference between the inlet and outlet coolant of MNSR increases; the buoyancy force and circulating head will increase to make the flow velocity high, which in turn will limit the rise in temperature and the consequent increase in power.

2.4.2.7 Limited excess reactivity and reactivity feedback characteristics

Any significant deterioration in heat removal capability will eventually result in an automatic decrease in reactor power to match up with the new heat removal capacity [3].

2.4.3 Significance of the Research in Monitoring Safety Design and Operational Limits

- The present work will provide in depth understanding of the behaviour of operational Thermalhydraulic parameters of the GHARR-1 and allow the development of improved analytical models contributing to safety.

University of Ghana http://ugspace.ug.edu.gh

- The analysis performed in this work will provide sufficient evidence for the safety of the GHARR-1 MNSR design as well as its operational ability to keep within its thermal safety limits in compliance with regulatory requirements.
- The application of STAR-CCM+ CFD code in this work will enable modelling of the actual specifications of the GHARR-1 core configuration which in turn will provide accurate and reliable prediction of performance of the GHARR-1 under normal and accident conditions.
- The study will provide detailed information on the behaviour of the temperature field in the GHARR-1 core and coolant which form some of the key concerns in reactor operations and safety.
- Thermalhydraulic studies performed in this work will improve the existing knowledge on the local temperature and flow fields around fuel geometry and in internal components of the GHARR-1.

2.4.4 Safety Related Thermalhydraulic Parameters

2.4.4.1 Departure from Nucleate Boiling Ratio (DNBR)

The boiling crisis under subcooled flow boiling conditions is referred to as the departure from nucleate boiling (DNB). The heat flux at which the boiling crisis occurs is called critical heat flux (CHF) [36]. The parameter most used to evaluate margin to failure by boiling crisis is the critical heat flux ratio (CHFR), or departure from nucleate boiling ratio (DNBR). This is the ratio of critical heat flux to the most limiting heat flux condition in the reactor [22].

The design criteria of thermal-hydraulic design requires that the burnout ratio or Departure from Nucleate Boiling Ratio (DNBR) should be larger than the calculated burnout heat flux i.e. DNBR > 2.5. Under normal operational condition for the GHARR-1 at power of 30 kW, the maximum temperature is about 70^{o}C, much lower than the melting point of U-Al alloy, which has a melting point temperature greater than 640^{o}C [3].

University of Ghana http://ugspace.ug.edu.gh

2.4.4.2 Minimum Departure from Nucleate Boiling Ratio (MDNBR)

The performance metric for DNB is the MDNBR which is the minimum ratio of the Critical Heat flux to the actual heat flux found in the core [37]. For transient calculations, it was found out that the reactor power increased from zero to 76 kW in about 300s for the prototype MNSR. The maximum temperature on the outer surface of the cladding was 91.2^{o}C, while the saturation temperature of the reactor water was about 113^{o}C. Therefore, it is impossible for boiling to occur and there could not be any boiling crisis within the reactor. Under this transient condition, the heat flux of the fuel elements for burnout was more than 2.5 times that at the rated power. Therefore, the minimum burnout ratio MDNBR is at least greater than 2.5 and this fulfils the requirement of thermal-hydraulic design criteria [3].

2.5 STAR-CCM+ Simulation

2.5.1 Background

STAR-CCM+ is a mathematical idealisation (representation) of real materials such as solids, fluids and gases. Continuum mechanics is concerned with the behaviour of such representations. It is based on laws of conservation (of mass, energy, momentum, moment of momentum and entropy), and is aided by a mathematical apparatus specifically developed for it [38].

2.5.2 Principle of Operation

STAR-CCM+ is based on numerical solution of equations governing fluid flow by the finite volume method. This entails transforming the governing equations into a system of (in general non-linear) algebraic equations, whose subsets approximate each conservation equation [38]. Time, space and equations relating values of dependent variables are treated as basic unknowns at a finite number of locations (grid-points) in the calculation domain. Continuous information contained in the exact solution of differential equations is replaced with discrete values for the distribution of dependent variables. This process is

University of Ghana http://ugspace.ug.edu.gh

called discretization and the algebraic equations involving unknown values of the dependent variables at each grid point are referred to as discretization equations.

Time discretization entails subdivision of a given time interval into a number of smaller subintervals or time steps. Space discretization consists of defining a numerical mesh consisting of a finite number of computational points, thus replacing the continuous functions by their values at those points. Replacement of individual terms in the governing equations by algebraic expressions connecting nodal values on a numerical mesh is called equation discretization [38]. An illustration of the discretization process is shown in on the diagram below.

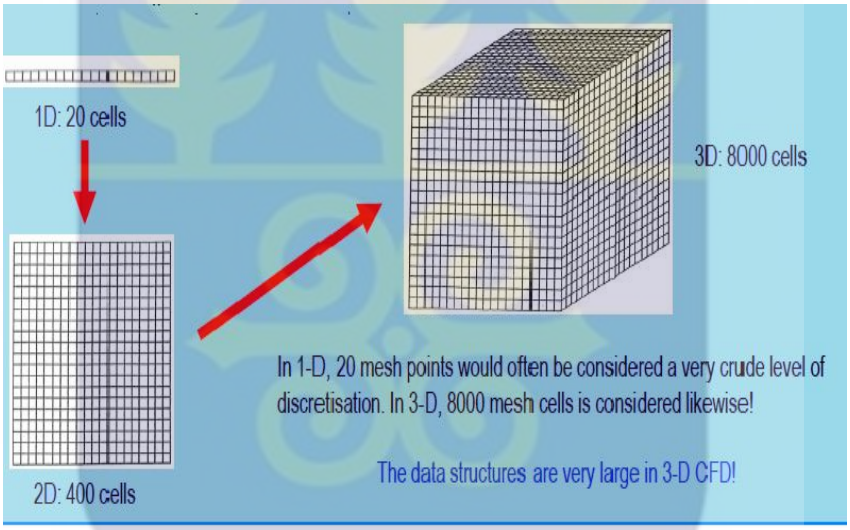

Figure 2.3: Illustration of the finite volume method [39]

STAR-CCM+ is inherently a computational fluid dynamics (CFD) code hence it comprises three main elements: (i) a pre-processor, (ii) a solver and (iii) a post-processor. Pre-processing entails defining the problem, geometry generation with the aid of inbuilt geometry modeller together with facilities for importation of external computer aided design (CAD) models, mesh generation and physics set-up.

Solvers are mathematical software libraries that take the generic form of the problem and calculate the solution. A discretized version of the transport equations is solved for each cell in a mesh when the solver is run. Velocity and pressure solvers apply the Semi

University of Ghana http://ugspace.ug.edu.gh

Implicit Method for Pressure Linked Equations (SIMPLE) algorithm. The discretized continuity equation takes the form of a pressure correction equation and estimated values of its solution are placed at all grid points in a mesh. Tentative values of the coefficients in the discretization equation are then calculated and the equation is discretized into a set of linear algebraic equations. The equations are solved to get the new values of velocity and pressure which are reused to calculate values of the coefficients of the discretization equation. The process is repeated until further repetitions (iterations) cease to produce any significant changes in the values of velocity and pressure. The final unchanging state is called the convergence of the iterations [40].

Energy solvers compute the conservation of energy within each control volume or cell in the mesh. The solver similarly proceeds from an initial guess of the energy distribution in each cell and performs a series of iteration to obtain a converged solution of discretized algebraic equations for the transport and distribution of energy in the domain. The k-ε turbulent solver computes the solution of transport equations for two scalar properties of the turbulence. It solves k equation which is a model for the turbulent kinetic energy and the ε-equation which is a model for the dissipation rate of turbulent kinetic energy in the domain. The k- ω solver computes the solution of two convective transport equations namely the turbulent kinetic energy (k) and its specific dissipation rate (ω) in the computational domain.

Data generated by the solver is post processed using various data visualization tools. The Plots node, which has a pop-up menu, is the object manager for all monitor plots and XY plots that have been created in the simulation. It exists even when empty to allow creation of the first plot, but will typically contain a Residuals plot, which is created automatically once you start iterating. The plotting features in STAR-CCM+ allow you to create three kinds of two-dimensional plots:

- **Monitor plots**

Display data from the simulation as it steps through the solution in two varieties namely monitor plots based on various monitored quantities (scalar and vector) and residual plots. The residual in each cell represents the degree to which the discretized equation is

University of Ghana http://ugspace.ug.edu.gh

satisfied. When the solver is run, a discretized version of the transport equations is solved for each cell in the mesh. Residual monitors keep a record of this global quantity for each of the transport equations solved in the continua within the simulation. The residual plot is a monitor plot that is automatically created from the active residual monitors on semi-log axes when iterating starts. All active residuals are displayed in the residual plot by default.

- **XY plots**

Based on the solution data from the simulation and/or simulation data.

- **Histogram plots**

Display data typically for particles [41].

2.6 Governing Equations

Essentially, STAR-CCM+ is a flow solver for the governing integral conservation equations of mass, momentum and energy [42]. The governing equations of fluid flow are mathematical statements of the conservation laws of physics:

- The mass of a fluid is conserved
- The rate of change of momentum equals the sum of the forces on a fluid particle (Newton's second law)
- The rate of change of energy is equal to the sum of the rate of heat addition to and the rate of work done on a fluid particle (first law of thermodynamics) [43].

The equations are stated as follows:

2.6.1 Continuity Equation

$$\frac{\partial \rho}{\partial t} + div(\rho u) = 0 \qquad (1.13)$$

Where:

$\frac{\partial \rho}{\partial t}$ – Change in density with time.

University of Ghana http://ugspace.ug.edu.gh

$div(\rho u)$– Convective term, describes net flow of mass out of the element across its boundaries.

2.6.2 X- Component of momentum equation

$$\rho \frac{Du}{Dt} = \frac{\partial(-p + \tau_{xx})}{\partial x} + \frac{\partial \tau_{xx}}{\partial y} + \frac{\partial \tau_{zx}}{\partial y} + S_{Mx} \quad (1.14)$$

Where:

ρ - Density

u- x-component of velocity

p- Pressure

τ - Viscous Stresses

1st three terms at the RHS- total force in the *x*-direction on the element due to surface stresses.

S_{Mx}- Source of *x*-momentum per unit volume per unit time

2.6.3 Y- Component of momentum equation

$$\rho \frac{Dv}{Dt} = \frac{\partial \tau_{xy}}{\partial x} + \frac{\partial(-p + \tau_{yy})}{\partial y} + \frac{\partial \tau_{zy}}{\partial z} + S_{My} \quad (1.15)$$

Where:

ρ - Density

v- y- component of velocity

P- Pressure

τ - Viscous Stresses

1st three terms at the RHS- total force in the *y*-direction on the element due to surface stresses

University of Ghana http://ugspace.ug.edu.gh

S_{Mx}- Source of *y*-momentum per unit volume per unit time.

2.6.4 Z- Component of momentum equation

$$\rho\frac{Dw}{Dt}=\frac{\partial\tau_{xz}}{\partial x}+\frac{\partial\tau_{yz}}{\partial y}+\frac{\partial(-p+\tau_{zz})}{\partial z}+S_{Mz} \quad (1.16)$$

Where:

ρ - Density

w- z-component of velocity

P- Pressure

τ - Viscous Stresses

1st three terms at the RHS- total force in the y-direction on the element due to surface stresses

S_{My}- Source of *y*-momentum per unit volume per unit time. The sign associated with the pressure is opposite to that associated with the normal viscous stress, because the usual sign convention takes a tensile stress to be the positive normal stress so that the pressure, which is by definition a compressive normal stress, has a minus sign [43].

2.6.5 Energy Equation (Temperature Based)

$$\rho c\frac{DT}{Dt}=div(kgradT)+\tau_{xx}\frac{\partial u}{\partial x}+\tau_{yx}\frac{\partial u}{\partial y}+\tau_{zx}\frac{\partial u}{\partial z}+\tau_{xy}\frac{\partial v}{\partial x}+\tau_{yy}\frac{\partial v}{\partial x}+\tau_{zy}\frac{\partial v}{\partial z}+\tau_{xz}\frac{\partial w}{\partial x}+\tau_{yz}\frac{\partial w}{\partial y}+\tau_{zz}\frac{\partial w}{\partial z}+S_i$$

Where: (1.16)

ρ - Density

c- Specific heat capacity

k- Thermal conductivity

University of Ghana http://ugspace.ug.edu.gh

T- Temperature

τ - Viscous Stresses

u- x - component of velocity

v- y- component of velocity

w- z-component of velocity

S_i - Source of internal energy per unit volume per unit time.

2.7 Meshing Models

A mesh is a discretized representation of the computational domain, which the physics solvers use to provide a numerical solution. There are different meshing strategies, and each one has its pros and cons, being more suited for one or other applications. The domain will be discretized by the application of surface remesher, polyhedral meshing and prism layer meshing models

2.7.1 Surface Remesher

Remeshes the initial surface to improve the overall quality of an existing surface and optimize it for the volume mesh models. It is used to retriangulate the surface based on a user defined target edge length and can also omit specific surfaces or boundaries preserving the original triangulation from the imported mesh [41].

2.7.2 Polyhedral Meshing Model

The polyhedral meshing model generates a volume mesh which is composed of polyhedral-shaped cells. It is created from the evolution of an automatically inserted underlying tetrahedral mesh by the application of a special dualization scheme. It is numerically more stable, less diffusive and more accurate than an equivalent tetrahedral mesh. Moreover polyhedral mesh contains approximately five times fewer cells than a tetrahedral mesh for a given starting surface [41].

University of Ghana http://ugspace.ug.edu.gh

2.7.3 Prism Layer Mesher

A prism layer is defined in terms of thickness, number of cell layers, size distribution of the layers and the function that is used to generate the distribution. The prism layer mesh model is used in conjunction with a core volume mesh to generate orthogonal prismatic cells next to wall surfaces or boundaries. This layer of cells allows the solver to resolve near wall flow accurately, which is critical in determining flow features such as separation together with forces and heat transfer on walls. Additionally, separation affects pressure drop or drag whose accurate prediction depends on resolving the velocity and temperature gradients normal to the wall.

2.8 Physics Models

A physics model defines how a physical phenomenon in a continuum is represented. Essentially, physics models define the primary variables of the simulation (such as pressure, temperature, and velocity) and the type of mathematical formulation used to generate the solution. In STAR-CCM+ the models have varying levels of functionality and complexity, but their major purpose is to work with solvers to obtain a solution and to help present the information to the user. A typical physics model avails relevant field functions and places initial conditions and reference values in its continuum [42].

2.8.1 K-Epsilon model

The K-epsilon model is one of the most common turbulence models, although it just doesn't perform well in cases of large adverse pressure gradients [44]. It is a two equation model that means, it includes two extra transport equations to represent the turbulent properties of the flow. This allows a two equation model to account for history effects like convection and diffusion of turbulent energy [45].

The Standard K-epsilon model solves the transport equations for turbulent kinetic energy (k) and its dissipation (ε). The turbulent kinetic energy equation is given as;

University of Ghana http://ugspace.ug.edu.gh

$$\frac{\partial}{\partial t}(\rho k)+\frac{\partial}{\partial x_i}(\rho k u_i)=\frac{\partial}{\partial x_j}\left[\left(\mu+\frac{\mu_t}{\sigma_k}\right)\frac{\partial k}{\partial x_j}\right]+P_k+P_b-\rho\varepsilon-Y_M+S_k \quad \textbf{(1.36)}$$

The turbulent dissipation equation is given as;

$$\frac{\partial}{\partial t}(\rho\varepsilon)+\frac{\partial}{\partial x_i}(\rho\varepsilon u_i)=\frac{\partial}{\partial x_j}\left[\left(\mu+\frac{\mu_t}{\sigma_\varepsilon}\right)\frac{\partial \varepsilon}{\partial x_j}\right]+C_{1\varepsilon}\frac{\varepsilon}{k}(P_k+C_{3\varepsilon}P_b)-C_{2\varepsilon}\rho\frac{\varepsilon^2}{k}+S_\varepsilon$$

(1.17)

Where;

$$P_k=-\rho\overline{u_i'u_j'}\frac{\partial u_j}{\partial x_i}$$

(1.18)

u_i Represents the velocity component in corresponding direction

$$P_k=-\mu_t S^2$$

(1.19)

Where S is the modulus of the mean rate of strain tensor and is given in Equation (1.20);

$$S\equiv\sqrt{2S_{ij}S_{i,j}}$$

(1.20)

The effect of buoyancy is defined as;

$$P_b=\beta g_i\frac{\mu_t}{\mathrm{Pr}_t}\frac{\partial T}{\partial x_i} \quad (1.21)$$

Where;

Pr_t - Turbulent Prandtl number for energy and g_i is the component of the gravitational vector in the direction.

University of Ghana http://ugspace.ug.edu.gh

The coefficient of thermal expansion β, is defined as;

$$\beta = -\frac{1}{\rho}\left(\frac{\partial \rho}{\partial T}\right)_P \quad (1.22)$$

Model constants are given as;

$$C_{1\varepsilon} = 1.44, C_{2\varepsilon} = 1.92,\ \sigma_k = 1.0 \text{ and } \sigma_\varepsilon = 1.3$$

$C_{3\varepsilon}$ Depends on the literature reference and is meant to be used only with P_b term.

The turbulent dissipation (ε) is the variable that determines the scale of the turbulence, whereas *k*, determines the energy in the turbulence [45].

K-epsilon model has been shown to be useful for free-shear layer flows with relatively small pressure gradients, accuracy has been shown experimentally to be reduced for flows containing large adverse pressure gradients [46].

2.8.2 Turbulent Boundary Layer

In a flow bounded by a wall, different scales and physical processes are dominant in the inner portion near the wall, and the outer portion approaching the free stream. The flow near a wall is characterized by three layers:

1. The inner layer, or sublayer, where viscous shear dominates
2. The outer layer, or defect layer, where large scale turbulent eddy shear dominates
3. The overlap layer, or log layer, where velocity profiles exhibit a logarithmic variation

University of Ghana http://ugspace.ug.edu.gh

Convection and pressure gradients are assumed negligible in the inner layer consistent with Prandtl and Von Karman who postulated that the important variables determining the mean velocity in the inner layer are the viscosity (μ), density (ρ), wall shear stress (τ_w) and distance from the wall (y). The combination of these variables can be expressed as:

$$U = f(\mu, \rho, \tau_w, y) \tag{1.23}$$

Viscous effects are assumed negligible in the outer layer but the pressure gradient and Convection are included. Mean velocity is thus influenced by the wall shear stress (τ_w), density, boundary layer thickness, pressure gradient, and the distance from the wall. The combination of these variables gives:

$$U = f\left(\tau_w, \rho, \delta, y, \frac{\partial P}{\partial x}\right)$$

Inner and outer layers merge at the log layer which is defined by the logarithmic velocity profile law of the wall as:

$$U^+ = \frac{1}{\kappa}\ln(y^+) + B \tag{1.24}$$

Where:

$\kappa \cong 0.42$, $B \approx 5.0$ are constants [47].

2.8.3 Wall Y+

In wall-attached boundary layers, the normal gradients in some flow variables become large as the wall distance reduces to zero. A large number of mesh points packed close to the wall is required to resolve these gradients thus increasing computational burden in terms of CPU and RAM requirements in the domain. As the wall is approached, turbulent fluctuations are suppressed and viscous effects become important in the region known as the viscous sub-layer.

University of Ghana http://ugspace.ug.edu.gh

In order to overcome the above-mentioned limitations, the wall region is characterized in terms of dimensionless variables with respect to the wall conditions. These dimensionless variables are defined in terms of the wall friction velocity (U_τ) given by the relation:

$$U_\tau = \left(\frac{\tau_w}{\rho}\right)^{\frac{1}{2}} \tag{1.25}$$

Where:

τ_w - Wall shear stress

ρ - Density

The dimensionless velocity (U^+) defined by the logarithmic velocity profile can also be related as:

$$U^+ = \frac{U}{U_\tau} \tag{1.26}$$

The dimensionless wall distance (Y^+) is defined by the relation:

$$Y^+ = \frac{Y\rho U_\tau}{\mu}$$ [48]

Accuracy of a simulation is a function of computation of the flux of dependent variables in the entire domain. The Y^+ enables the capturing of the flux of flow parameters in the wall region and thus optimizes the available mesh cells at the boundary.

University of Ghana http://ugspace.ug.edu.gh

CHAPTER THREE:

METHODOLOGY

This chapter furnishes insight on the procedure undertaken in the study of heat transfer and distribution in the GHARR-1 core together with the experimentation and acquisition of data for validation of the work.

3.1 Experimental

The Ghana Research Reactor 1(GHARR-1) located at the National Nuclear Research Institute (NNRI) of the Ghana Atomic Energy Commission (GAEC) was used to conduct an experiment at different power levels under normal operating conditions. The power was varied from 5- 30kW in equal steps of 5kW and six readings at an interval of 30 minutes were taken for each power level noting Inlet and outlet temperatures measured by two pairs of NiCr-NiAl thermocouples.

At 15kW, a constant neutron flux of 4.68×10^{11}ncm^{-2}s was recorded on the neutron flux monitor despite variation of the control rod position from 129 mm (minimum) to a maximum of 143mm. The average inlet and outlet temperatures were 313.42 K and323.59K respectively. The neutron flux was set to 6.67×10^{11} ncm^{-2}s with a variable control rod position which ranged from 152-169mm for the 20kW power. Five inlet and outlet temperatures were measured at 10 minute intervals and averages of 316.65 K and 327.91 K were obtained respectively. The neutron flux was increased to 8.33×10^{11} ncm^{-2}s and the reactor attained a power of 25kW. The Control rod position was varied from160-182mm to obtain an average measured inlet and outlet temperature of 314.39 K and 328.25 K respectively.

The neutron flux was further increased to 1.0×10^{12} ncm^{-2}s and reactor power of 30kW was attained. Seven inlet and outlet temperatures at a minimum and maximum control rod position of 165-185mm with intervals that ranged between 2mm and 5mm were

University of Ghana http://ugspace.ug.edu.gh

recorded. Computed values for the mean inlet and outlet temperature were 316.32 K and 321.26 K respectively.

A flux lower than 4.68×10^{11} ncm^{-2}s and control rod position greater than 129 mm was employed to obtain inlet and outlet temperatures of 38.5K and 38.75K for a rector power of 5 kW as well as 42.85 K and 46.5 K for 10 kW respectively.

3.2 CFD Model Description

3.2.1 Geometry Modelling

STAR-CCM+ 3D-CAD (3Dimensional-Computer Aided Design) tools were used to generate the model of the geometry used in the research. Dimensions of the model in mm were obtained from an extract of the GHARR-1 core configuration as illustrated in Figure 3.1.

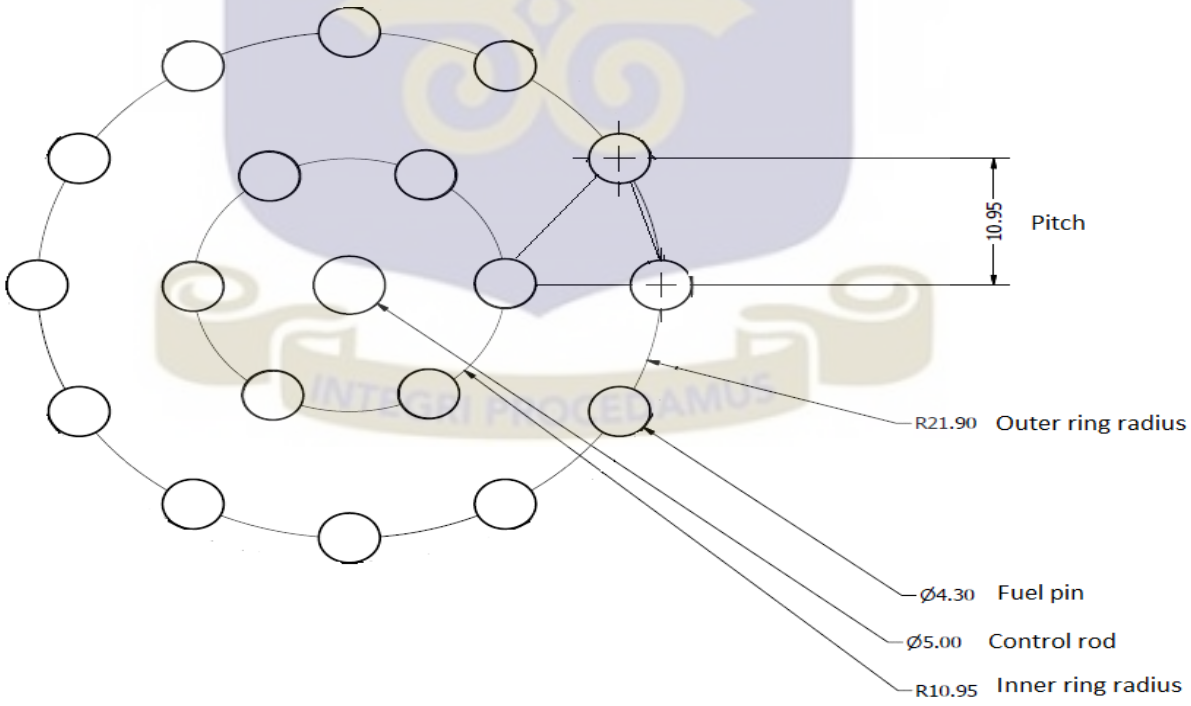

Figure 3.1: Schematic Diagram of the first 2 Concentric Rings of the GHARR-1 Core

University of Ghana http://ugspace.ug.edu.gh

The computational geometry was split into 21 axial segments consistent to the PARET code geometry used by Ampomah- Amoako et al., [12] whose results were used to compute the heat fluxes for the present work. The fuel rods in the outer ring were halved so as to optimize the available computational resources. Schematic diagrams of the plan and transparent view of the 3D geometry are shown in Figures 3.2 and 3.3 respectively. The transparent view shows the actual shape of the axial segments.

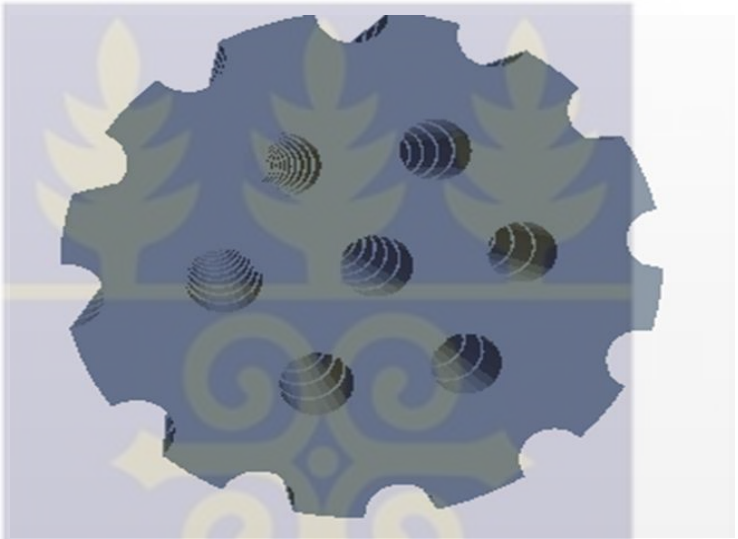

Figure 3.2: Plan View of the Computational Geometry

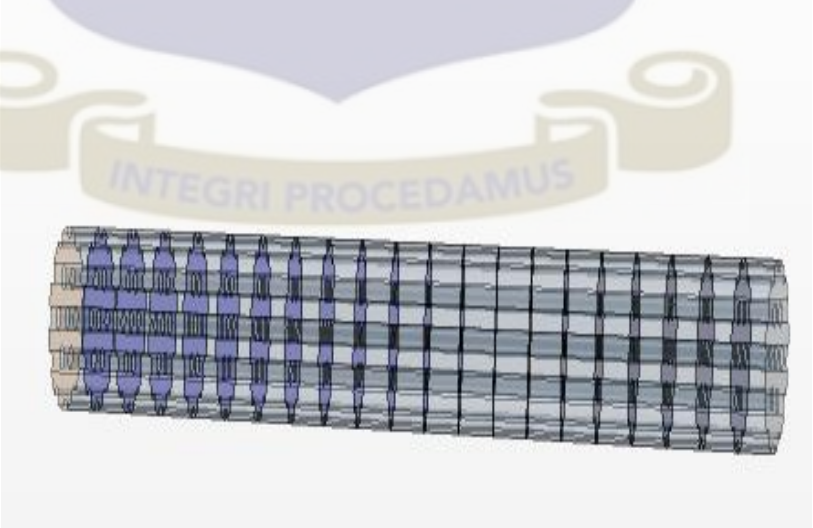

Figure 3.3: Transparent View of the Computational Geometry

University of Ghana http://ugspace.ug.edu.gh

3.2.2 Mesh Generation

Region-Based Meshing was employed for the 21- axial segments of the computational domain. This entailed generating a mesh for subdivisions of all the 18 fuel pins and the central control rod in each axial segment. These components represented the boundaries and continua for each segment thus each segment was defined as a region.

The following meshing models were applied in the mesh generation pipeline:

- surface remesher
- polyhedral mesher
- prism layer mesher

Specifications of the applied meshing models are shown in Table 3.1

Table 3.1: Meshing Specifications

S/No	Mesh Settings	Specification
1	Base Size	1 mm
2	Number of Prism layers	4
3	Number of Mesh Cells	3675839
4	Prism layer Thickness	0.5 mm
5	Near wall Prism layer Thickness	0.01 mm
6	Surface Growth Rate	1.1

Application of the above mentioned specifications generated the mesh represented in Figure 3.4.

University of Ghana http://ugspace.ug.edu.gh

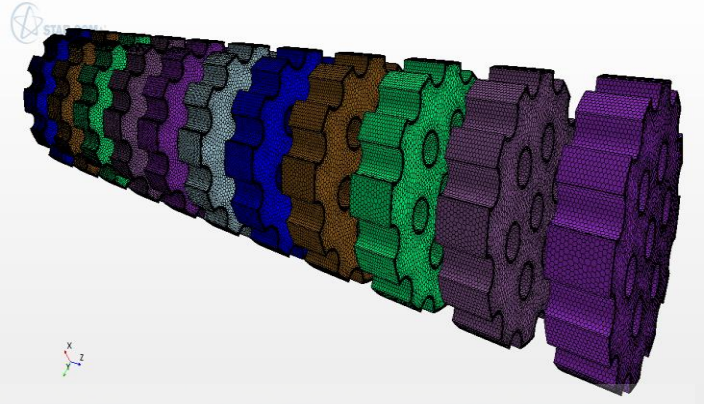

Figure 3.4: Mesh Scene of the Computational Geometry

3.2.3 Physics Modelling

Tables 3.2 and 3.3 display the relevant initial conditions, physics models and boundary conditions employed in the present work.

Table 3.2: Initial Conditions

S/No	Initial Condition	Specification
1	Reference Pressure	1.0 Atm
2	Temperature	288.15K
3	Turbulence Intensity	0.01
4	Velocity	0.1m/s
5	Reference Density	1000kg/cm^3

University of Ghana http://ugspace.ug.edu.gh

Table 3.3: Physics and Boundary Specifications

S/No	Physics Model	Specification
1	Space Model	3-Dimensional
2	Time Model	Steady State
3	Material	Water
4	Energy of State Model	Constant Density
5	Flow Model	Segregated Flow
6	Energy Model	Segregated Fluid Temperature
7	Viscous Regime Model	Turbulent
8	Turbulence Model	K-Epsilon
9	Wall Function	All Y^+ Treatment
10	Convection Scheme	2^{ND} Order Upwind
11	Inlet	Mass Flow
12	Outlet	Pressure
13	Wall Surface	Adiabatic

Initial conditions employed mimicked the actual operating environment of the GHARR-1. These conditions allowed the system to start up and stabilize thus enabling acquisition of simulation data by the code.

A 3-Dimensional space model was selected to enable radial and axial analysis of the geometry. The present work considered a steady state analysis of heat transfer and distribution consistent with the usage of the steady state model. Water at constant density was selected as the coolant to mimic the natural convection cooling employed in the GHARR-1.

The segregated flow model solves the conservation equations for mass, momentum, and energy in series using a pseudo-time-marching approach. The transport of a scalar quantity ϕ in a continuum is represented by the equation below.

University of Ghana http://ugspace.ug.edu.gh

$$\frac{\partial}{\partial t}\iiint_V \rho\phi dV + \iint_S \rho\phi\vec{u}.d\vec{A} = \iint_S \Gamma_\phi \vec{\nabla}.d\vec{A} + \iiint_V S_\phi dV \qquad (3.1)$$

The terms in this equation are transient term and the convective flux on the left side, together with the diffusive flux and the volumetric source on the right side [41].
The segregated fluid temperature model enabled the fluid temperature to vary as heat is transferred at all nodes in the trajectory of the fluid throughout the computational domain.

A turbulent viscous regime was selected to capture the occurrence of turbulence in the coolant flow. Coolant flow in the GHARR-1 is predominantly laminar and transitions to turbulent when there is an increase in power. The turbulence intensity increases on the upper part of the fuel elements due to the fact that the buoyancy force in natural circulation must overcome friction on the surface of the fuel rods. The discretized momentum, continuity and energy equations are solved to capture the effects of laminar flow thus the turbulence model was implemented to solve the turbulent kinetic energy and its dissipation rate.

The standard K-epsilon model solved the transport equations for turbulent kinetic energy (k) and its dissipation (ε) in the geometry. The model was best suited for the characteristic low pressure gradient flow of the GHARR-1.

All Y^+ Treatment was used as the set of mathematical relations for analysing the flux of the flow parameters at the wall. The Y^+ is a dimensionless variable with respect to the wall conditions which enables the capturing of the flux of flow parameters in the wall region and thus optimizes the available mesh cells at the boundary. A non-slip boundary condition was also applied at the wall to ensure that the fluid is retained within the boundary. The fluid takes the velocity of the wall at all fluid- wall boundaries.

The second order upwind convection scheme was selected to minimize numerical errors associated with the calculation of mesh cell gradients and face interpolations used by the discretized transport equations for the movement of the flux of flow parameters in each mesh cell in the computational domain. The second order upwind scheme uses a larger

University of Ghana http://ugspace.ug.edu.gh

stencil size which increases the accuracy of determining cell centers and faces to enable storage and transport of field data within the computational domain.

A mass flow inlet boundary condition was imposed at the inlet such that at each power level a coolant mass flow rate which varied from 0.11-0.15kg/s was imposed. Pressure was imposed at the outlet so as to establish a pressure gradient for coolant flow and the wall surface was considered to be adiabatic.

Thermometric input parameters (temperature, density, viscosity and thermal conductivity) which also served as boundary conditions were computed using the National Institute of Standards and Technology (NIST) online database and presented in Appendix 1.

Residual plots (Appendix III) were used to monitor convergence of flow parameters represented by conservation equations in the domain. The residual indicates the extent at which a conservation equation is solved with each iteration. Convergence is an indicator of overall conservation of flow properties within the entire computational domain.

3.3 Calculation of Power Peaking Factors

GHARR-1 power peaking factors (PPF) were calculated based on the PARET code which divided the hottest and cold fuel pins in the core to a maximum of 21 axial segments. The MCNP code was used to compute the temperature of each segment [12]. The core average temperature was obtained by finding the average of the total core temperature and the power peaking factor of each particular segment was evaluated by dividing its temperature by the core average temperature. The results of the calculation for the 18 fuel pins used in this work were tabulated as shown in Appendix II.

3.4 Calculation of Heat Flux

The tabulated Power Peaking factors were used to compute the heat flux as follows:

University of Ghana http://ugspace.ug.edu.gh

- The Power Peaking factor (F_q) for each segment was divided by the total power peaking factor of all the 21 axial segments for each rod and multiplied by the operating power (P_r) to obtain the power in each fuel rod segment using equation 3.2.

$$P_s = \frac{F_q}{\sum F_q} \times P_r \qquad (3.2)$$

- The Power in each fuel rod segment (P_s) calculated by equation 3.2 was based on the actual GHARR-1 core configuration comprising 344 pins. The segment power for the 18 pin geometry employed in this work was evaluated by direct proportion.
- The surface area (A_s) of each fuel segment was calculated using equation 3.3

$$A_s = 2\pi rh + 2\pi r^2 \qquad (3.3)$$

Where:

r - Segment radius (2.15mm)

h - Segment length (1.095mm)

- The imposed heat flux for each fuel rod segment in the geometry was computed by dividing the segment power by the surface area using equation 3.4

$$\Phi = \frac{P_s}{A_s} \qquad (3.4)$$

- The computed heat fluxes for the 12 rods in the second concentric ring were halved consistent with the geometry modelling.

University of Ghana http://ugspace.ug.edu.gh

CHAPTER FOUR

RESULTS AND DISCUSSIONS

4.1. Introduction

The simulations were ran until convergence by monitoring of residual plots. A simulation was declared converged when oscillations of each residual with each iteration at a given time were observed to be minimal and follow a constant pattern. A typical converged simulation is illustrated in the Figure 4.1.

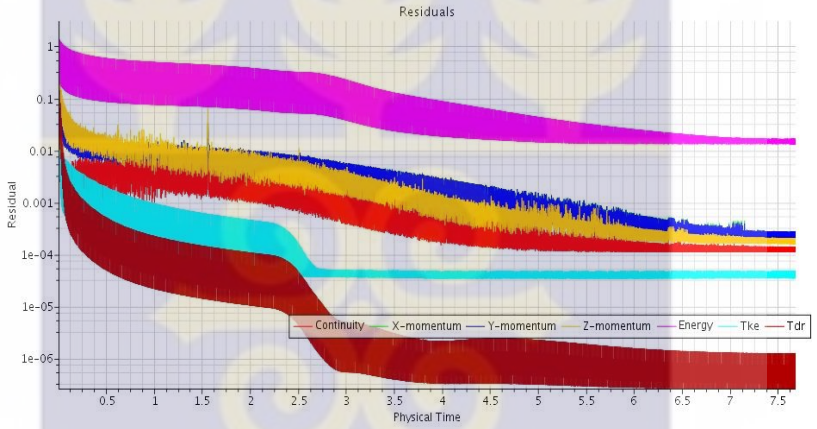

Figure 4.1: Residual Plot of a Converged Simulation

A constrained plane which divided the geometry into flow channels was designed and applied on each converged simulation. The channels resembled triangular pitch distances between individual fuel rods in a bid to analyse heat transfer between them. Flow channels in the first ring were subdivided with respect to the central control rod. Flow channels in the second ring and in the region between the 2 rings where necessary were further subdivided in a bid to enhance accuracy of data acquisition and thus optimize usage of the constrained plane. Temperature, pressure, mass flow rate and turbulent intensity were measured. The code computed the average values of the above mentioned

University of Ghana http://ugspace.ug.edu.gh

flow parameters on the surface of each of the 21 axial segments. Figure 4.1 below shows the constrained plane and the associated flow channels in which the geometry was split into for data acquisition.

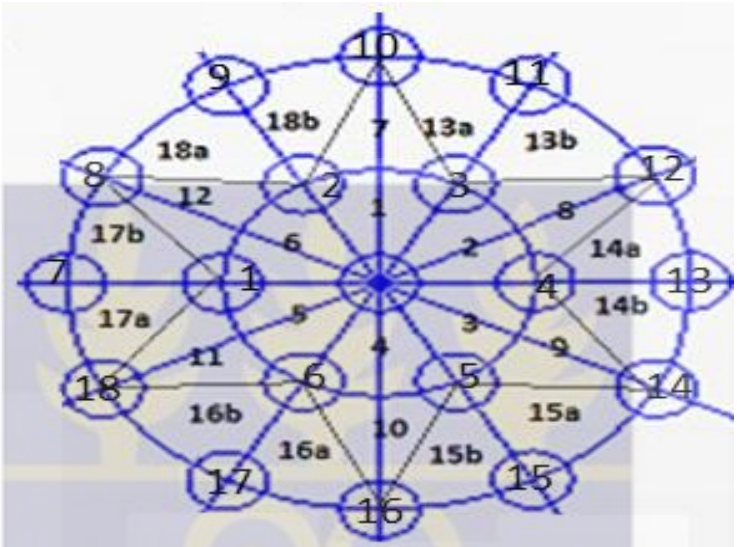

Figure 4.2: Schematic Diagram of the Constrained Plane

The hottest and coldest flow channel at each power rating and coolant mass flow rate were identified by finding the channel with the highest and lowest average temperature. Each segment had a uniform length of 0.0101m. An extra segment length of 0.0099m was added to cover the full length of the geometry which measured 0.2299m in length. Plots of the 4 measured flow parameters against position in meters were generated from the code for each simulation. Comparisons were made between the 2 rings and between the hottest and coldest channels.

University of Ghana http://ugspace.ug.edu.gh

4.2 Analysis of Flow Parameters at Fixed Mass Flow Rate

4.2.1 Flow Parameters analysis at 15kW

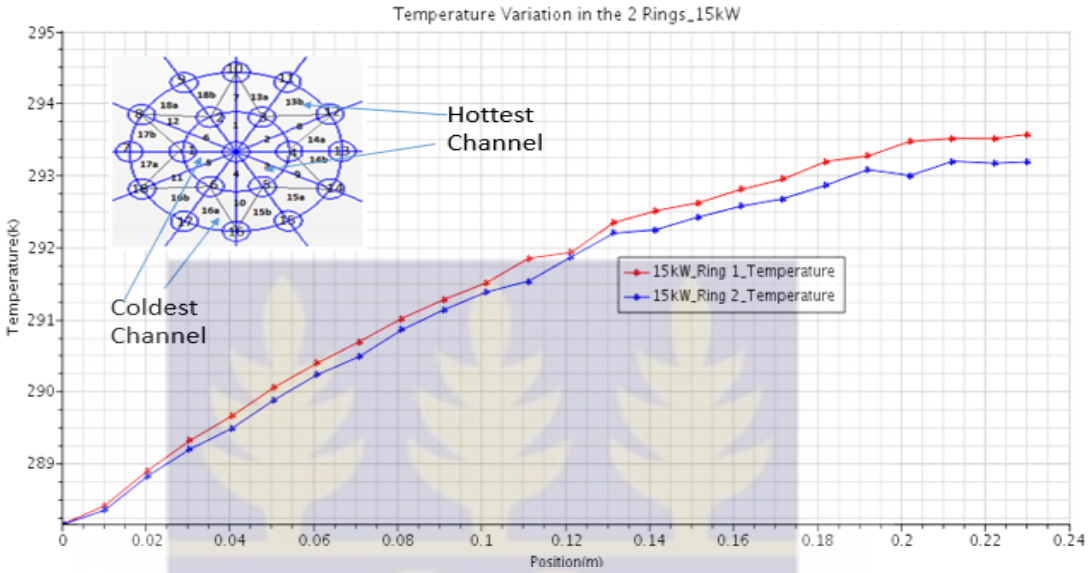

Figure 4.3: Comparison of Temperature in the 2 rings at 15kW and 0.11kg/s

Sectional Average Temperature was observed to increase steadily along the flow channel from the inlet to the outlet and levelling off to a constant value as the coolant exits the domain. The temperature is higher at the upper part of the fuel rods as indicated by the trend. The hottest flow channel in the 1st ring was observed to be in flow channel 3 on the triangular pitch segment bounded by rods 4, 5 and the control rod. The hottest channel in the 2nd ring was observed to be in channel 13b on the triangular pitch bounded by rods 11, 12 and 3. The coldest channel in the 1st ring was observed to be in channel 5 on the triangular pitch bounded by rods 1, 6 and the control rod. Likewise the coldest channel in the 2nd ring was observed to be in channel 16a on the triangular pitch segment bounded by rods 16, 17 and 6.The varying Heat fluxes (Appendix III) imposed on the surfaces of each rod contribute to the heat generated in the system by each rod. The sectional average temperatures were observed to vary slightly at each axial position.

University of Ghana http://ugspace.ug.edu.gh

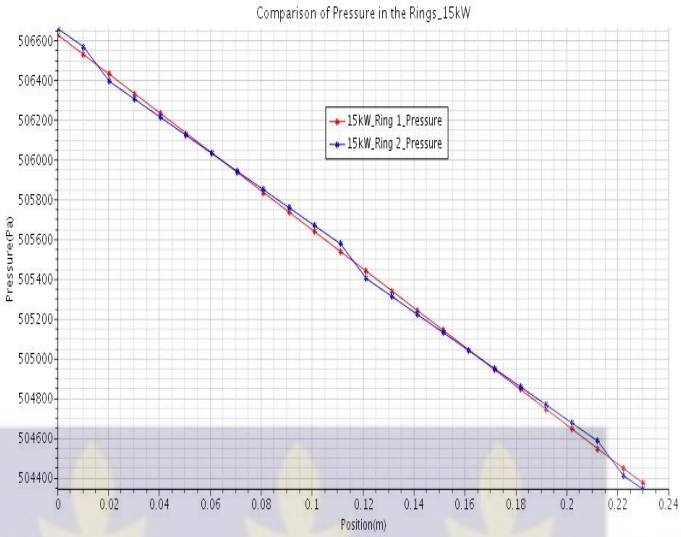

Figure 4.4: Comparison of Pressure in the 2 Rings at 15kW and 0.11kg/s

The temperature gradient in natural circulation is responsible for moving the coolant in the system. Pressure is maximum at the inlet due to the fact that at low temperature the density of the coolant is high. The temperature increases steadily in the domain and consequently the density decreases thus a pressure gradient is set up as the coolant flows from the inlet to the outlet. The minimum pressure at the outlet as a result of low density shows that the temperature of the fuel rods is higher at the top.

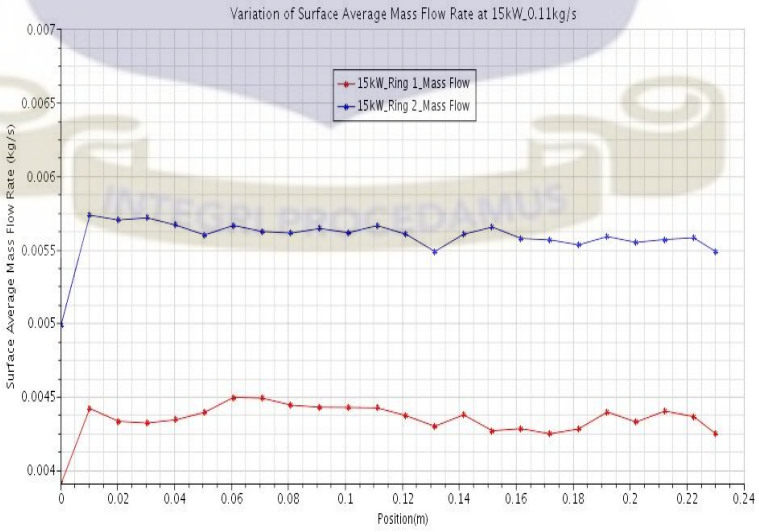

Figure 4.5: Comparison of Mass Flow Rate in the 2 Rings at 15kW and 0.11kg/s

University of Ghana http://ugspace.ug.edu.gh

A mass flow rate of 0.11kg/s was set at the inlet to initialise the system. The mass flow rate was not fixed at the outlet hence as the coolant flows within the domain it establishes a varying mas flow rate depending on temperature variations which influence the temperature gradient responsible for natural convection. The mass flow rate was observed to be higher in the second ring. However there is a slight difference in the values of mass flow rate between the two rings due to the small difference in temperature between them.

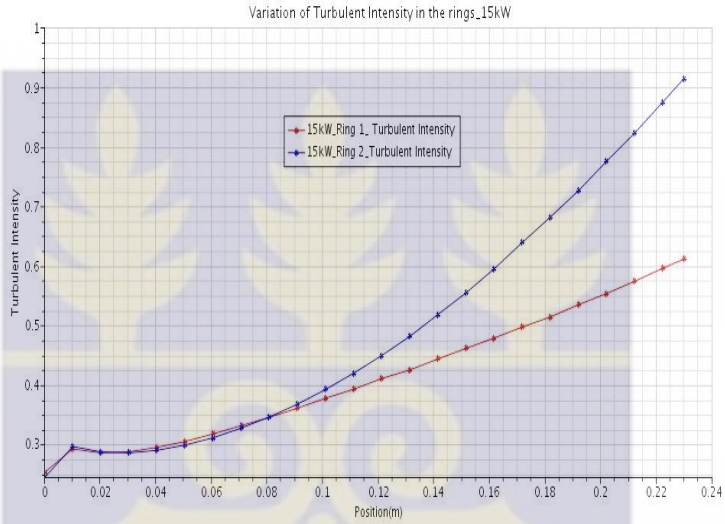

Figure 4.6: Comparison of Turbulent Intensity in the 2 Rings at 15kW and 0.11kg/s

The initial surge observed in the turbulent intensity is due to the fact that the fluid is instantly injected into the domain and as a result the flow will not have fully developed. The turbulence becomes slightly constant as the flow develops and increases. Turbulent intensity peaks at the upper part of the fuel rods consistent with the findings recorded in the Safety Analysis Report as the buoyancy force in natural circulation must overcome friction. The turbulent intensity is higher in the second ring due to the fact that the mass flow rate in ring 2 is slightly higher than in ring 1 as shown in fig 4.4 hence the effect of turbulence is more visible in the second ring.

University of Ghana http://ugspace.ug.edu.gh

4.2.2 Flow Parameters analysis at 30 kW

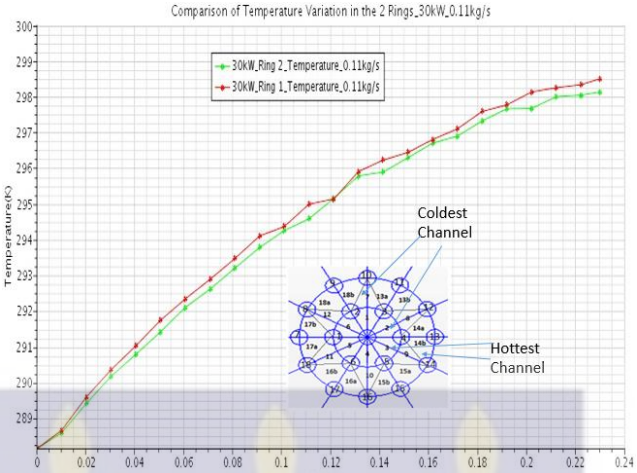

Figure 4.7: Comparison of Temperature in the 2 rings at 30 kW and 0.11 kg/s

The outlet sectional average temperature at 30 kW was observed to be higher than at 15 kW due to the fact that at 30 kW the control rod is raised at higher level thus fission rate and hence the heat generated is higher than at 15 kW. A similar trend as reported at 15 kW was observed. The hottest flow channel in the 1st ring was observed to be in channel 3 on the triangular pitch segment bounded by rods 4, 5 and the control rod. The hottest flow channel in the 2nd ring was observed to be in channel 14b on the triangular pitch bounded by rods 13, 14 and 4. The coldest channel in the 1st ring was observed to be in channel 2 on the triangular pitch bounded by rods 3, 4 and the control rod. The coldest channel in the 2nd ring was observed to be in channel 7 on the triangular pitch segment bounded by rods 2, 3 and 10.

University of Ghana http://ugspace.ug.edu.gh

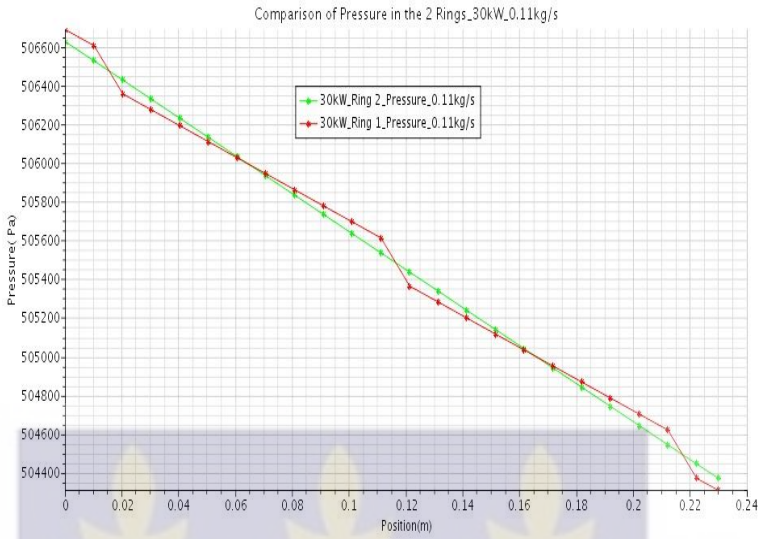

Figure 4.8: Comparison of Pressure in the 2 Rings at 30 kW and 0.11 kg/s

The pressure follows a generally similar trend throughout all the simulations. The sudden drop observed at the centre of the reactor core and at the outlet in the 1st ring can be attributed to spikes in temperature as the fluid mixes with the heat resulting in reduction in density and consequently pressure.

University of Ghana http://ugspace.ug.edu.gh

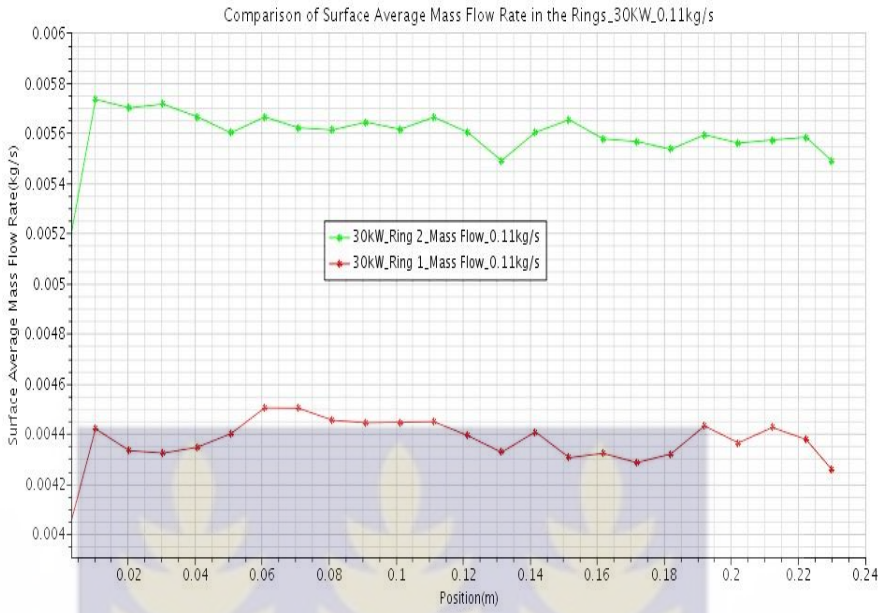

Figure 4.9: Comparison of Mass Flow in the 2 Rings at 30 kW and 0.11 kg/s

The sectional Average mass flow rate at 30 kW what was observed to be marginally higher than that at 15 kW but following a similar trend. The slight difference in the values of the coolant mass flow rate in the system is as a result of the marginal difference in temperature between the 2 rings

University of Ghana http://ugspace.ug.edu.gh

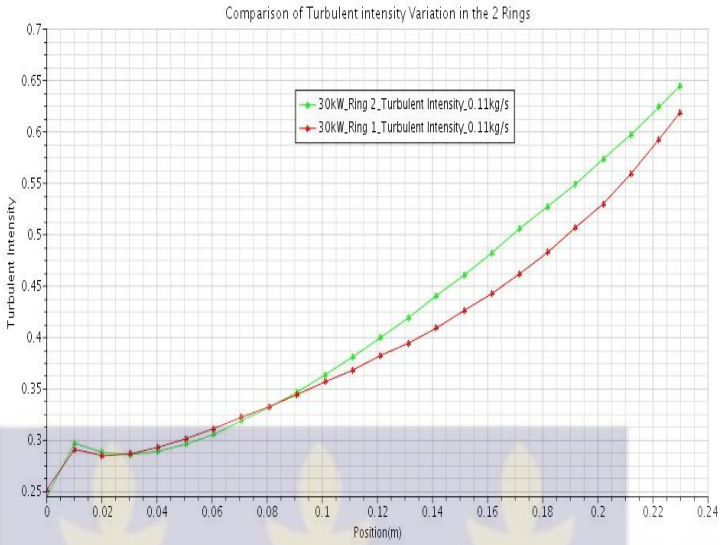

Figure 4.10: Comparison of Turbulent Intensity in the 2 Rings at 30kW and 0.11kg/s

The Sectional Average turbulent intensity at 30 kW follows a similar trend to the observations at 15 kW. Both rings were observed to have an almost similar variation at 30kW due to slight differences in the average temperature at each axial position. The effect of increase in power on turbulent intensity significantly reduces the maximum value at the outlet.

University of Ghana http://ugspace.ug.edu.gh

4.3 Analysis of Flow Parameters at Fixed Power and Varying Mass Flow Rate

4.3.1 1 Flow Parameters analysis at 30 kW and Mass Flow Rate of 0.13 kg/s

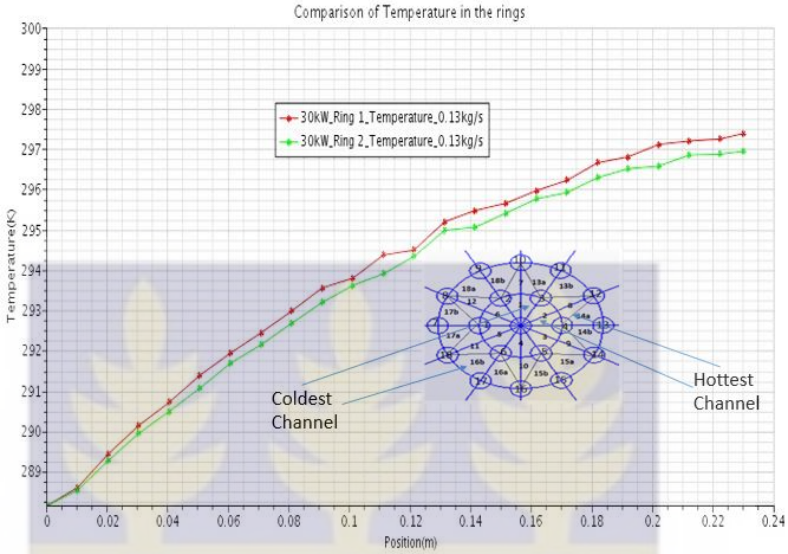

Figure 4.11: Comparison of Temperature in the 2 rings at 30 kW and 0.13 kg/s

The outlet temperature was observed to be reduced due to the increase in coolant mass flow rate and consequently the heat transfer rate. The hottest channel in the 1st ring was observed to be in channel 2 on the triangular pitch segment bounded by rods 3, 4 and the control rod. The hottest channel in the 2nd ring was observed to be in channel 14a on the triangular pitch bounded by rods 12, 13 and 4. The coldest channel in the 1st ring was observed to be in channel 1 on the triangular pitch bounded by rods 2, 3 and the control rod. The coldest channel in the 2nd ring was observed to be in channel 16b on the triangular pitch segment bounded by rods 17, 18 and 6.

University of Ghana http://ugspace.ug.edu.gh

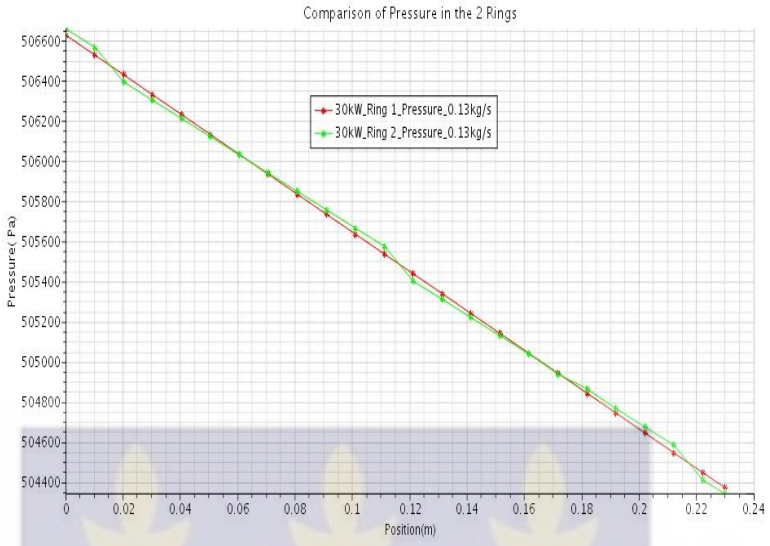

Figure 4.12: Comparison of Pressure in the 2 Rings at 30 kW and 0.13 kg/s

A more uniform decrease in pressure with significantly reduced spikes is observed when the inlet mass flow rate is increased to 0.13 kg/s due to the increase in mixing as a larger volume of coolant is available in the domain.

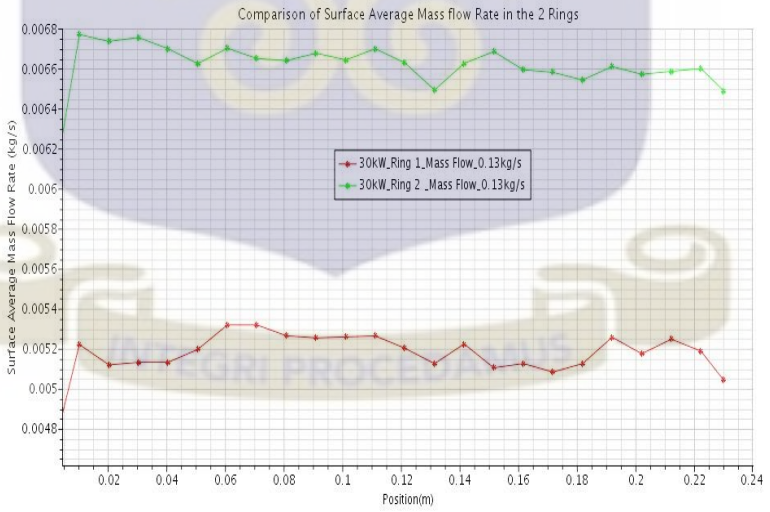

Figure 4.13: Comparison of Mass Flow Rate in the 2 Rings at 30 kW and 0.13 kg/s

University of Ghana http://ugspace.ug.edu.gh

The mass flow rate generated by the system was observed to increase slightly when the inlet mass flow rate was increased to 0.13 kg/s at the inlet. A similar trend was observed between the two rings.

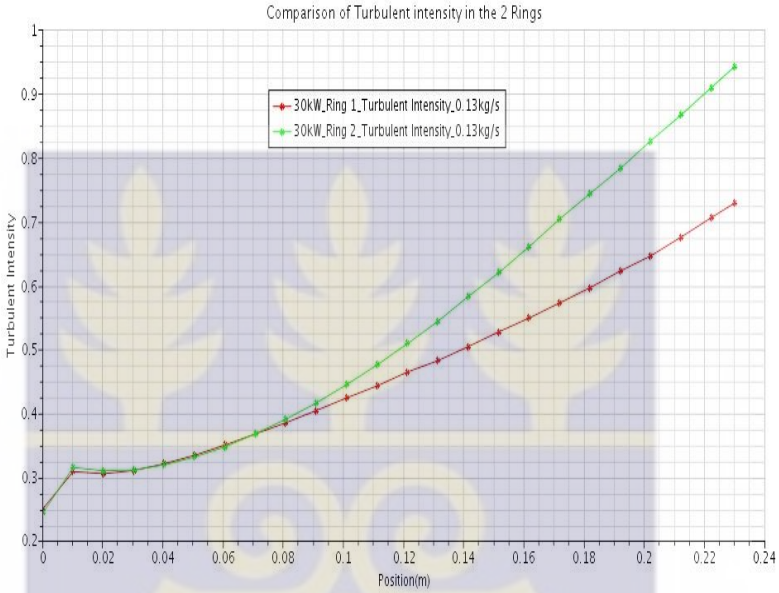

Figure 4.14: Comparison of Turbulent Intensity in the 2 Rings at 30kW and 0.13kg/s

Increase in coolant mass flow rate resulted in a significant surge in turbulent intensity at the inlet due to the fact that a larger volume of coolant is being introduced into the system. The peak turbulent intensity at upper part of the fuel rods was therefore observed to be larger than at 0.11 kg/s.

University of Ghana http://ugspace.ug.edu.gh

4.3.2 Flow Parameters analysis at 30kW and Mass Flow Rate of 0.15 kg/s

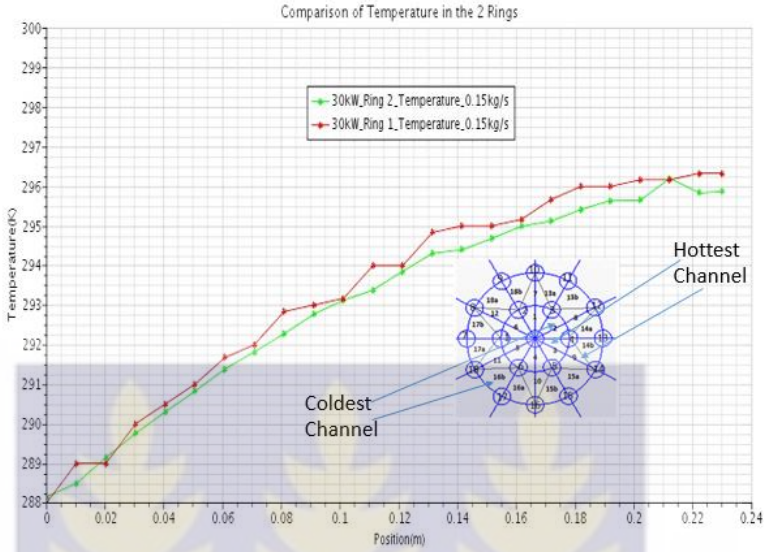

Figure 4.15: Comparison of Temperature in the 2 rings at 30 kW and 0.15 kg/s

Increasing the coolant mass flow rate to 0.15 kg/s further reduced the outlet temperature as the heat transfer rate increased. The hottest channel in the 1st ring was observed to be in channel 3 on the triangular pitch segment bounded by rods 4, 5 and the control rod. The hottest channel in the 2nd ring was observed to be in channel 9 on the triangular pitch bounded by rods 4, 5 and 14. The coldest channel in the 1st ring was observed to be in channel 2 on the triangular pitch bounded by rods 3, 4 and the control rod. The coldest channel in the 2nd ring was observed to be in channel 16b on the triangular pitch segment bounded by rods 17, 18 and 6. Average temperature in the hottest and coldest flow channels is in influenced by the heat generated by the rods as a result of the imposed heat flux applied at the surface of the rods.

University of Ghana http://ugspace.ug.edu.gh

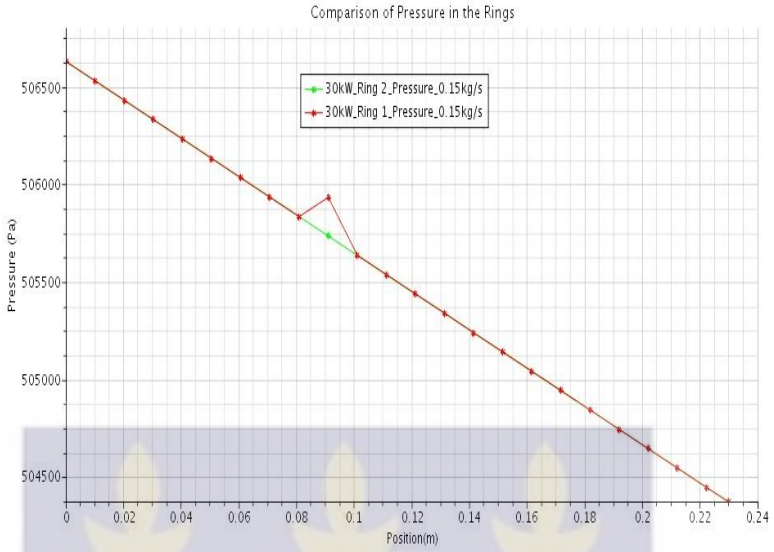

Figure 4.16: Comparison of Pressure in the 2 rings at 30kW and 0.15kg/s

A predominantly uniform pressure gradient was observed when the mass flow rate was increased to 0.15 kg/s. The single spike could be attributed to an errors in computation by the code since there is no significant drop in temperature at the same point in Figure 14.15 that could result in a corresponding increase in density and consequently an increase in pressure at that point.

University of Ghana http://ugspace.ug.edu.gh

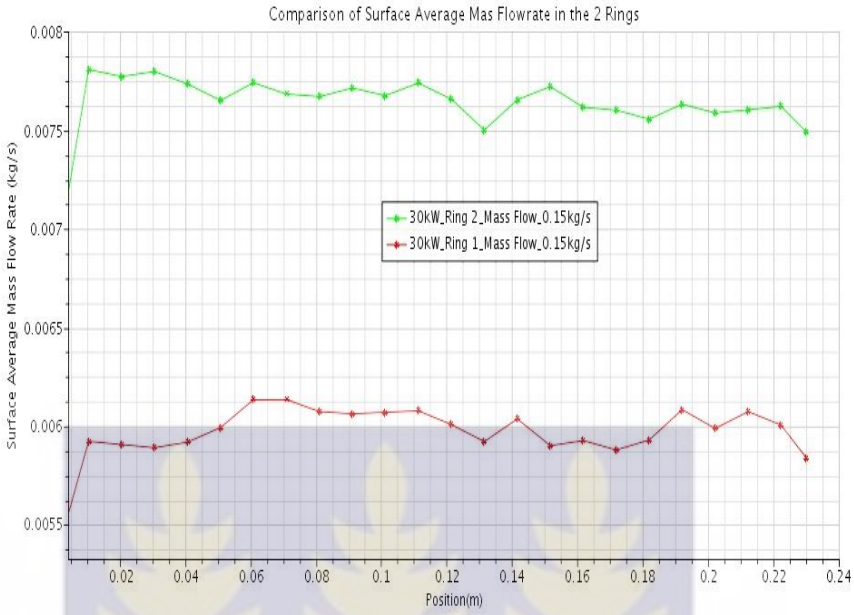

Figure 4.17: Comparison of Mass Flow Rate in the 2 rings at 30 kW and 0.15 kg/s

The Sectional Average mass flow rate generated by the system was observed to increase significantly when the inlet mass flow rate was increased to the maximum operating value of 0.15kg/s at the inlet. A similar trend was observed between the two rings.

University of Ghana http://ugspace.ug.edu.gh

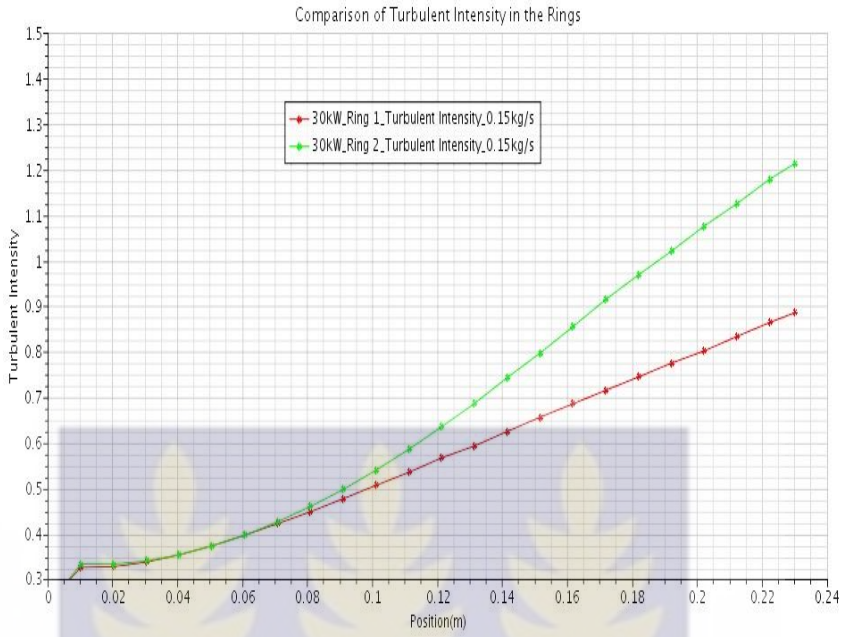

Figure 4.18: Comparison of Turbulent Intensity in the 2 rings at 30 kW and 0.15 kg/s

The minimum sectional average turbulent Intensity at the inlet increased when the coolant mass flow rate at the inlet was set to0.15 kg/s as a result of further increase in the volume of coolant. The size of the surge at the inlet dropped significantly since the coolant is moving at a faster rate and thus the flow develops faster in comparison to the previous simulations. The peak turbulent intensity at upper part of the fuel rods further increased.

University of Ghana http://ugspace.ug.edu.gh

4.4 Analysis of Temperature at low Mass Flow Rate

4.4.1 Temperature at 15 kW at Mass Flow Rate of 0.01 kg/s

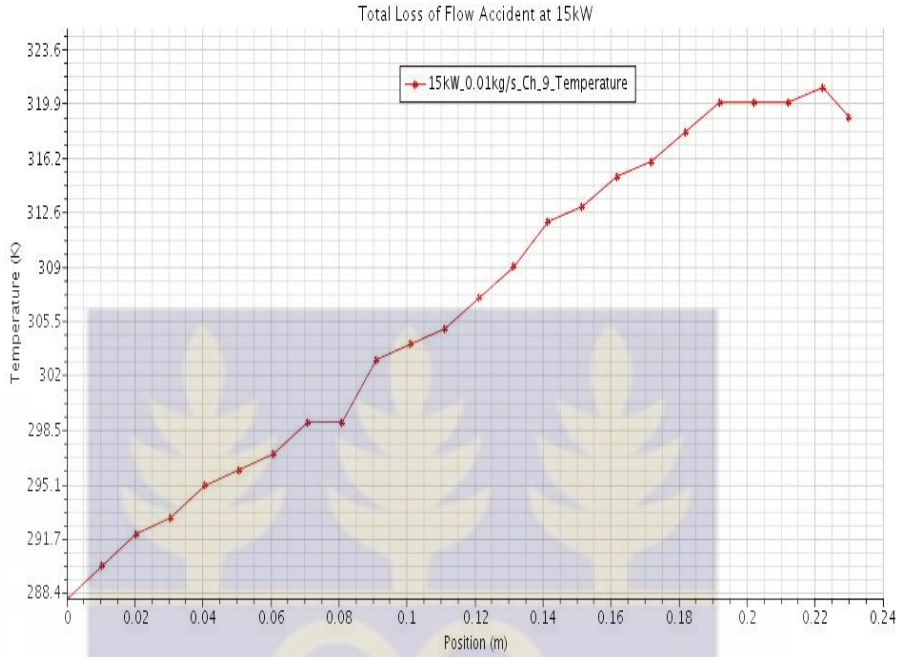

Figure 4.19: Temperature Variation in the Hottest Channel at 15kWand 0.01kg/s

The average temperature of the hottest flow channel is 306.399 K. A maximum temperature of 321.08 K on the axial located at 0.2222 m was computed. An outlet Temperature of 319.47 K was computed. All calculated temperatures were below the maximum cladding temperature at 30kW and the melting point of the U-Al alloy as reported in the Safety Analysis Report as 313.15 K and 640 ^{o}c respectively [3]. Based on these findings the reactor satisfies the regulatory requirements consistent with the specifications outlined in the Safety Analysis Report and its inherent safety features prevent structural damage together with radioactive contamination under accident conditions.

University of Ghana http://ugspace.ug.edu.gh

4.4.2 Temperature at 30 kW at Mass Flow Rate of 0.01 kg/s

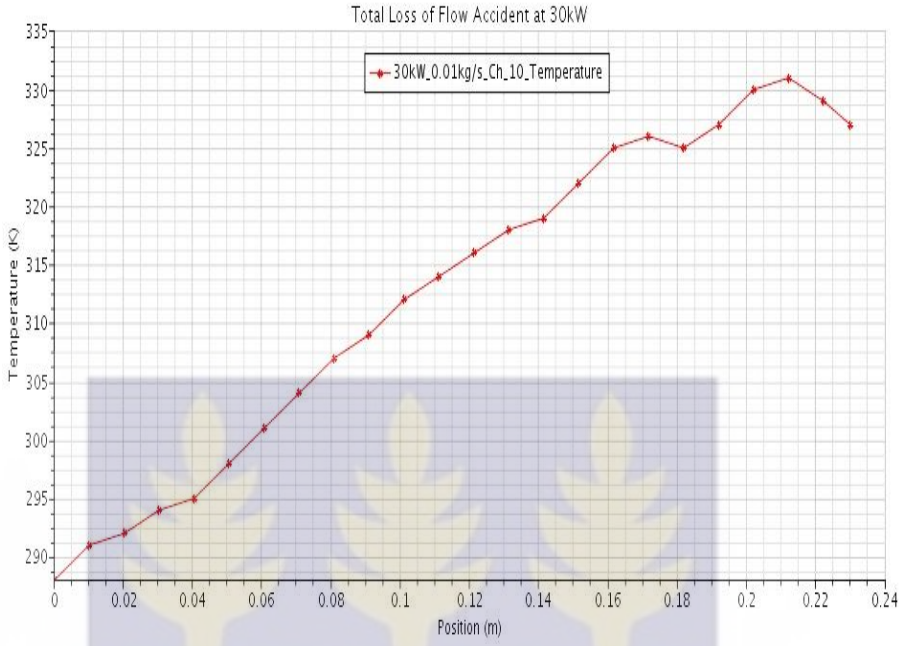

Figure 4.20: Temperature Variation in the Hottest Channel at 30kWand 0.01kg/s

The sectional average temperature of the hottest flow channel is 312.45 K. A maximum temperature of 330.68 K on the axial segment located at 0.2121 m was computed. An outlet Temperature of 327.39 K was computed. The maximum and outlet temperatures were observed to be above the maximum cladding temperature at 30kW. However, all the computed temperatures were below the melting point (640 ^{o}c) of the U-Al alloy. Therefore the integrity of the fuel is not compromised and thus there is no possibility of radiation leakage and radioactive contamination. Based on these findings the reactor satisfies the regulatory requirements consistent with the specifications outlined in the Safety Analysis Report.

University of Ghana http://ugspace.ug.edu.gh

CHAPTER FIVE

CONCLUSION AND RECOMMENDATIONS

5.1. Conclusion

The steady state thermal hydraulic behaviour of the GHARR-1 under natural convection cooling together with its operational safety as stipulated by the regulatory requirements were investigated in this study.

The following conclusions were drawn under evaluation of the steady state thermal hydraulic behaviour of GHARR-1 by numerical simulation using STAR-CCM+ CFD code:

i. Surface Average temperature increases along the flow channel from the inlet to the outlet in conformity with operating trends reported in the GHARR-1 Safety Analysis Report.

ii. Effective heat transfer and cooling of the reactor is achieved at the maximum operating coolant mass flow rate of 0.15 kg/s

The following conclusions were drawn under flow channel mapping and zoning of the GHARR-1 core:

i. The highest surface average temperature in the normal operating power range (15-30 kW)was observed to be 296.21 K at 30 kW and coolant mass flow rate of 0.11 kg/s

ii. The hottest flow channel is located between the inner and outer ring on the triangular pitch distance bounded by rods 4, 5 and 14.

The following conclusions were drawn under determination of the extent to which failure of the heat transfer will compromise safe operation of the reactor based on limits approved by the Regulatory Authority

University of Ghana http://ugspace.ug.edu.gh

i. The maximum temperatures attained under normal and accident operations are were below the melting point of the U-Al alloy fuel hence there is no possibility of radiation leakage and radioactive contamination

ii. The Inherent safety features of the reactor enable it to operate safely during accidents thus satisfying regulatory requirements.

The following contributions were made to current knowledge of heat generated in the core of the GHARR-1 Miniature Neutron Source Reactor (MNSR):

i. The temperature of the hottest segment is 301.85 K located at an axial distance of 0.2020 cm. This is below the maximum cladding Temperature of 333.15 K thus the reactor is operating safely.

ii. Results of the numerical simulation and Coolant flow channel zoning and mapping have provided a more detailed analysis on the steady state thermal hydraulic behaviour of the GHARR-1 under natural convection cooling

5.2. Recommendations

i. Acquisition of a high performance server to enable efficient and quick running of simulations and modelling the entire core.

ii. Experiments to determine inlet and outlet temperatures must be performed on the LEU core once the core conversion is completed.

iii. A similar study should be performed after the commissioning of the LEU core.

iv. Further study should cover simulation and modelling of the full geometry of the GHARR-1 core.

v. Computational features available in CFD codes for simulation of heat transfer in current operating Power reactors and experimental Reactor designs.

University of Ghana http://ugspace.ug.edu.gh

REFERENCES

[1] U.S. Department of Energy FSC-6910 Washington, D.C. 20585 (1992) DOE Fundamentals Handbook Thermodynamics, Heat Transfer, and Fluid Flow Volume 1 of 3

[2] Kyei A.Y, Annafi T.A, Annor-Nyarko M, Quaye C.R, Bansah C. (2014) Modelling the Velocity Profile of Coolant Flow in the GHARR-1 Fuel Channel. Journal of Nuclear Energy Science and Power Generation Technology 2014, 3:2 http://dx.doi.org/10.4172/2325-9809.1000123

[3] Akaho, E.H.K., S. Anim-Sampong, D.N.A. Dodoo-Amoo, B.T. Maakuu, G. Emi-Reynolds, E.K. Osae, H.O. Boadu and S. Akoto-Bamford, 2003. Final Safety Analysis Report for Ghana Research Reactor-1, GAEC-NNRI-RT-90.

[4] Yusuf A Ahmed, Tulshi Bezboruah, Manoj Johri and E.H.K. Akaho. (2006). The low power miniature neutron source reactors: design, safety and applications. http://www.researchgate.net/publication/265148122

[5] S. Yamoah, E.H.K. Akaho, B.J.B. Nyarko, M. Asamoah, A.G. Ampong and E.O. Amponsah-Abu (2011). Analysis of thermal-hydraulic transients for the Miniature Neutron Source Reactor (MNSR) in Ghana. Research Journal of Applied Sciences, Engineering and Technology 3(8): 737-745 ISSN:2040-7467

[6] Nuclear Regulatory Authority Act Section 23(b), 2015 (ACT 895)

[7] Nikolay Ivanov Kolev (2005) "Multiphase Flow Dynamics-Nuclear Thermal Hydraulics" springer.com Library of Congress Control Number: 2009920195

[8] E.H.K. Akaho. (2013) Thermal Hydraulics Notes

[9] Keng-Yen Chiang. (2012) Thermal Hydraulic Limits Analysis for the MIT Research Reactor Low Enrichment Uranium Core Conversion Using Statistical Propagation of Parametric Uncertainties. Research Thesis submitted to the Massachusetts Institute of Technology.

[10] Sadaf Waqar, Sikander M. Mirza, Nasir M. Mirza, Tariq Asad. (2008) A comparative neutronic study of the standard HEU core and various potential LEU alternatives for a typical MNSR system. Nuclear Engineering and Design 238 (2008) 2302–2307

[11] B.J.B. Nyarko, E.H.K. Akaho, Y. Serfor-Armah. (2008) The 30 kW Research Reactor Facility in Ghana: Past, Present and Future Programmes. https://www.researchgate.net/publication/242371685

University of Ghana http://ugspace.ug.edu.gh

[12] E. Ampomah-Amoako, E.H.K. Akaho, S. Anim-Sampong, B.J.B. Nyarko (2009) Transient analysis of Ghana Research Reactor-1 using PARET/ANL thermal–hydraulic code. Nuclear Engineering and Design 239: 2479–2483

[13] Briesmeister, J.F. (Ed.), (2000). MCNP™—a general Monte Carlo N-particle transport Code. Version 4c. LA-13709-M.

[14] Anim-Sampong, S., (2001). Three-dimensional Monte Carlo modeling and particle

Transport simulation of the Ghana Research Reactor-1, technical report,

NNRI/GAEC/ICTP/ENEA-TR.01/2001.

[15] C.A. Adjei, A.G. Ayensu, E.H.K. Akaho, F.K. Quashie, A.B. Asumadu-Sakyi and E.O. Amartey. (2010) Equalisation of Transient Temperature Profile within the Fuel Pin of a Miniature Neutron Source Reactor (MNSR) During Total Loss of Coolant. Research Journal of Applied Sciences, Engineering and Technology 2(7): 661-668, 2010

ISSN: 2040-7467

[16] N.A. Adoo, B.J.B. Nyarko, E.H.K. Akaho, E. Alhassan, V.Y. Agbodemegbe, C.Y. Bansah, R. Della (2010) Determination of thermal hydraulic data of GHARR-1 under reactivity insertion transients using the PARET/ANL code. Nuclear Engineering and Design. Journal homepage:www.elsevier.com/locate/nucengdes

[17] M. Annor-Nyarko, A.A Gyeabour, T.A. Annafi, C. R. Quaye, A. Y. Kyei. (2014) Control Volume Finite Difference Analysis of Thermal Stresses Induced In GHARR-1 Reactor Vessel by Coolant Heating. International Journal of Scientific & Technology Research Volume 3, Issue 8, August 2014.

[18] T. A. Annafi, A. A. Gyeabour I, E. H. K. Akaho, M. Annor-Nyarko and C. R. Quaye (2014) Finite Difference Analysis of the Transient Temperature Profile within GHARR-1 Fuel Element. International Journal of Scientific and Technology Research. 3:8 2277-8616.

[19] S. Mohammed (2015) Investigation of Heat Transfer and Distribution in the Core of Ghana Research Reactor-1 (GHARR-1) using STAR-CCM+ CFD Code. Thesis submitted to the University of Ghana.

[20] H. Omar, N. Ghazi, F. Alhabit, A. Hainoun (2009) Thermal hydraulic analysis of Syrian MNSR research reactor using RELAP5/Mod3.2 code. Annals of Nuclear Energy. Journal homepage: www.elsevier.com/locate/anucene

[21] S.A. Agbo, Y.A. Ahmed, I.O.B. Ewa and M. Abubakar (2015) An experimental testing of coolant flow rate and velocity in the core of Nigeria Research Reactor-1. Int. J. Nuclear Energy Science and Technology, Vol. 9, No. 2.

University of Ghana http://ugspace.ug.edu.gh

[22] Harvey W. Graves Jr. (1979) Nuclear Fuel Management. John Wiley & Sons, Inc., New York

[23] Tong, L. S. (1967). "Heat Transfer in Water Cooled Nuclear Reactors," Nucl. Eng. and Design, 6, Pp.301

[24] Chris Long, Nasser Sayma and bookboon.com (2009) Heat Transfer 1st Edition ISBN 978-87-7681-432-8

[25] John H. Leinhard IV and John H. Leinhard V (2008) A Heat Transfer Textbook 3rd Edition

[26] https://en.wikipedia.org/wiki/Natural_convection 27/2/2016

[27] J. Michael Doster and Paul Turinsky (2007) NE 405/505 Reactor Systems. www4.nscu.edu

[28] Donald Olander and Arthur Motta (2011) Light Water Reactor Materials. http://www.mne.psu.edu/motta/Book.html

[29] Bowlesf (2010) NET 2010 Thermal Sciences http://www.tarleton.edu/COSTWEB/tpc/Nuclear_Plant_Systems/Handouts/Thermal%20Science%20STP4.pdf

[30] In Ho Bae, Man Gyun Na, Yoon Joon Lee, Goon Cherl Pak (2008). Calculation of the power peaking factor in a nuclear reactor using support vector regression models. Annals of Nuclear Energy 35(12).

[31] RRRP-7225-EBEAN-002-REV0-Ch05 (e).doc. 5.8-1. 5.8 (2004) Thermal and Hydraulic Design. 5.8.1 www.arpansa.gov.au/pubs/regulatory/opal/op/SAR/ch5e.pdf

[32] Simon Adu, Ivan Horvatovic, Francesco D'AURIA (2014). Application of Best Estimate plus Uncertainty in Review of Research Reactor Safety Analysis. 23rd International Conference Nuclear Energy for Europe

[33]] Simon Adu, B.J. Benjamin Nyarko, Geoffrey Emi Reynolds, Emmanuel O. Darko, Ivan Horvatovic, Francesco D'AURIA (2015) Analysis of Channel Blockage of the MNSR Reactor using System thermal hydraulic Code RELAP5/MOD 3.3. 24th International Conference Nuclear Energy for Europe

[34] Susan Maria Sipaun (2014) Thermal-fluid modeling of the Missouri S&T reactor. Doctoral Dissertation submitted to the Missouri University of Science & Technology.

[35] Shi Shaungkai (1984) Core Thermohydraulic Calculation of Strong Neutron Source Reactor (SNSR) CIAE Technical Report.

[36] H. C. Odoi, E. H. K. Akaho, B. J. B. Nyarko, R. G. Abrefah, E. Ampomah-Amoako, R. B. M. Sogbadji, S. A. Birikorang, J. Gbadago J. E. Matos, J. Liaw, J. Morman, M. Kalimullah and S. C. Mo. Current Studies of Conversion of Ghana Research Reactor Core to Low Enriched Uranium. http://www.rertr.anl.gov/RERTR33/pdfs/S10-P2_Odoi.pdf

University of Ghana http://ugspace.ug.edu.gh

[37] Shuffler, Carter Alexander (2004). Optimization of hydride fueled pressurized water reactor cores. S.M. Thesis MIT department of Nuclear Engineering

[38] Alojz Ivankovic (2009) Lecture notes for the course Computational Continuum Mechanics (CCM) UCD School of Electrical, Electronic and Mechanical Engineering Dublin www.ucd.ie/mecheng/ccm/CCM.pdf

[39] B. L. Smith (2013). Thermal Hydraulics Laboratory on the Use of Computational Fluid Dynamics (CFD) in Reactor Technology. Paul Scherrer Institut

[40] Suhas V.Pantakar (1980) Numerical Heat Transfer and fluid Flow. Washington, DC, Hemisphere Publishing Corp., 1980. 210.

[41] CD-ADAPCO (2008). CFD Basics. Americas Agency Training Document.

[42] CD-ADAPCO (2015) "User Guide STAR-CCM+, Version 10.06.009" New York.

[43] Versteeg H. K., Malalasekera, W. (2007). An Introduction to Computational Fluid Dynamics, the Finite Volume Method. Second edition.

[44] André Bakker (2002) Lecture-10: Turbulence Models. Applied Computational Fluid Dynamics.

[45] Markus Schatz (2004) Numerical Simulation Method. https://www.cfd.tu.-berlin.de /research/flow control/ gurneys/node4.html

[46] J.E Bardina, P.G. Haung and T.J. Coakley (1997) Turbulence Modeling, Validation, Testing and Development. 28th Fluid Dynamics Conference, Fluid Dynamics and Co-located Conferences. http://dx.doi.org/10.2514/6.1997-2121

[47] Ishmael B.Celik (1999) Introductory Turbulence Modeling Lecture Notes. West Virginia University Mechanical & Aerospace Engineering Dept.

[48] http://www.compassis.com info@compassis.com (2015) Turbulence Handbook

[49] The NIST Reference on Constants, Units, and Uncertainty

http://physics.nist.gov/cuu/Units/units.html

University of Ghana http://ugspace.ug.edu.gh

APPENDICES

Appendix I

Thermophysical Properties

Temperature (K)	Density (kg/m^3)	Viscosity (Pa*s)	Thermal Conductivity (W/m*K)
274	9.9984E+02	1.7400E-03	5.6263E-01
274.5	9.9987E+02	1.7106E-03	5.6358E-01
275	9.9989E+02	1.6820E-03	5.6453E-01
275.5	9.9990E+02	1.6542E-03	5.6548E-01
276	9.9991E+02	1.6271E-03	5.6643E-01
276.5	9.9992E+02	1.6007E-03	5.6738E-01
277	9.9992E+02	1.5750E-03	5.6834E-01
277.5	9.9992E+02	1.5499E-03	5.6929E-01
278	9.9992E+02	1.5255E-03	5.7024E-01
278.5	9.9991E+02	1.5017E-03	5.7119E-01
279	9.9990E+02	1.4785E-03	5.7214E-01
279.5	9.9988E+02	1.4558E-03	5.7309E-01
280	9.9986E+02	1.4337E-03	5.7404E-01
280.5	9.9984E+02	1.4121E-03	5.7499E-01
281	9.9981E+02	1.3910E-03	5.7593E-01
281.5	9.9978E+02	1.3705E-03	5.7688E-01
282	9.9975E+02	1.3504E-03	5.7783E-01
282.5	9.9971E+02	1.3308E-03	5.7877E-01
283	9.9967E+02	1.3116E-03	5.7972E-01
283.5	9.9962E+02	1.2929E-03	5.8066E-01
284	9.9958E+02	1.2746E-03	5.8160E-01
284.5	9.9952E+02	1.2568E-03	5.8254E-01
285	9.9947E+02	1.2393E-03	5.8348E-01
285.5	9.9941E+02	1.2222E-03	5.8441E-01
286	9.9935E+02	1.2055E-03	5.8534E-01
286.5	9.9929E+02	1.1891E-03	5.8628E-01
287	9.9922E+02	1.1731E-03	5.8721E-01
287.5	9.9915E+02	1.1575E-03	5.8813E-01
288	9.9908E+02	1.1421E-03	5.8906E-01
288.5	9.9900E+02	1.1272E-03	5.8998E-01
289	9.9892E+02	1.1125E-03	5.9090E-01
289.5	9.9884E+02	1.0981E-03	5.9182E-01
290	9.9876E+02	1.0840E-03	5.9273E-01
290.5	9.9867E+02	1.0702E-03	5.9364E-01
291	9.9858E+02	1.0567E-03	5.9455E-01
291.5	9.9849E+02	1.0435E-03	5.9545E-01
292	9.9839E+02	1.0305E-03	5.9636E-01
292.5	9.9829E+02	1.0178E-03	5.9725E-01
293	9.9819E+02	1.0053E-03	5.9815E-01
293.5	9.9809E+02	9.9312E-04	5.9904E-01

University of Ghana http://ugspace.ug.edu.gh

294	9.9798E+02	9.8114E-04	5.9993E-01
294.5	9.9787E+02	9.6939E-04	6.0081E-01
295	9.9776E+02	9.5787E-04	6.0169E-01
295.5	9.9765E+02	9.4657E-04	6.0257E-01
296	9.9753E+02	9.3548E-04	6.0344E-01
296.5	9.9741E+02	9.2460E-04	6.0431E-01
297	9.9729E+02	9.1392E-04	6.0518E-01
297.5	9.9717E+02	9.0344E-04	6.0604E-01
298	9.9704E+02	8.9315E-04	6.0689E-01
298.5	9.9691E+02	8.8306E-04	6.0775E-01
299	9.9678E+02	8.7314E-04	6.0859E-01
299.5	9.9665E+02	8.6340E-04	6.0944E-01
300	9.9651E+02	8.5384E-04	6.1028E-01
300.5	9.9638E+02	8.4445E-04	6.1111E-01
301	9.9623E+02	8.3523E-04	6.1194E-01
301.5	9.9609E+02	8.2616E-04	6.1277E-01
302	9.9595E+02	8.1726E-04	6.1359E-01
302.5	9.9580E+02	8.0851E-04	6.1440E-01
303	9.9565E+02	7.9991E-04	6.1522E-01
303.5	9.9550E+02	7.9145E-04	6.1602E-01
304	9.9535E+02	7.8314E-04	6.1682E-01
304.5	9.9519E+02	7.7498E-04	6.1762E-01
305	9.9503E+02	7.6695E-04	6.1841E-01
305.5	9.9487E+02	7.5905E-04	6.1920E-01
306	9.9471E+02	7.5128E-04	6.1998E-01
306.5	9.9455E+02	7.4365E-04	6.2076E-01
307	9.9438E+02	7.3613E-04	6.2153E-01
307.5	9.9421E+02	7.2874E-04	6.2229E-01
308	9.9404E+02	7.2147E-04	6.2305E-01
308.5	9.9387E+02	7.1432E-04	6.2381E-01
309	9.9370E+02	7.0728E-04	6.2456E-01
309.5	9.9352E+02	7.0036E-04	6.2531E-01
310	9.9334E+02	6.9354E-04	6.2605E-01
310.5	9.9316E+02	6.8683E-04	6.2678E-01
311	9.9298E+02	6.8022E-04	6.2751E-01
311.5	9.9280E+02	6.7372E-04	6.2823E-01
312	9.9261E+02	6.6732E-04	6.2895E-01
312.5	9.9242E+02	6.6102E-04	6.2967E-01
313	9.9223E+02	6.5481E-04	6.3037E-01
313.5	9.9204E+02	6.4870E-04	6.3108E-01
314	9.9185E+02	6.4268E-04	6.3177E-01
314.5	9.9165E+02	6.3675E-04	6.3246E-01
315	9.9146E+02	6.3091E-04	6.3315E-01
315.5	9.9126E+02	6.2516E-04	6.3383E-01
316	9.9106E+02	6.1949E-04	6.3450E-01
316.5	9.9085E+02	6.1391E-04	6.3517E-01

University of Ghana http://ugspace.ug.edu.gh

317	9.9065E+02	6.0841E-04	6.3584E-01
317.5	9.9044E+02	6.0299E-04	6.3650E-01
318	9.9024E+02	5.9764E-04	6.3715E-01
318.5	9.9003E+02	5.9238E-04	6.3780E-01
319	9.8981E+02	5.8718E-04	6.3844E-01
319.5	9.8960E+02	5.8207E-04	6.3907E-01
320	9.8939E+02	5.7702E-04	6.3971E-01
320.5	9.8917E+02	5.7205E-04	6.4033E-01
321	9.8895E+02	5.6715E-04	6.4095E-01
321.5	9.8873E+02	5.6231E-04	6.4156E-01
322	9.8851E+02	5.5755E-04	6.4217E-01
322.5	9.8829E+02	5.5285E-04	6.4278E-01
323	9.8806E+02	5.4821E-04	6.4337E-01
323.5	9.8784E+02	5.4364E-04	6.4397E-01
324	9.8761E+02	5.3913E-04	6.4455E-01
324.5	9.8738E+02	5.3468E-04	6.4514E-01
325	9.8715E+02	5.3029E-04	6.4571E-01
325.5	9.8692E+02	5.2596E-04	6.4628E-01
326	9.8668E+02	5.2169E-04	6.4685E-01
326.5	9.8645E+02	5.1748E-04	6.4741E-01
327	9.8621E+02	5.1332E-04	6.4796E-01
327.5	9.8597E+02	5.0921E-04	6.4851E-01
328	9.8573E+02	5.0516E-04	6.4905E-01
328.5	9.8549E+02	5.0117E-04	6.4959E-01
329	9.8524E+02	4.9722E-04	6.5013E-01
329.5	9.8500E+02	4.9333E-04	6.5065E-01
330	9.8475E+02	4.8949E-04	6.5118E-01
330.5	9.8450E+02	4.8569E-04	6.5169E-01
331	9.8425E+02	4.8195E-04	6.5220E-01
331.5	9.8400E+02	4.7825E-04	6.5271E-01
332	9.8375E+02	4.7460E-04	6.5321E-01
332.5	9.8349E+02	4.7100E-04	6.5371E-01
333	9.8324E+02	4.6744E-04	6.5420E-01
333.5	9.8298E+02	4.6392E-04	6.5469E-01
334	9.8272E+02	4.6045E-04	6.5517E-01
334.5	9.8246E+02	4.5702E-04	6.5564E-01
335	9.8220E+02	4.5364E-04	6.5611E-01
335.5	9.8194E+02	4.5029E-04	6.5658E-01
336	9.8167E+02	4.4699E-04	6.5704E-01
336.5	9.8141E+02	4.4373E-04	6.5750E-01
337	9.8114E+02	4.4051E-04	6.5795E-01
337.5	9.8087E+02	4.3732E-04	6.5839E-01
338	9.8060E+02	4.3418E-04	6.5883E-01
338.5	9.8033E+02	4.3107E-04	6.5927E-01
339	9.8005E+02	4.2800E-04	6.5970E-01
339.5	9.7978E+02	4.2497E-04	6.6013E-01

University of Ghana http://ugspace.ug.edu.gh

340	9.7950E+02	4.2197E-04	6.6055E-01
340.5	9.7923E+02	4.1901E-04	6.6096E-01
341	9.7895E+02	4.1608E-04	6.6138E-01
341.5	9.7867E+02	4.1319E-04	6.6178E-01
342	9.7839E+02	4.1033E-04	6.6218E-01
342.5	9.7810E+02	4.0750E-04	6.6258E-01
343	9.7782E+02	4.0471E-04	6.6298E-01
343.5	9.7753E+02	4.0195E-04	6.6336E-01
344	9.7725E+02	3.9922E-04	6.6375E-01
344.5	9.7696E+02	3.9652E-04	6.6413E-01
345	9.7667E+02	3.9385E-04	6.6450E-01
345.5	9.7638E+02	3.9121E-04	6.6487E-01
346	9.7609E+02	3.8861E-04	6.6524E-01
346.5	9.7579E+02	3.8603E-04	6.6560E-01
347	9.7550E+02	3.8348E-04	6.6595E-01
347.5	9.7520E+02	3.8096E-04	6.6631E-01
348	9.7490E+02	3.7847E-04	6.6665E-01
348.5	9.7461E+02	3.7600E-04	6.6700E-01
349	9.7431E+02	3.7356E-04	6.6734E-01
349.5	9.7400E+02	3.7115E-04	6.6767E-01
350	9.7370E+02	3.6877E-04	6.6800E-01
350.5	9.7340E+02	3.6641E-04	6.6833E-01
351	9.7309E+02	3.6408E-04	6.6865E-01
351.5	9.7279E+02	3.6177E-04	6.6897E-01
352	9.7248E+02	3.5949E-04	6.6928E-01
352.5	9.7217E+02	3.5723E-04	6.6959E-01
353	9.7186E+02	3.5500E-04	6.6990E-01
353.5	9.7155E+02	3.5279E-04	6.7020E-01
354	9.7124E+02	3.5060E-04	6.7050E-01
354.5	9.7092E+02	3.4844E-04	6.7079E-01
355	9.7061E+02	3.4630E-04	6.7108E-01
355.5	9.7029E+02	3.4419E-04	6.7136E-01
356	9.6997E+02	3.4209E-04	6.7164E-01
356.5	9.6965E+02	3.4002E-04	6.7192E-01
357	9.6933E+02	3.3797E-04	6.7220E-01
357.5	9.6901E+02	3.3594E-04	6.7247E-01
358	9.6869E+02	3.3393E-04	6.7273E-01
358.5	9.6836E+02	3.3194E-04	6.7299E-01
359	9.6804E+02	3.2997E-04	6.7325E-01
359.5	9.6771E+02	3.2803E-04	6.7351E-01
360	9.6739E+02	3.2610E-04	6.7376E-01
360.5	9.6706E+02	3.2419E-04	6.7400E-01
361	9.6673E+02	3.2230E-04	6.7425E-01
361.5	9.6640E+02	3.2043E-04	6.7449E-01
362	9.6606E+02	3.1858E-04	6.7472E-01
362.5	9.6573E+02	3.1675E-04	6.7495E-01

University of Ghana http://ugspace.ug.edu.gh

363	9.6540E+02	3.1494E-04	6.7518E-01
363.5	9.6506E+02	3.1314E-04	6.7541E-01
364	9.6472E+02	3.1137E-04	6.7563E-01
364.5	9.6438E+02	3.0961E-04	6.7585E-01
365	9.6405E+02	3.0787E-04	6.7606E-01
365.5	9.6370E+02	3.0614E-04	6.7627E-01
366	9.6336E+02	3.0443E-04	6.7648E-01
366.5	9.6302E+02	3.0274E-04	6.7669E-01
367	9.6268E+02	3.0107E-04	6.7689E-01
367.5	9.6233E+02	2.9941E-04	6.7709E-01
368	9.6198E+02	2.9777E-04	6.7728E-01
368.5	9.6164E+02	2.9614E-04	6.7747E-01
369	9.6129E+02	2.9453E-04	6.7766E-01
369.5	9.6094E+02	2.9294E-04	6.7784E-01
370	9.6059E+02	2.9136E-04	6.7802E-01
370.5	9.6023E+02	2.8979E-04	6.7820E-01
371	9.5988E+02	2.8824E-04	6.7838E-01
371.5	9.5953E+02	2.8671E-04	6.7855E-01
372	9.5917E+02	2.8519E-04	6.7872E-01
372.5	9.5881E+02	2.8368E-04	6.7888E-01
373	9.5846E+02	2.8219E-04	6.7904E-01
373.5	9.5810E+02	2.8071E-04	6.7920E-01
374	9.5774E+02	2.7924E-04	6.7936E-01
374.5	9.5738E+02	2.7779E-04	6.7951E-01
375	9.5701E+02	2.7636E-04	6.7966E-01
375.5	9.5665E+02	2.7493E-04	6.7981E-01
376	9.5629E+02	2.7352E-04	6.7995E-01
376.5	9.5592E+02	2.7213E-04	6.8009E-01
377	9.5555E+02	2.7074E-04	6.8023E-01
377.5	9.5518E+02	2.6937E-04	6.8037E-01
378	9.5482E+02	2.6801E-04	6.8050E-01
378.5	9.5445E+02	2.6666E-04	6.8063E-01
379	9.5407E+02	2.6533E-04	6.8075E-01
379.5	9.5370E+02	2.6400E-04	6.8088E-01
380	9.5333E+02	2.6269E-04	6.8100E-01
380.5	9.5295E+02	2.6139E-04	6.8111E-01
381	9.5258E+02	2.6011E-04	6.8123E-01
381.5	9.5220E+02	2.5883E-04	6.8134E-01
382	9.5182E+02	2.5756E-04	6.8145E-01
382.5	9.5144E+02	2.5631E-04	6.8156E-01
383	9.5106E+02	2.5507E-04	6.8166E-01
383.5	9.5068E+02	2.5384E-04	6.8176E-01
384	9.5030E+02	2.5262E-04	6.8186E-01
384.5	9.4991E+02	2.5141E-04	6.8195E-01
385	9.4953E+02	2.5021E-04	6.8205E-01
385.5	9.4914E+02	2.4902E-04	6.8214E-01

University of Ghana http://ugspace.ug.edu.gh

386	9.4876E+02	2.4784E-04	6.8222E-01
386.5	9.4837E+02	2.4667E-04	6.8231E-01
387	9.4798E+02	2.4551E-04	6.8239E-01
387.5	9.4759E+02	2.4437E-04	6.8247E-01
388	9.4720E+02	2.4323E-04	6.8255E-01
388.5	9.4681E+02	2.4210E-04	6.8262E-01
389	9.4641E+02	2.4098E-04	6.8269E-01
389.5	9.4602E+02	2.3987E-04	6.8276E-01
390	9.4562E+02	2.3877E-04	6.8283E-01
390.5	9.4523E+02	2.3768E-04	6.8289E-01
391	9.4483E+02	2.3660E-04	6.8295E-01
391.5	9.4443E+02	2.3553E-04	6.8301E-01
392	9.4403E+02	2.3446E-04	6.8307E-01
392.5	9.4363E+02	2.3341E-04	6.8312E-01
393	9.4323E+02	2.3236E-04	6.8317E-01
393.5	9.4282E+02	2.3133E-04	6.8322E-01
394	9.4242E+02	2.3030E-04	6.8327E-01
394.5	9.4201E+02	2.2928E-04	6.8331E-01
395	9.4161E+02	2.2827E-04	6.8335E-01
395.5	9.4120E+02	2.2726E-04	6.8339E-01
396	9.4079E+02	2.2627E-04	6.8343E-01
396.5	9.4038E+02	2.2528E-04	6.8346E-01
397	9.3997E+02	2.2431E-04	6.8350E-01
397.5	9.3956E+02	2.2333E-04	6.8353E-01
398	9.3915E+02	2.2237E-04	6.8355E-01
398.5	9.3873E+02	2.2142E-04	6.8358E-01
399	9.3832E+02	2.2047E-04	6.8360E-01
399.5	9.3790E+02	2.1953E-04	6.8362E-01
400	9.3749E+02	2.1860E-04	6.8364E-01
400.5	9.3707E+02	2.1767E-04	6.8365E-01
401	9.3665E+02	2.1676E-04	6.8367E-01
401.5	9.3623E+02	2.1585E-04	6.8368E-01
402	9.3581E+02	2.1494E-04	6.8369E-01
402.5	9.3538E+02	2.1405E-04	6.8369E-01
403	9.3496E+02	2.1316E-04	6.8370E-01
403.5	9.3454E+02	2.1228E-04	6.8370E-01
404	9.3411E+02	2.1140E-04	6.8370E-01
404.5	9.3368E+02	2.1054E-04	6.8370E-01
405	9.3326E+02	2.0968E-04	6.8369E-01
405.5	9.3283E+02	2.0882E-04	6.8368E-01
406	9.3240E+02	2.0797E-04	6.8368E-01
406.5	9.3197E+02	2.0713E-04	6.8366E-01
407	9.3154E+02	2.0630E-04	6.8365E-01
407.5	9.3110E+02	2.0547E-04	6.8363E-01
408	9.3067E+02	2.0465E-04	6.8362E-01
408.5	9.3023E+02	2.0383E-04	6.8359E-01

University of Ghana http://ugspace.ug.edu.gh

409	9.2980E+02	2.0303E-04	6.8357E-01
409.5	9.2936E+02	2.0222E-04	6.8355E-01
410	9.2892E+02	2.0143E-04	6.8352E-01
410.5	9.2848E+02	2.0063E-04	6.8349E-01
411	9.2804E+02	1.9985E-04	6.8346E-01
411.5	9.2760E+02	1.9907E-04	6.8343E-01
412	9.2716E+02	1.9830E-04	6.8339E-01
412.5	9.2671E+02	1.9753E-04	6.8335E-01
413	9.2627E+02	1.9677E-04	6.8331E-01
413.5	9.2582E+02	1.9601E-04	6.8327E-01
414	9.2538E+02	1.9526E-04	6.8323E-01
414.5	9.2493E+02	1.9452E-04	6.8318E-01
415	9.2448E+02	1.9378E-04	6.8313E-01
415.5	9.2403E+02	1.9305E-04	6.8308E-01
416	9.2358E+02	1.9232E-04	6.8303E-01
416.5	9.2312E+02	1.9159E-04	6.8297E-01
417	9.2267E+02	1.9088E-04	6.8292E-01
417.5	9.2222E+02	1.9016E-04	6.8286E-01
418	9.2176E+02	1.8946E-04	6.8279E-01
418.5	9.2130E+02	1.8875E-04	6.8273E-01
419	9.2085E+02	1.8806E-04	6.8267E-01
419.5	9.2039E+02	1.8737E-04	6.8260E-01
420	9.1993E+02	1.8668E-04	6.8253E-01
420.5	9.1947E+02	1.8600E-04	6.8246E-01
421	9.1901E+02	1.8532E-04	6.8238E-01
421.5	9.1854E+02	1.8465E-04	6.8231E-01
422	9.1808E+02	1.8398E-04	6.8223E-01
422.5	9.1761E+02	1.8332E-04	6.8215E-01
423	9.1715E+02	1.8266E-04	6.8207E-01
423.5	9.1668E+02	1.8200E-04	6.8198E-01
424	9.1621E+02	1.8135E-04	6.8190E-01
424.5	9.1574E+02	1.8071E-04	6.8181E-01
425	9.1527E+02	1.8007E-04	6.8172E-01
425.5	9.1480E+02	1.7943E-04	6.8163E-01
426	9.1433E+02	1.7880E-04	6.8153E-01
426.5	9.1385E+02	1.7818E-04	6.8143E-01
427	9.1338E+02	1.7755E-04	6.8134E-01
427.5	9.1290E+02	1.7694E-04	6.8124E-01
428	9.1243E+02	1.7632E-04	6.8113E-01
428.5	9.1195E+02	1.7571E-04	6.8103E-01
429	9.1147E+02	1.7511E-04	6.8092E-01
429.5	9.1099E+02	1.7451E-04	6.8081E-01
430	9.1051E+02	1.7391E-04	6.8070E-01
430.5	9.1002E+02	1.7332E-04	6.8059E-01
431	9.0954E+02	1.7273E-04	6.8047E-01
431.5	9.0906E+02	1.7214E-04	6.8036E-01

University of Ghana http://ugspace.ug.edu.gh

432	9.0857E+02	1.7156E-04	6.8024E-01
432.5	9.0808E+02	1.7098E-04	6.8012E-01
433	9.0760E+02	1.7041E-04	6.7999E-01
433.5	9.0711E+02	1.6984E-04	6.7987E-01
434	9.0662E+02	1.6928E-04	6.7974E-01
434.5	9.0613E+02	1.6871E-04	6.7961E-01
435	9.0563E+02	1.6816E-04	6.7948E-01
435.5	9.0514E+02	1.6760E-04	6.7935E-01
436	9.0465E+02	1.6705E-04	6.7921E-01
436.5	9.0415E+02	1.6650E-04	6.7907E-01
437	9.0365E+02	1.6596E-04	6.7893E-01
437.5	9.0315E+02	1.6542E-04	6.7879E-01
438	9.0266E+02	1.6488E-04	6.7865E-01
438.5	9.0216E+02	1.6435E-04	6.7850E-01
439	9.0165E+02	1.6382E-04	6.7836E-01
439.5	9.0115E+02	1.6329E-04	6.7821E-01
440	9.0065E+02	1.6277E-04	6.7805E-01
440.5	9.0014E+02	1.6225E-04	6.7790E-01
441	8.9964E+02	1.6173E-04	6.7774E-01
441.5	8.9913E+02	1.6122E-04	6.7759E-01
442	8.9862E+02	1.6071E-04	6.7743E-01
442.5	8.9811E+02	1.6020E-04	6.7726E-01
443	8.9760E+02	1.5970E-04	6.7710E-01

INTEGRI PROCEDAMUS

University of Ghana http://ugspace.ug.edu.gh

Appendix II

Power Peaking Factors for the 18 Fuel Rods [12]

Segment	Pin 1	Pin 2	Pin 3	Pin 4	Pin 5	Pin 6	Pin 7
1	0.39705629	0.42395157	0.41222161	0.42485287	0.41076487	0.39769118	0.38010275
2	0.87064803	0.89361208	0.85434101	0.87659279	0.87934601	0.88846863	0.89298199
3	0.94847789	0.94120446	0.95894972	0.94075929	0.95668962	0.95055308	0.93208184
4	1.00538465	0.99711814	0.98913243	0.98312602	1.02630776	1.00836388	0.97085980
5	1.08365284	1.04833353	1.03321821	1.03527970	1.05410708	1.05941491	1.03639606
6	1.07575616	1.12134869	1.10795927	1.07355770	1.09402879	1.08668686	1.12452654
7	1.10393901	1.14822342	1.15154509	1.10255556	1.17016700	1.11087001	1.17343388
8	1.17963205	1.20184959	1.18775474	1.15963353	1.18428924	1.15452432	1.16120191
9	1.21396514	1.16017459	1.18598775	1.19604180	1.20304128	1.16444140	1.19026826
10	1.21352681	1.23567586	1.23790172	1.21147902	1.18971350	1.20124005	1.17909785
11	1.23075842	1.18800130	1.20427407	1.16416059	1.23140220	1.22380687	1.20288376
12	1.18946010	1.20265775	1.17207097	1.18438513	1.20061681	1.16891367	1.18269347
13	1.17697472	1.16033896	1.15305867	1.16311273	1.17934440	1.16535229	1.14347034
14	1.13652565	1.14525788	1.14738101	1.16187309	1.15449008	1.15462020	1.08828949
15	1.13236157	1.10908932	1.09861749	1.08717998	1.10107621	1.09885720	1.07157154
16	1.06603770	1.08608417	1.03995744	1.03714943	1.04738155	1.04757331	1.04725142
17	0.99877555	0.99627573	0.99496076	1.00054939	0.95948393	0.95294332	0.94154005
18	0.95100510	0.93066414	0.92765751	0.94262216	0.88855081	0.91023414	0.91416536
19	0.81497406	0.83338365	0.82175438	0.83130847	0.86112133	0.81501515	0.79663979
20	0.75587568	0.73917143	0.75032814	0.77258677	0.76181360	0.72809691	0.74382178
21	0.65657890	0.65189706	0.65015472	0.65121834	0.63971440	0.62961446	0.64923424

Segment	Pin 8	Pin 9	Pin 10	Pin 11	Pin 12	Pin 13	Pin 14
1	0.39892602	0.39768912	0.40590016	0.41260583	0.42850054	0.39499617	0.39657208
2	0.89588589	0.86082683	0.88877682	0.86127885	0.88645508	0.91337775	0.86810027
3	0.91667887	0.97642104	0.93997852	0.94311528	0.96280560	0.92106211	0.94680678
4	0.96026469	1.02315731	0.97872908	0.98478343	1.00085074	0.95145028	0.93508847
5	1.01280191	1.08280359	1.06344201	1.05453855	1.05964092	1.01271288	1.03125260
6	1.05488099	1.12803997	1.07813955	1.11779416	1.09991876	1.04076560	1.08399528
7	1.15842814	1.14115544	1.13696397	1.18076211	1.11555460	1.10918520	1.15336687
8	1.16135258	1.15967462	1.15681182	1.16282508	1.17152991	1.13869672	1.16073619
9	1.18875467	1.16714668	1.23874413	1.25063366	1.21194474	1.22105365	1.16558515
10	1.20749986	1.22675871	1.20836281	1.21928666	1.22085504	1.17335855	1.19743896
11	1.18678906	1.21579377	1.17336539	1.23518959	1.20132908	1.20034970	1.15905823
12	1.21009556	1.25626338	1.17094776	1.18878206	1.19336392	1.17891293	1.21136944
13	1.19711706	1.20617119	1.16492766	1.15230531	1.15468869	1.16142792	1.15259296
14	1.15368877	1.11890366	1.06690065	1.11480807	1.14929183	1.07826968	1.13097126
15	1.10676072	1.09495338	1.06409264	1.05964092	1.06664040	1.11945842	1.04414206

University of Ghana http://ugspace.ug.edu.gh

16	1.00239857	1.03445100	1.07652323	1.02002056	1.05500427	1.02030821	0.99439916
17	0.97722235	0.97712646	0.97047627	0.96273711	1.00094662	0.94277284	0.98551625
18	0.90790555	0.91572004	0.92419202	0.88314710	0.87650376	0.88323614	0.89879663
19	0.85420403	0.84604025	0.80217363	0.80672809	0.78780483	0.81020044	0.84931398
20	0.75130752	0.77560710	0.71695390	0.76186154	0.69920863	0.77562080	0.73416496
21	0.66813011	0.64618173	0.65757061	0.70881751	0.63939798	0.64229982	0.65697751

Segment	**Pin 15**	**Pin 16**	**Pin 17**	**Pin 18**
1	0.42481315	0.41372424	0.40603987	0.40701035
2	0.85445059	0.86986041	0.90851509	0.90013900
3	0.98224937	0.95006682	0.92482211	0.95044350
4	1.01054180	0.99346087	1.00609008	0.99970014
5	1.07457817	1.05268938	1.07923536	1.07610545
6	1.11142476	1.10254871	1.11394513	1.13099181
7	1.16787265	1.14286765	1.09804219	1.16800963
8	1.16109918	1.19267219	1.14209373	1.20182220
9	1.17264627	1.26281769	1.18779584	1.18826840
10	1.16268125	1.15328469	1.20902714	1.17897457
11	1.17250244	1.21651974	1.21016405	1.21751282
12	1.21899216	1.17173538	1.21656083	1.17904991
13	1.15707893	1.13334780	1.17325581	1.14832615
14	1.14921649	1.11428757	1.12651269	1.14621671
15	1.09983658	1.07637256	1.02687621	1.14638109
16	0.98866671	1.02906098	1.03786855	1.01021306
17	0.97667444	0.97906468	0.95039556	0.96153172
18	0.92089089	0.91396674	0.87705166	0.90706314
19	0.81507679	0.76818984	0.83592456	0.86360745
20	0.71294050	0.71781685	0.72813800	0.76323130
21	0.61880772	0.64739397	0.61181851	0.68665477

University of Ghana http://ugspace.ug.edu.gh

Appendix III

Heat Fluxes for Fuel Rods

Rod 1 Segments	Heat flux 5kW	Heat Flux 10kW	Heat Flux 15kW	Heat Flux 20kW	Heat Flux 25kW	Heat Flux 30kW
1	1.187E+05	4.272E+06	3.560E+05	4.747E+05	5.934E+05	7.120E+05
2	2.602E+05	9.368E+06	7.807E+05	1.041E+06	1.301E+06	1.561E+06
3	2.835E+05	1.021E+07	8.505E+05	1.134E+06	1.417E+06	1.701E+06
4	3.005E+05	1.082E+07	9.015E+05	1.202E+06	1.502E+06	1.803E+06
5	3.239E+05	1.166E+07	9.717E+05	1.296E+06	1.619E+06	1.943E+06
6	3.215E+05	1.157E+07	9.646E+05	1.286E+06	1.608E+06	1.929E+06
7	3.299E+05	1.188E+07	9.898E+05	1.320E+06	1.650E+06	1.980E+06
8	3.526E+05	1.269E+07	1.058E+06	1.410E+06	1.763E+06	2.115E+06
9	3.628E+05	1.306E+07	1.088E+06	1.451E+06	1.814E+06	2.177E+06
10	3.627E+05	1.306E+07	1.088E+06	1.451E+06	1.814E+06	2.176E+06
11	3.679E+05	1.324E+07	1.104E+06	1.471E+06	1.839E+06	2.207E+06
12	3.555E+05	1.280E+07	1.067E+06	1.422E+06	1.778E+06	2.133E+06
13	3.518E+05	1.266E+07	1.055E+06	1.407E+06	1.759E+06	2.111E+06
14	3.397E+05	1.223E+07	1.019E+06	1.359E+06	1.698E+06	2.038E+06
15	3.384E+05	1.218E+07	1.015E+06	1.354E+06	1.692E+06	2.031E+06
16	3.186E+05	1.147E+07	9.559E+05	1.274E+06	1.593E+06	1.912E+06
17	2.985E+05	1.075E+07	8.955E+05	1.194E+06	1.493E+06	1.791E+06
18	2.842E+05	1.023E+07	8.527E+05	1.137E+06	1.421E+06	1.705E+06
19	2.436E+05	8.769E+06	7.307E+05	9.743E+05	1.218E+06	1.461E+06
20	2.259E+05	8.133E+06	6.778E+05	9.037E+05	1.130E+06	1.356E+06
21	1.962E+05	7.065E+06	5.887E+05	7.850E+05	9.812E+05	1.177E+06
Rod 2 Segments	Heat flux 5kW	Heat Flux 10kW	Heat Flux 15kW	Heat Flux 20kW	Heat Flux 25kW	Heat Flux 30kW
1	1.266E+05	2.533E+05	3.799E+05	5.065E+05	6.332E+05	7.598E+05
2	2.669E+05	5.338E+05	8.008E+05	1.068E+06	1.335E+06	1.602E+06
3	2.811E+05	5.623E+05	8.434E+05	1.125E+06	1.406E+06	1.687E+06
4	2.978E+05	5.957E+05	8.935E+05	1.191E+06	1.489E+06	1.787E+06
5	3.131E+05	6.263E+05	9.394E+05	1.253E+06	1.566E+06	1.879E+06
6	3.349E+05	6.699E+05	1.005E+06	1.340E+06	1.675E+06	2.010E+06
7	3.430E+05	6.859E+05	1.029E+06	1.372E+06	1.715E+06	2.058E+06
8	3.590E+05	7.180E+05	1.077E+06	1.436E+06	1.795E+06	2.154E+06
9	3.465E+05	6.931E+05	1.040E+06	1.386E+06	1.733E+06	2.079E+06
10	3.691E+05	7.382E+05	1.107E+06	1.476E+06	1.845E+06	2.215E+06
11	3.549E+05	7.097E+05	1.065E+06	1.419E+06	1.774E+06	2.129E+06
12	3.592E+05	7.185E+05	1.078E+06	1.437E+06	1.796E+06	2.155E+06
13	3.466E+05	6.932E+05	1.040E+06	1.386E+06	1.733E+06	2.080E+06
14	3.421E+05	6.842E+05	1.026E+06	1.368E+06	1.710E+06	2.053E+06
15	3.313E+05	6.626E+05	9.939E+05	1.325E+06	1.656E+06	1.988E+06
16	3.244E+05	6.488E+05	9.732E+05	1.298E+06	1.622E+06	1.946E+06
17	2.976E+05	5.952E+05	8.928E+05	1.190E+06	1.488E+06	1.786E+06
18	2.780E+05	5.560E+05	8.340E+05	1.112E+06	1.390E+06	1.668E+06

University of Ghana http://ugspace.ug.edu.gh

19	2.489E+05	4.979E+05	7.468E+05	9.957E+05	1.245E+06	1.494E+06
20	2.208E+05	4.416E+05	6.624E+05	8.832E+05	1.104E+06	1.325E+06
21	1.947E+05	3.894E+05	5.842E+05	7.789E+05	9.736E+05	1.168E+06
Rod 3 Segments	Heat flux 5kW	Heat Flux 10kW	Heat Flux 15kW	Heat Flux 20kW	Heat Flux 25kW	Heat Flux 30kW
1	1.239E+05	2.478E+05	3.718E+05	4.957E+05	6.196E+05	7.435E+05
2	2.568E+05	5.137E+05	7.705E+05	1.027E+06	1.284E+06	1.541E+06
3	2.883E+05	5.765E+05	8.648E+05	1.153E+06	1.441E+06	1.730E+06
4	2.973E+05	5.947E+05	8.920E+05	1.189E+06	1.487E+06	1.784E+06
5	3.106E+05	6.212E+05	9.318E+05	1.242E+06	1.553E+06	1.864E+06
6	3.331E+05	6.661E+05	9.992E+05	1.332E+06	1.665E+06	1.998E+06
7	3.462E+05	6.923E+05	1.039E+06	1.385E+06	1.731E+06	2.077E+06
8	3.571E+05	7.141E+05	1.071E+06	1.428E+06	1.785E+06	2.142E+06
9	3.565E+05	7.131E+05	1.070E+06	1.426E+06	1.783E+06	2.139E+06
10	3.721E+05	7.443E+05	1.116E+06	1.489E+06	1.861E+06	2.233E+06
11	3.620E+05	7.240E+05	1.086E+06	1.448E+06	1.810E+06	2.172E+06
12	3.523E+05	7.047E+05	1.057E+06	1.409E+06	1.762E+06	2.114E+06
13	3.466E+05	6.933E+05	1.040E+06	1.387E+06	1.733E+06	2.080E+06
14	3.449E+05	6.898E+05	1.035E+06	1.380E+06	1.725E+06	2.070E+06
15	3.303E+05	6.605E+05	9.908E+05	1.321E+06	1.651E+06	1.982E+06
16	3.126E+05	6.253E+05	9.379E+05	1.251E+06	1.563E+06	1.876E+06
17	2.991E+05	5.982E+05	8.973E+05	1.196E+06	1.495E+06	1.795E+06
18	2.789E+05	5.577E+05	8.366E+05	1.115E+06	1.394E+06	1.673E+06
19	2.470E+05	4.941E+05	7.411E+05	9.881E+05	1.235E+06	1.482E+06
20	2.256E+05	4.511E+05	6.767E+05	9.022E+05	1.128E+06	1.353E+06
21	1.954E+05	3.909E+05	5.863E+05	7.818E+05	9.772E+05	1.173E+06
Rod 4 Segments	Heat flux 5kW	Heat Flux 10kW	Heat Flux 15kW	Heat Flux 20kW	Heat Flux 25kW	Heat Flux 30kW
1	1.282E+05	2.564E+05	3.846E+05	5.128E+05	6.410E+05	7.692E+05
2	2.645E+05	5.290E+05	7.935E+05	1.058E+06	1.323E+06	1.587E+06
3	2.839E+05	5.677E+05	8.516E+05	1.135E+06	1.419E+06	1.703E+06
4	2.967E+05	5.933E+05	8.900E+05	1.187E+06	1.483E+06	1.780E+06
5	3.124E+05	6.248E+05	9.372E+05	1.250E+06	1.562E+06	1.874E+06
6	3.239E+05	6.479E+05	9.718E+05	1.296E+06	1.620E+06	1.944E+06
7	3.327E+05	6.654E+05	9.981E+05	1.331E+06	1.663E+06	1.996E+06
8	3.499E+05	6.998E+05	1.050E+06	1.400E+06	1.750E+06	2.100E+06
9	3.609E+05	7.218E+05	1.083E+06	1.444E+06	1.805E+06	2.165E+06
10	3.656E+05	7.311E+05	1.097E+06	1.462E+06	1.828E+06	2.193E+06
11	3.513E+05	7.026E+05	1.054E+06	1.405E+06	1.756E+06	2.108E+06
12	3.574E+05	7.148E+05	1.072E+06	1.430E+06	1.787E+06	2.144E+06
13	3.510E+05	7.019E+05	1.053E+06	1.404E+06	1.755E+06	2.106E+06
14	3.506E+05	7.012E+05	1.052E+06	1.402E+06	1.753E+06	2.104E+06
15	3.281E+05	6.561E+05	9.842E+05	1.312E+06	1.640E+06	1.968E+06
16	3.130E+05	6.259E+05	9.389E+05	1.252E+06	1.565E+06	1.878E+06
17	3.019E+05	6.038E+05	9.057E+05	1.208E+06	1.510E+06	1.811E+06
18	2.844E+05	5.689E+05	8.533E+05	1.138E+06	1.422E+06	1.707E+06

University of Ghana http://ugspace.ug.edu.gh

19	2.508E+05	5.017E+05	7.525E+05	1.003E+06	1.254E+06	1.505E+06
20	2.331E+05	4.663E+05	6.994E+05	9.325E+05	1.166E+06	1.399E+06
21	1.965E+05	3.930E+05	5.895E+05	7.860E+05	9.825E+05	1.179E+06
Rod 5 Segments	Heat flux 5kW	Heat Flux 10kW	Heat Flux 15kW	Heat Flux 20kW	Heat Flux 25kW	Heat Flux 30kW
1	1.228E+05	2.456E+05	3.684E+05	4.913E+05	6.141E+05	1.578E+06
2	2.629E+05	5.258E+05	7.888E+05	1.052E+06	1.315E+06	1.716E+06
3	2.860E+05	5.721E+05	8.581E+05	1.144E+06	1.430E+06	1.841E+06
4	3.069E+05	6.137E+05	9.206E+05	1.227E+06	1.534E+06	1.891E+06
5	3.152E+05	6.303E+05	9.455E+05	1.261E+06	1.576E+06	1.963E+06
6	3.271E+05	6.542E+05	9.813E+05	1.308E+06	1.636E+06	2.099E+06
7	3.499E+05	6.997E+05	1.050E+06	1.399E+06	1.749E+06	2.125E+06
8	3.541E+05	7.082E+05	1.062E+06	1.416E+06	1.770E+06	2.158E+06
9	3.597E+05	7.194E+05	1.079E+06	1.439E+06	1.799E+06	2.134E+06
10	3.557E+05	7.114E+05	1.067E+06	1.423E+06	1.779E+06	2.209E+06
11	3.682E+05	7.364E+05	1.105E+06	1.473E+06	1.841E+06	2.154E+06
12	3.590E+05	7.180E+05	1.077E+06	1.436E+06	1.795E+06	2.116E+06
13	3.526E+05	7.052E+05	1.058E+06	1.410E+06	1.763E+06	2.071E+06
14	3.452E+05	6.904E+05	1.036E+06	1.381E+06	1.726E+06	1.975E+06
15	3.292E+05	6.584E+05	9.876E+05	1.317E+06	1.646E+06	1.879E+06
16	3.132E+05	6.263E+05	9.395E+05	1.253E+06	1.566E+06	1.721E+06
17	2.869E+05	5.738E+05	8.606E+05	1.148E+06	1.434E+06	1.594E+06
18	2.657E+05	5.313E+05	7.970E+05	1.063E+06	1.328E+06	1.545E+06
19	2.575E+05	5.149E+05	7.724E+05	1.030E+06	1.287E+06	1.367E+06
20	2.278E+05	4.556E+05	6.833E+05	9.111E+05	1.139E+06	1.148E+06
21	1.913E+05	3.825E+05	5.738E+05	7.651E+05	9.564E+05	3.802E+07
Rod 6 Segments	Heat flux 5kW	Heat Flux 10kW	Heat Flux 15kW	Heat Flux 20kW	Heat Flux 25kW	Heat Flux 30kW
1	1.205E+05	2.410E+05	3.614E+05	4.819E+05	6.024E+05	7.229E+05
2	2.692E+05	5.383E+05	8.075E+05	1.077E+06	1.346E+06	1.615E+06
3	2.880E+05	5.759E+05	8.639E+05	1.152E+06	1.440E+06	1.728E+06
4	3.055E+05	6.110E+05	9.164E+05	1.222E+06	1.527E+06	1.833E+06
5	3.209E+05	6.419E+05	9.628E+05	1.284E+06	1.605E+06	1.926E+06
6	3.292E+05	6.584E+05	9.876E+05	1.317E+06	1.646E+06	1.975E+06
7	3.365E+05	6.731E+05	1.010E+06	1.346E+06	1.683E+06	2.019E+06
8	3.498E+05	6.995E+05	1.049E+06	1.399E+06	1.749E+06	2.099E+06
9	3.528E+05	7.055E+05	1.058E+06	1.411E+06	1.764E+06	2.117E+06
10	3.639E+05	7.278E+05	1.092E+06	1.456E+06	1.820E+06	2.183E+06
11	3.707E+05	7.415E+05	1.112E+06	1.483E+06	1.854E+06	2.224E+06
12	3.541E+05	7.082E+05	1.062E+06	1.416E+06	1.771E+06	2.125E+06
13	3.530E+05	7.061E+05	1.059E+06	1.412E+06	1.765E+06	2.118E+06
14	3.498E+05	6.996E+05	1.049E+06	1.399E+06	1.749E+06	2.099E+06
15	3.329E+05	6.658E+05	9.987E+05	1.332E+06	1.664E+06	1.997E+06
16	3.174E+05	6.347E+05	9.521E+05	1.269E+06	1.587E+06	1.904E+06
17	2.887E+05	5.774E+05	8.661E+05	1.155E+06	1.443E+06	1.732E+06
18	2.757E+05	5.515E+05	8.272E+05	1.103E+06	1.379E+06	1.654E+06

University of Ghana http://ugspace.ug.edu.gh

19	2.469E+05	4.938E+05	7.407E+05	9.876E+05	1.235E+06	1.481E+06
20	2.206E+05	4.411E+05	6.617E+05	8.823E+05	1.103E+06	1.323E+06
21	1.907E+05	3.815E+05	5.722E+05	7.629E+05	9.537E+05	1.144E+06
Rod 7 Segments	Heat flux 5kW	Heat Flux 10kW	Heat Flux 15kW	Heat Flux 20kW	Heat Flux 25kW	Heat Flux 30kW
1	5.205E+05	1.157E+05	1.735E+05	2.313E+05	2.892E+05	3.470E+05
2	1.223E+06	2.718E+05	4.076E+05	5.435E+05	6.794E+05	8.153E+05
3	1.276E+06	2.837E+05	4.255E+05	5.673E+05	7.091E+05	8.510E+05
4	1.330E+06	2.955E+05	4.432E+05	5.909E+05	7.386E+05	8.864E+05
5	1.419E+06	3.154E+05	4.731E+05	6.308E+05	7.885E+05	9.462E+05
6	1.540E+06	3.422E+05	5.133E+05	6.844E+05	8.555E+05	1.027E+06
7	1.607E+06	3.571E+05	5.357E+05	7.142E+05	8.928E+05	1.071E+06
8	1.590E+06	3.534E+05	5.301E+05	7.068E+05	8.834E+05	1.060E+06
9	1.630E+06	3.622E+05	5.433E+05	7.244E+05	9.056E+05	1.087E+06
10	1.615E+06	3.588E+05	5.382E+05	7.176E+05	8.971E+05	1.076E+06
11	1.647E+06	3.661E+05	5.491E+05	7.321E+05	9.152E+05	1.098E+06
12	1.620E+06	3.599E+05	5.399E+05	7.198E+05	8.998E+05	1.080E+06
13	1.566E+06	3.480E+05	5.220E+05	6.960E+05	8.700E+05	1.044E+06
14	1.490E+06	3.312E+05	4.968E+05	6.624E+05	8.280E+05	9.936E+05
15	1.467E+06	3.261E+05	4.892E+05	6.522E+05	8.153E+05	9.783E+05
16	1.434E+06	3.187E+05	4.781E+05	6.374E+05	7.968E+05	9.561E+05
17	1.289E+06	2.865E+05	4.298E+05	5.731E+05	7.163E+05	8.596E+05
18	1.252E+06	2.782E+05	4.173E+05	5.564E+05	6.955E+05	8.346E+05
19	1.091E+06	2.424E+05	3.637E+05	4.849E+05	6.061E+05	7.273E+05
20	1.019E+06	2.264E+05	3.395E+05	4.527E+05	5.659E+05	6.791E+05
21	8.891E+05	1.976E+05	2.964E+05	3.952E+05	4.939E+05	5.927E+05
Rod 8 Segments	Heat flux 5kW	Heat Flux 10kW	Heat Flux 15kW	Heat Flux 20kW	Heat Flux 25kW	Heat Flux 30kW
1	6.027E+04	1.205E+05	1.808E+05	2.411E+05	3.014E+05	3.616E+05
2	1.354E+05	2.707E+05	4.061E+05	5.414E+05	6.768E+05	8.121E+05
3	1.385E+05	2.770E+05	4.155E+05	5.540E+05	6.925E+05	8.310E+05
4	1.451E+05	2.902E+05	4.352E+05	5.803E+05	7.254E+05	8.705E+05
5	1.530E+05	3.060E+05	4.590E+05	6.121E+05	7.651E+05	9.181E+05
6	1.594E+05	3.187E+05	4.781E+05	6.375E+05	7.969E+05	9.562E+05
7	1.750E+05	3.500E+05	5.251E+05	7.001E+05	8.751E+05	1.050E+06
8	1.755E+05	3.509E+05	5.264E+05	7.018E+05	8.773E+05	1.053E+06
9	1.796E+05	3.592E+05	5.388E+05	7.184E+05	8.980E+05	1.078E+06
10	1.824E+05	3.649E+05	5.473E+05	7.297E+05	9.122E+05	1.095E+06
11	1.793E+05	3.586E+05	5.379E+05	7.172E+05	8.965E+05	1.076E+06
12	1.828E+05	3.656E+05	5.485E+05	7.313E+05	9.141E+05	1.097E+06
13	1.809E+05	3.617E+05	5.426E+05	7.235E+05	9.043E+05	1.085E+06
14	1.743E+05	3.486E+05	5.229E+05	6.972E+05	8.715E+05	1.046E+06
15	1.672E+05	3.344E+05	5.016E+05	6.688E+05	8.361E+05	1.003E+06
16	1.514E+05	3.029E+05	4.543E+05	6.058E+05	7.572E+05	9.087E+05
17	1.476E+05	2.953E+05	4.429E+05	5.906E+05	7.382E+05	8.858E+05
18	1.372E+05	2.743E+05	4.115E+05	5.487E+05	6.858E+05	8.230E+05

University of Ghana http://ugspace.ug.edu.gh

19	1.291E+05	2.581E+05	3.872E+05	5.162E+05	6.453E+05	7.743E+05
20	1.135E+05	2.270E+05	3.405E+05	4.540E+05	5.675E+05	6.811E+05
21	1.009E+05	2.019E+05	3.028E+05	4.038E+05	5.047E+05	6.057E+05
Rod 9 Segments	Heat flux 5kW	Heat Flux 10kW	Heat Flux 15kW	Heat Flux 20kW	Heat Flux 25kW	Heat Flux 30kW
1	5.929E+04	1.186E+05	1.779E+05	2.372E+05	2.965E+05	3.558E+05
2	1.283E+05	2.567E+05	3.850E+05	5.134E+05	6.417E+05	7.701E+05
3	1.456E+05	2.912E+05	4.367E+05	5.823E+05	7.279E+05	8.735E+05
4	1.525E+05	3.051E+05	4.576E+05	6.102E+05	7.627E+05	9.153E+05
5	1.614E+05	3.229E+05	4.843E+05	6.458E+05	8.072E+05	9.686E+05
6	1.682E+05	3.364E+05	5.045E+05	6.727E+05	8.409E+05	1.009E+06
7	1.701E+05	3.403E+05	5.104E+05	6.806E+05	8.507E+05	1.021E+06
8	1.729E+05	3.458E+05	5.187E+05	6.916E+05	8.645E+05	1.037E+06
9	1.740E+05	3.480E+05	5.220E+05	6.961E+05	8.701E+05	1.044E+06
10	1.829E+05	3.658E+05	5.487E+05	7.316E+05	9.145E+05	1.097E+06
11	1.813E+05	3.625E+05	5.438E+05	7.251E+05	9.063E+05	1.088E+06
12	1.873E+05	3.746E+05	5.619E+05	7.492E+05	9.365E+05	1.124E+06
13	1.798E+05	3.597E+05	5.395E+05	7.193E+05	8.992E+05	1.079E+06
14	1.668E+05	3.336E+05	5.005E+05	6.673E+05	8.341E+05	1.001E+06
15	1.632E+05	3.265E+05	4.897E+05	6.530E+05	8.162E+05	9.795E+05
16	1.542E+05	3.085E+05	4.627E+05	6.169E+05	7.711E+05	9.254E+05
17	1.457E+05	2.914E+05	4.370E+05	5.827E+05	7.284E+05	8.741E+05
18	1.365E+05	2.731E+05	4.096E+05	5.461E+05	6.826E+05	8.192E+05
19	1.261E+05	2.523E+05	3.784E+05	5.046E+05	6.307E+05	7.568E+05
20	1.156E+05	2.313E+05	3.469E+05	4.626E+05	5.782E+05	6.938E+05
21	9.634E+04	1.927E+05	2.890E+05	3.854E+05	4.817E+05	5.780E+05
Rod 10 Segments	Heat flux 5kW	Heat Flux 10kW	Heat Flux 15kW	Heat Flux 20kW	Heat Flux 25kW	Heat Flux 30kW
1	6.158E+04	1.232E+05	1.847E+05	2.463E+05	3.079E+05	3.695E+05
2	1.348E+05	2.697E+05	4.045E+05	5.394E+05	6.742E+05	8.090E+05
3	1.426E+05	2.852E+05	4.278E+05	5.704E+05	7.130E+05	8.556E+05
4	1.485E+05	2.970E+05	4.455E+05	5.939E+05	7.424E+05	8.909E+05
5	1.613E+05	3.227E+05	4.840E+05	6.453E+05	8.067E+05	9.680E+05
6	1.636E+05	3.271E+05	4.907E+05	6.543E+05	8.178E+05	9.814E+05
7	1.725E+05	3.450E+05	5.175E+05	6.900E+05	8.625E+05	1.035E+06
8	1.755E+05	3.510E+05	5.265E+05	7.020E+05	8.775E+05	1.053E+06
9	1.879E+05	3.759E+05	5.638E+05	7.517E+05	9.397E+05	1.128E+06
10	1.833E+05	3.666E+05	5.500E+05	7.333E+05	9.166E+05	1.100E+06
11	1.780E+05	3.560E+05	5.340E+05	7.121E+05	8.901E+05	1.068E+06
12	1.776E+05	3.553E+05	5.329E+05	7.106E+05	8.882E+05	1.066E+06
13	1.767E+05	3.535E+05	5.302E+05	7.069E+05	8.837E+05	1.060E+06
14	1.619E+05	3.237E+05	4.856E+05	6.474E+05	8.093E+05	9.712E+05
15	1.614E+05	3.229E+05	4.843E+05	6.457E+05	8.072E+05	9.686E+05
16	1.633E+05	3.266E+05	4.900E+05	6.533E+05	8.166E+05	9.799E+05
17	1.472E+05	2.945E+05	4.417E+05	5.889E+05	7.362E+05	8.834E+05
18	1.402E+05	2.804E+05	4.206E+05	5.608E+05	7.011E+05	8.413E+05

University of Ghana http://ugspace.ug.edu.gh

19	1.217E+05	2.434E+05	3.651E+05	4.868E+05	6.085E+05	7.302E+05
20	1.088E+05	2.175E+05	3.263E+05	4.351E+05	5.439E+05	6.526E+05
21	9.976E+04	1.995E+05	2.993E+05	3.990E+05	4.988E+05	5.986E+05
Rod 11 Segments	Heat flux 5kW	Heat Flux 10kW	Heat Flux 15kW	Heat Flux 20kW	Heat Flux 25kW	Heat Flux 30kW
1	6.201E+04	1.240E+05	1.860E+05	2.480E+05	3.101E+05	3.721E+05
2	1.294E+05	2.589E+05	3.883E+05	5.178E+05	6.472E+05	7.766E+05
3	1.417E+05	2.835E+05	4.252E+05	5.670E+05	7.087E+05	8.504E+05
4	1.480E+05	2.960E+05	4.440E+05	5.920E+05	7.400E+05	8.880E+05
5	1.585E+05	3.170E+05	4.755E+05	6.339E+05	7.924E+05	9.509E+05
6	1.680E+05	3.360E+05	5.040E+05	6.720E+05	8.400E+05	1.008E+06
7	1.775E+05	3.549E+05	5.324E+05	7.098E+05	8.873E+05	1.065E+06
8	1.748E+05	3.495E+05	5.243E+05	6.990E+05	8.738E+05	1.049E+06
9	1.880E+05	3.759E+05	5.639E+05	7.518E+05	9.398E+05	1.128E+06
10	1.832E+05	3.665E+05	5.497E+05	7.330E+05	9.162E+05	1.099E+06
11	1.856E+05	3.713E+05	5.569E+05	7.425E+05	9.282E+05	1.114E+06
12	1.787E+05	3.573E+05	5.360E+05	7.146E+05	8.933E+05	1.072E+06
13	1.732E+05	3.464E+05	5.195E+05	6.927E+05	8.659E+05	1.039E+06
14	1.675E+05	3.351E+05	5.026E+05	6.702E+05	8.377E+05	1.005E+06
15	1.593E+05	3.185E+05	4.778E+05	6.370E+05	7.963E+05	9.555E+05
16	1.533E+05	3.066E+05	4.599E+05	6.132E+05	7.665E+05	9.198E+05
17	1.447E+05	2.894E+05	4.341E+05	5.788E+05	7.234E+05	8.681E+05
18	1.327E+05	2.655E+05	3.982E+05	5.309E+05	6.636E+05	7.964E+05
19	1.212E+05	2.425E+05	3.637E+05	4.850E+05	6.062E+05	7.275E+05
20	1.145E+05	2.290E+05	3.435E+05	4.580E+05	5.725E+05	6.870E+05
21	1.065E+05	2.131E+05	3.196E+05	4.261E+05	5.326E+05	6.392E+05
Rod 12 Segments	Heat flux 5kW	Heat Flux 10kW	Heat Flux 15kW	Heat Flux 20kW	Heat Flux 25kW	Heat Flux 30kW
1	6.470E+04	1.294E+05	1.941E+05	9.317E+06	3.235E+05	3.882E+05
2	1.339E+05	2.677E+05	4.016E+05	1.928E+07	6.693E+05	8.031E+05
3	1.454E+05	2.908E+05	4.362E+05	2.094E+07	7.269E+05	8.723E+05
4	1.511E+05	3.023E+05	4.534E+05	2.176E+07	7.557E+05	9.068E+05
5	1.600E+05	3.200E+05	4.800E+05	2.304E+07	8.000E+05	9.600E+05
6	1.661E+05	3.322E+05	4.983E+05	2.392E+07	8.304E+05	9.965E+05
7	1.685E+05	3.369E+05	5.054E+05	2.426E+07	8.423E+05	1.011E+06
8	1.769E+05	3.538E+05	5.307E+05	2.547E+07	8.845E+05	1.061E+06
9	1.830E+05	3.660E+05	5.490E+05	2.635E+07	9.150E+05	1.098E+06
10	1.844E+05	3.687E+05	5.531E+05	2.655E+07	9.218E+05	1.106E+06
11	1.814E+05	3.628E+05	5.442E+05	2.612E+07	9.070E+05	1.088E+06
12	1.802E+05	3.604E+05	5.406E+05	2.595E+07	9.010E+05	1.081E+06
13	1.744E+05	3.487E+05	5.231E+05	2.511E+07	8.718E+05	1.046E+06
14	1.735E+05	3.471E+05	5.206E+05	2.499E+07	8.677E+05	1.041E+06
15	1.611E+05	3.221E+05	4.832E+05	2.319E+07	8.053E+05	9.664E+05
16	1.593E+05	3.186E+05	4.779E+05	2.294E+07	7.965E+05	9.558E+05
17	1.511E+05	3.023E+05	4.534E+05	2.176E+07	7.557E+05	9.069E+05
18	1.324E+05	2.647E+05	3.971E+05	1.906E+07	6.618E+05	7.941E+05

University of Ghana http://ugspace.ug.edu.gh

19	1.190E+05	2.379E+05	3.569E+05	1.713E+07	5.948E+05	7.138E+05
20	1.056E+05	2.112E+05	3.167E+05	1.520E+07	5.279E+05	6.335E+05
21	9.655E+04	1.931E+05	2.897E+05	1.390E+07	4.828E+05	5.793E+05
Rod 13 Segments	Heat flux 5kW	Heat Flux 10kW	Heat Flux 15kW	Heat Flux 20kW	Heat Flux 25kW	Heat Flux 30kW
1	6.049E+04	1.210E+05	1.815E+05	2.420E+05	3.024E+05	3.629E+05
2	1.399E+05	2.797E+05	4.196E+05	5.595E+05	6.994E+05	8.392E+05
3	1.410E+05	2.821E+05	4.231E+05	5.642E+05	7.052E+05	8.463E+05
4	1.457E+05	2.914E+05	4.371E+05	5.828E+05	7.285E+05	8.742E+05
5	1.551E+05	3.102E+05	4.653E+05	6.203E+05	7.754E+05	9.305E+05
6	1.594E+05	3.188E+05	4.781E+05	6.375E+05	7.969E+05	9.563E+05
7	1.699E+05	3.397E+05	5.096E+05	6.794E+05	8.493E+05	1.019E+06
8	1.744E+05	3.488E+05	5.231E+05	6.975E+05	8.719E+05	1.046E+06
9	1.870E+05	3.740E+05	5.610E+05	7.480E+05	9.350E+05	1.122E+06
10	1.797E+05	3.594E+05	5.391E+05	7.187E+05	8.984E+05	1.078E+06
11	1.838E+05	3.676E+05	5.515E+05	7.353E+05	9.191E+05	1.103E+06
12	1.805E+05	3.611E+05	5.416E+05	7.221E+05	9.027E+05	1.083E+06
13	1.779E+05	3.557E+05	5.336E+05	7.114E+05	8.893E+05	1.067E+06
14	1.651E+05	3.302E+05	4.954E+05	6.605E+05	8.256E+05	9.907E+05
15	1.714E+05	3.429E+05	5.143E+05	6.857E+05	8.572E+05	1.029E+06
16	1.562E+05	3.125E+05	4.687E+05	6.250E+05	7.812E+05	9.375E+05
17	1.444E+05	2.887E+05	4.331E+05	5.775E+05	7.219E+05	8.662E+05
18	1.353E+05	2.705E+05	4.058E+05	5.410E+05	6.763E+05	8.115E+05
19	1.241E+05	2.481E+05	3.722E+05	4.963E+05	6.204E+05	7.444E+05
20	1.188E+05	2.376E+05	3.563E+05	4.751E+05	5.939E+05	7.127E+05
21	9.836E+04	1.967E+05	2.951E+05	3.934E+05	4.918E+05	5.902E+05
Rod 14 Segments	Heat flux 5kW	Heat Flux 10kW	Heat Flux 15kW	Heat Flux 20kW	Heat Flux 25kW	Heat Flux 30kW
1	6.054E+04	1.211E+05	1.816E+05	2.421E+05	3.027E+05	3.632E+05
2	1.325E+05	2.650E+05	3.975E+05	5.300E+05	6.626E+05	7.951E+05
3	1.445E+05	2.891E+05	4.336E+05	5.781E+05	7.226E+05	8.672E+05
4	1.427E+05	2.855E+05	4.282E+05	5.710E+05	7.137E+05	8.564E+05
5	1.574E+05	3.148E+05	4.723E+05	6.297E+05	7.871E+05	9.445E+05
6	1.655E+05	3.309E+05	4.964E+05	6.619E+05	8.273E+05	9.928E+05
7	1.761E+05	3.521E+05	5.282E+05	7.042E+05	8.803E+05	1.056E+06
8	1.772E+05	3.544E+05	5.315E+05	7.087E+05	8.859E+05	1.063E+06
9	1.779E+05	3.558E+05	5.338E+05	7.117E+05	8.896E+05	1.068E+06
10	1.828E+05	3.656E+05	5.484E+05	7.311E+05	9.139E+05	1.097E+06
11	1.769E+05	3.539E+05	5.308E+05	7.077E+05	8.846E+05	1.062E+06
12	1.849E+05	3.698E+05	5.547E+05	7.396E+05	9.246E+05	1.109E+06
13	1.759E+05	3.519E+05	5.278E+05	7.038E+05	8.797E+05	1.056E+06
14	1.726E+05	3.453E+05	5.179E+05	6.906E+05	8.632E+05	1.036E+06
15	1.594E+05	3.188E+05	4.782E+05	6.375E+05	7.969E+05	9.563E+05
16	1.518E+05	3.036E+05	4.554E+05	6.072E+05	7.590E+05	9.107E+05
17	1.504E+05	3.009E+05	4.513E+05	6.017E+05	7.522E+05	9.026E+05
18	1.372E+05	2.744E+05	4.116E+05	5.488E+05	6.860E+05	8.232E+05

University of Ghana http://ugspace.ug.edu.gh

19	1.296E+05	2.593E+05	3.889E+05	5.186E+05	6.482E+05	7.779E+05
20	1.121E+05	2.241E+05	3.362E+05	4.483E+05	5.603E+05	6.724E+05
21	1.003E+05	2.006E+05	3.009E+05	4.011E+05	5.014E+05	6.017E+05
Rod 15 Segments	Heat flux 5kW	Heat Flux 10kW	Heat Flux 15kW	Heat Flux 20kW	Heat Flux 25kW	Heat Flux 30kW
1	6.424E+04	1.285E+05	1.927E+05	2.569E+05	3.212E+05	3.854E+05
2	1.292E+05	2.584E+05	3.876E+05	5.168E+05	6.460E+05	7.752E+05
3	1.485E+05	2.971E+05	4.456E+05	5.941E+05	7.426E+05	8.912E+05
4	1.528E+05	3.056E+05	4.584E+05	6.112E+05	7.640E+05	9.168E+05
5	1.625E+05	3.250E+05	4.875E+05	6.500E+05	8.124E+05	9.749E+05
6	1.681E+05	3.361E+05	5.042E+05	6.722E+05	8.403E+05	1.008E+06
7	1.766E+05	3.532E+05	5.298E+05	7.064E+05	8.830E+05	1.060E+06
8	1.756E+05	3.511E+05	5.267E+05	7.023E+05	8.779E+05	1.053E+06
9	1.773E+05	3.546E+05	5.320E+05	7.093E+05	8.866E+05	1.064E+06
10	1.758E+05	3.516E+05	5.274E+05	7.032E+05	8.791E+05	1.055E+06
11	1.773E+05	3.546E+05	5.319E+05	7.092E+05	8.865E+05	1.064E+06
12	1.843E+05	3.687E+05	5.530E+05	7.373E+05	9.216E+05	1.106E+06
13	1.750E+05	3.499E+05	5.249E+05	6.999E+05	8.748E+05	1.050E+06
14	1.738E+05	3.476E+05	5.213E+05	6.951E+05	8.689E+05	1.043E+06
15	1.663E+05	3.326E+05	4.989E+05	6.652E+05	8.315E+05	9.979E+05
16	1.495E+05	2.990E+05	4.485E+05	5.980E+05	7.475E+05	8.970E+05
17	1.477E+05	2.954E+05	4.431E+05	5.907E+05	7.384E+05	8.861E+05
18	1.393E+05	2.785E+05	4.178E+05	5.570E+05	6.963E+05	8.355E+05
19	1.232E+05	2.465E+05	3.697E+05	4.930E+05	6.162E+05	7.395E+05
20	1.078E+05	2.156E+05	3.234E+05	4.312E+05	5.390E+05	6.468E+05
21	9.357E+04	1.871E+05	2.807E+05	3.743E+05	4.679E+05	5.614E+05
Rod 16 Segments	Heat flux 5kW	Heat Flux 10kW	Heat Flux 15kW	Heat Flux 20kW	Heat Flux 25kW	Heat Flux 30kW
1	6.271E+04	1.254E+05	1.881E+05	2.509E+05	3.136E+05	3.763E+05
2	1.319E+05	2.637E+05	3.956E+05	5.274E+05	6.593E+05	7.911E+05
3	1.440E+05	2.880E+05	4.320E+05	5.761E+05	7.201E+05	8.641E+05
4	1.506E+05	3.012E+05	4.518E+05	6.024E+05	7.530E+05	9.036E+05
5	1.596E+05	3.191E+05	4.787E+05	6.383E+05	7.979E+05	9.574E+05
6	1.671E+05	3.343E+05	5.014E+05	6.685E+05	8.356E+05	1.003E+06
7	1.732E+05	3.465E+05	5.197E+05	6.930E+05	8.662E+05	1.039E+06
8	1.808E+05	3.616E+05	5.424E+05	7.232E+05	9.039E+05	1.085E+06
9	1.914E+05	3.828E+05	5.743E+05	7.657E+05	9.571E+05	1.149E+06
10	1.748E+05	3.496E+05	5.245E+05	6.993E+05	8.741E+05	1.049E+06
11	1.844E+05	3.688E+05	5.532E+05	7.376E+05	9.220E+05	1.106E+06
12	1.776E+05	3.552E+05	5.328E+05	7.105E+05	8.881E+05	1.066E+06
13	1.718E+05	3.436E+05	5.154E+05	6.872E+05	8.590E+05	1.031E+06
14	1.689E+05	3.378E+05	5.067E+05	6.756E+05	8.445E+05	1.013E+06
15	1.632E+05	3.263E+05	4.895E+05	6.526E+05	8.158E+05	9.790E+05
16	1.560E+05	3.120E+05	4.680E+05	6.240E+05	7.799E+05	9.359E+05
17	1.484E+05	2.968E+05	4.452E+05	5.936E+05	7.421E+05	8.905E+05
18	1.385E+05	2.771E+05	4.156E+05	5.542E+05	6.927E+05	8.313E+05

University of Ghana http://ugspace.ug.edu.gh

19	1.164E+05	2.329E+05	3.493E+05	4.658E+05	5.822E+05	6.987E+05
20	1.088E+05	2.176E+05	3.264E+05	4.352E+05	5.440E+05	6.529E+05
21	9.813E+04	1.963E+05	2.944E+05	3.925E+05	4.907E+05	5.888E+05
Rod 17 Segments	Heat flux 5kW	Heat Flux 10kW	Heat Flux 15kW	Heat Flux 20kW	Heat Flux 25kW	Heat Flux 30kW
1	6.164E+04	1.233E+05	1.849E+05	2.466E+05	3.082E+05	3.699E+05
2	1.379E+05	2.758E+05	4.138E+05	5.517E+05	6.896E+05	8.275E+05
3	1.404E+05	2.808E+05	4.212E+05	5.616E+05	7.020E+05	8.424E+05
4	1.527E+05	3.055E+05	4.582E+05	6.109E+05	7.637E+05	9.164E+05
5	1.638E+05	3.277E+05	4.915E+05	6.554E+05	8.192E+05	9.831E+05
6	1.691E+05	3.382E+05	5.073E+05	6.764E+05	8.456E+05	1.015E+06
7	1.667E+05	3.334E+05	5.001E+05	6.668E+05	8.335E+05	1.000E+06
8	1.734E+05	3.468E+05	5.202E+05	6.935E+05	8.669E+05	1.040E+06
9	1.803E+05	3.606E+05	5.410E+05	7.213E+05	9.016E+05	1.082E+06
10	1.835E+05	3.671E+05	5.506E+05	7.342E+05	9.177E+05	1.101E+06
11	1.837E+05	3.674E+05	5.512E+05	7.349E+05	9.186E+05	1.102E+06
12	1.847E+05	3.694E+05	5.541E+05	7.388E+05	9.234E+05	1.108E+06
13	1.781E+05	3.562E+05	5.343E+05	7.125E+05	8.906E+05	1.069E+06
14	1.710E+05	3.420E+05	5.131E+05	6.841E+05	8.551E+05	1.026E+06
15	1.559E+05	3.118E+05	4.677E+05	6.236E+05	7.795E+05	9.354E+05
16	1.576E+05	3.151E+05	4.727E+05	6.302E+05	7.878E+05	9.454E+05
17	1.443E+05	2.886E+05	4.328E+05	5.771E+05	7.214E+05	8.657E+05
18	1.331E+05	2.663E+05	3.994E+05	5.326E+05	6.657E+05	7.989E+05
19	1.269E+05	2.538E+05	3.807E+05	5.076E+05	6.345E+05	7.614E+05
20	1.105E+05	2.211E+05	3.316E+05	4.422E+05	5.527E+05	6.632E+05
21	9.288E+04	1.858E+05	2.786E+05	3.715E+05	4.644E+05	5.573E+05
Rod 18 Segments	Heat flux 5kW	Heat Flux 10kW	Heat Flux 15kW	Heat Flux 20kW	Heat Flux 25kW	Heat Flux 30kW
1	6.074E+04	1.215E+05	1.822E+05	2.430E+05	3.037E+05	3.644E+05
2	1.343E+05	2.687E+05	4.030E+05	5.373E+05	6.716E+05	8.060E+05
3	1.418E+05	2.837E+05	4.255E+05	5.673E+05	7.092E+05	8.510E+05
4	1.492E+05	2.984E+05	4.476E+05	5.967E+05	7.459E+05	8.951E+05
5	1.606E+05	3.212E+05	4.818E+05	6.424E+05	8.029E+05	9.635E+05
6	1.688E+05	3.376E+05	5.063E+05	6.751E+05	8.439E+05	1.013E+06
7	1.743E+05	3.486E+05	5.229E+05	6.972E+05	8.715E+05	1.046E+06
8	1.793E+05	3.587E+05	5.380E+05	7.174E+05	8.967E+05	1.076E+06
9	1.773E+05	3.547E+05	5.320E+05	7.093E+05	8.866E+05	1.064E+06
10	1.759E+05	3.519E+05	5.278E+05	7.038E+05	8.797E+05	1.056E+06
11	1.817E+05	3.634E+05	5.451E+05	7.268E+05	9.085E+05	1.090E+06
12	1.760E+05	3.519E+05	5.279E+05	7.038E+05	8.798E+05	1.056E+06
13	1.714E+05	3.427E+05	5.141E+05	6.855E+05	8.568E+05	1.028E+06
14	1.711E+05	3.421E+05	5.132E+05	6.842E+05	8.553E+05	1.026E+06
15	1.711E+05	3.422E+05	5.132E+05	6.843E+05	8.554E+05	1.026E+06
16	1.508E+05	3.015E+05	4.523E+05	6.030E+05	7.538E+05	9.045E+05
17	1.435E+05	2.870E+05	4.305E+05	5.740E+05	7.175E+05	8.609E+05
18	1.354E+05	2.707E+05	4.061E+05	5.414E+05	6.768E+05	8.122E+05

University of Ghana http://ugspace.ug.edu.gh

19	1.289E+05	2.578E+05	3.866E+05	5.155E+05	6.444E+05	7.733E+05
20	1.139E+05	2.278E+05	3.417E+05	4.556E+05	5.695E+05	6.834E+05
21	1.025E+05	2.049E+05	3.074E+05	4.099E+05	5.124E+05	6.148E+05

Appendix IV

Residual Plot

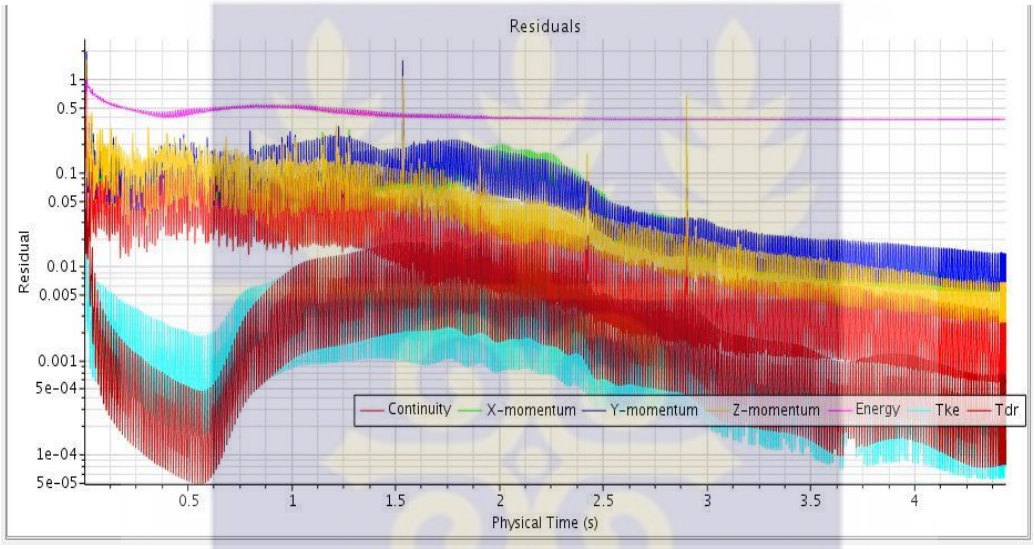

INTEGRI PROCEDAMUS